NTNU – Trondheim
Norwegian University of
Science and Technology

Preparation and Characterisation of Hydrophobically Modified Xanthan

Ina Beate Jenssen

Chemical Engineering and Biotechnology
Submission date: June 2014
Supervisor: Bjørn E. Christensen, IBT

Norwegian University of Science and Technology
Department of Biotechnology

Preface

This master thesis was performed during the spring of 2014. The laboratory work was performed at the biopolymer laboratory at the Department of Biotechnology, NTNU.

Professor Bjørn E. Christensen has been my supervisor during the work, and I would like to thank him very much for this interesting project, as well as excellent guidance and help with the experimental planning and writing of this thesis, and good discussions during the project.

I would also like to thank senior engineer Ann-Sissel T. Ulset for running SEC-MALLS analyses, and senior engineer Wenche I. Strand for running ^{1}H-NMR, and both for help with lab equipment, together with planning and performance of the experimental work. I will also thank the rest of the people in the biopolymer lab, for contributing to such a great working environment.

I will thank Professor Bjørn Torger Stokke at the Department of Physics for providing the sonicator.

I would like to thank PhD student Audrey Roy and Dr. Frédéric Renou at the University of Le Havre for help with experimental procedures and calculations, and also for the great opportunity to visit Le Havre, and for good discussions.

Last, but not least, I would like to thank my family and friends, and especially my classmates, for 5 great years at NTNU.

Trondheim, June 16th 2014

Ina Beate Jenssen

Abstract

Xanthan is a polysaccharide widely used in food, cosmetics, and enhanced oil recovery (EOR) by polymer flooding. In polymer flooding addition of polymers increases the viscosity of the injection water used for oil extraction from the oil producing wells. It is desirable to take advantage of biopolymers in EOR, due to their biodegradability and easily accessible raw materials of low costs.

By hydrophobically modifying xanthan the thickening properties may be improved, due to intra- and intermolecular interactions between hydrophobic side groups. In this master thesis xanthan was hydrophobically modified by grafting of octylamine using carbodiimide chemistry, applying a method adopted from the University of Le Havre, France.

Properties of non-modified and modified xanthan samples prepared from two different start xanthans, from Kelco and Statoil, were studied by SEC-MALLS, intrinsic viscosity measurements, and ^{1}H-NMR spectroscopy. In order to obtain xanthan molecules of a size suitable for these analysis methods, sonication was performed. Xanthan samples were sonicated for different times, and an obvious decreasing trend of the molecular weight and intrinsic viscosity as the sonication time increased was shown. Intrinsic viscosity dependence on molecular weight was in good accordance to previous reported results.

Depolymerisation by H_2O_2 and NaOH prior to ^{1}H-NMR analysis did not have the desirable effect on degradation of xanthan chains. The side groups were cut off, rather than breaking the β-1,4 bonds between the glucose units in the xanthan backbone.

By comparing the grafting density of octylamine for an acetyl and pyruvyl free xanthan sample and xanthan samples with these groups intact, it was shown for the first time that more than half of the octylamine binds to the carboxylic acid of the pyruvyl group on the β-D-mannose of xanthan.

Intrinsic viscosity determined by a single capillary viscometer was higher for modified xanthan than non-modified, while by a four-bulb shear dilution viscometer the opposite was shown. The intrinsic viscosity was shown to be dependent on shear rate by the four-bulb viscometer, and the intrinsic viscosities at zero shear for non-modified and modified xanthan was significantly higher than that determined by single capillary viscometer.

Sammendrag

Xanthan er et polysakkarid som er mye brukt i mat, kosmetikk, og økt oljeutvinning (EOR) ved polymerfløming. I polymerfløming økes viskositeten av injeksjonsvannet som brukes til å utvinne mer olje fra produksjonsbrønnene, ved å tilsette polymerer. Det er ønskelig å benytte biopolymerer i EOR, på grunn av deres biologiske nedbrytbarhet og lett tilgjengelige råstoffer med lave kostnader.

Ved å hydrofobmodifisere xantan kan fortykningsegenskapene forbedres som følge av intra-og intermolekylære vekselvirkninger mellom hydrofobe sidegrupper. I denne masteroppgaven ble xanthan hydrofobmodifisert ved å binde oktylamin ved hjelp av karbodiimidkjemi, ved å bruke en metode fra Universitetet i Le Havre i Frankrike.

Egenskapene til ikke-modifiserte og modifiserte xanthanprøver som var preparert fra to forskjellige startxanthaner, fra Kelco og Statoil, ble studert av SEC-MALLS, egenviskositetsmålinger, og ^{1}H-NMR-spektroskopi. For å oppnå xantanmolekyler med størrelser som er egnet for disse analysemetodene ble det utført sonikering. Xanthanprøver ble sonikert ved forskjellige tider, og det ble vist at både molekylvekt og egenviskositet ble redusert ettersom sonikeringstiden økte. Forholdet mellom egenviskositet og molekylvekt var i god overensstemmelse med tidligere rapporterte resultater.

Depolymerisering av H_2O_2 og NaOH før ^{1}H-NMR-analyse viste seg å ikke ha ønskelig effekt på nedbrytning av xanthankjedene. Sidegruppene ble kuttet av istedet for å bryte β -1,4 bindingene mellom glukoseenhetene i hovedkjeden av xanthan.

Ved å sammenligne festningsgraden av oktylamin for en acetyl- og pyruvylfri xanthanprøve med xantanprøver med disse gruppene intakt, ble det for første gang vist at mer enn halvparten av oktylamin bindes til karboksylsyren med pyruvylgruppen på den ytre β-D-mannosen av xanthan.

Egenviskositet bestemt ved kapillærviskometer var høyere for modifisert xanthan enn for ikke-modifisert, mens for målinger med "four-bulb shear dilution" viskometer ble det motsatte vist. Egenviskositeten ble vist å være avhengig av skjærhastigheten, ved fire-bulb-viskometeret, og egenviskositene ved null skjær for både ikke-modifisert of modifisert xanthan var betydelig høyere enn de bestemt fra målinger med kapillærviskometeret.

Table of Contents

List of Figures

List of Tables

Symbols and Abbreviations

Symbol	Description	Unit
$\%octyl$	Grafting density	%
ΔE	Energy difference between upper and lower spin state	J
$\dot{\gamma}$	Shear rate	s^{-1}
η	Viscosity	Ns/m^2
η_0	Viscosity of solvent	mL/g
η_s	Viscosity of solution	mL/g
η_{sp}	Specific viscosity	mL/g
σ	Shear stress	Pa
A	Area	m^2
a	Mark-Houwink-Sakurada exponent	
A_2	The second viral coefficient	
c	Concentration	g/mL, mol/L
dn/dc	Specific refractive index increment	mL/g
dv/dz	Flow gradient	s^{-1}
F	Force	N
h	Planck's constant	kJ/mol
I	Spin quantum number	
K	Mark-Houwink-Sakurada constant	mL/g
k	Partition coefficient	
k'	Huggins' constant	

K^*	Optical constant	
M	Molar mass	g/mol
M'_{RU}	Repeating unit molecular weight	g/mol
M_{H_2O}	Molecular weight of H_2O	g/mol
M_{octyl}	Molecular weight of octylamine	g/mol
M_{RU}	Molecular weight of non-modified xanthan	g/mol
n'_{RU}	Moles modified repeating units	mol
n_{octyl}	Moles octylamine	mol
$P(\theta)$	Particle scattering function	
R_θ	Excess Rayleigh ratio	
t_0	Flow-through time of solvent	s
T_m	Conformational temperature	°C
t_s	Flow-through time of solution	s
v	Frequency	Hz
V_m	Volume of mobile phase	mL
V_R	Retention volume	mL
V_s	Volume of stationary phase	mL
$[\eta]$	Intrinsic viscosity	mL/g
ABA	Aldobiuronic acid	
EDAC	*N*-ethyl-*N'*-(3-dimethylaminopropyl) carbodiimide hydrochloride	
MHS	Mark-Houwink-Sakurada	
NHS	N-hydroxysuccinimide	
NMR	Nuclear magnetic resonance	
TSP	2,2,3,3-d(4)-3(trimethylsilyl)propionic acid	
v%	Concentration on volume basis	mL/mL

Chapter 1

Introduction

1.1 General Background

The main background for this master thesis is the use of hydrophobically modified polysaccharide biopolymers, such as xanthan, for enhanced oil recovery (EOR).

Today fossil fuels already provides 85 % of the world's global energy, and with the energy consumption increasing and oil reservoirs being depleted, enhanced oil recovery becomes more and more important. Thus, it is important to take advantage of already existing oil fields (Sheng, 2010).

One method for increasing the oil recovery is polymer flooding, where the two most commonly applied polymers are polyacrylamide and xanthan gum. In fresh water polyacrylamide polymers are generally more viscous than polysaccharide biopolymers at equal concentrations. High viscosity is desirable for EOR polymers. In contrast to polyacrylamides, biopolymers are biodegradable, thus not harmful for the environment. In addition biopolymers are more resistant to mechanical degradation than polyacrylamides. However, the residual permeability reduction factor of biopolymers is low, and injectivity problems due to cell remnants from production may occur. Thus, today mainly polyacrylamides are used in EOR. It is desirable to develop and improve biopolymer for EOR application, such as xanthan. Water soluble hydrophobically modified polysaccharides with associating properties may increase solution viscosity, and they have a great potential in being used as mobility control agents at high salinity. Also, their flow properties may be of good advantage in drilling fluids. (Sheng, 2010, Taylor and Nasr-El-Din, 1998, Uhl et al., 1995).

1.2 Enhanced Oil Recovery

There are three phases of enhanced oil recovery (EOR):

1. Primary recovery phase
2. Secondary recovery phase
3. Tertiary recovery phase

In the primary phase, the efficiency of the oil recovery depends on the natural energy present in the reservoir, such as water drive, gravity, solution gas, and rock and fluid expansion. The secondary phase usually follows the primary phase, but may also be performed simultaneously in order to increase the oil production further. The most commonly used method for the secondary recovery phase is injection of water or gas. Following the secondary phase is the tertiary phase, which involves injection of chemicals, miscible gases, and thermal energy (Harnoy et al., 1989, Sheng, 2010).

1.2.1 Polymer Flooding

As a result of the immiscible properties of oil and water, neither is able to displace the other from an oil reservoir. The principle of polymer flooding is increasing the viscosity of the aqueous phase by adding a water-soluble polymer (Needham and Doe, 1987). This causes an increase in the sweep efficiency (the oil-water mobility ratio) in enhanced oil recovery processes (Chang, 1978, Taylor and Nasr-El-Din, 1998). A simplified illustration of polymer flooding is shown in Figure 1.2.1.

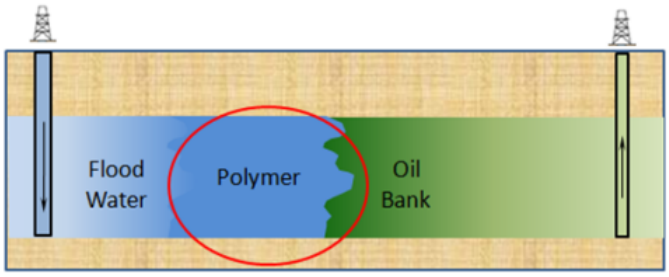

Figure 1.2.1: Simplified illustration of the principle of polymer flooding. The injected polymers cause increased oil recovery from the producing wells by increasing the viscosity and sweep efficiency of the injection water (PetroTel, 2010).

Properties of EOR Polymers

There are several characteristics that make polymers suitable for EOR. Some of the most important properties are water solubility, stability at different salt compositions, stability towards mechanical influence from valves and pumps, temperatures and pH. They should also be cost effective, and they should not degrade in the presence of free radicals, microorganisms or heavy metals. In addition the polymers should have high intrinsic viscosity, which provides a high viscosity of the injection water at low polymer concentrations. Shear thinning polymers is an advantage; they have low viscosity at high shear, thus they flow easily, while at low shear they have high viscosity. Biodegradability is also desirable, to prevent potential environmentally harmful leakages. (Christensen, 2013, Taylor and Nasr-El-Din, 1998)

Types of EOR Polymers

Both synthetic polymers and biopolymers are used in EOR. The most commonly used synthetic EOR polymers are polyacrylamide (PAM), partially hydrolysed polyacrylamide (HPAM), while the most common biopolymer is xanthan gum (Needham and Doe, 1987, Wever et al., 2011).

Polyacrylamide was the first polymer that was used for increasing viscosity of aqueous solutions used in EOR. It is mainly the high molecular weight of PAM that causes the viscosity increase. Previously it has been reported several attempts to chemically modify PAM in order to achieve properties such as shear resistance, better compatibility with brine, and stability towards temperature (Sabhapondit et al., 2003, Song et al., 2007, Vega et al., 2008, Wever et al., 2011).

In hydrolysed polyacrylamide, HPAM, parts of the acrylamide have been replaced by acrylic acid. The carboxylate groups of the acrylic acids cause repulsion of the ionic groups, giving a chain extension, thus the viscosity of a solution with HPAM increases (Needham and Doe, 1987). In EOR it is desirable to use PAMs and HPAMs with high molecular weights, as this influences the viscosity of the injection water. However, higher molecular weight gives higher capability for shear degradation (Taylor and Nasr-El-Din, 1998). The viscosity of HPAM will also decrease if there is an increase in the salinity or hardness of the water, due to shielding of the ionic groups (Nasr-El-Din et al., 1991).

The most commonly applied biopolymer in EOR is xanthan gum. Even though the cost of xanthan is higher than for the synthetic polymers, due to purification and removal of bacterial cells, xanthan is a more rigid polymer, and do not degrade easily at high shear rates, nor is it sensitive to increased salinity. In addition xanthan is biodegradable, thus it will not cause pollution in case of leakages. There may, however, occur problems with

injectivity due to remaining cell residues from the production process (Nasr-El-Din and Noy, 1992, Sheng, 2010).

Water-soluble hydrophobically associating polymers have small hydrophobic groups attached, which gives an increased solution viscosity. This increase is caused by association of the hydrophobic moieties, in order to minimise their exposure to the solvent, thus the hydrodynamic size of the polymer increases (Taylor and Nasr-El-Din, 1998, Uhl et al., 1995).

1.3 Xanthan

Xanthan is a polysaccharide that is extracellularly produced by the bacterium *Xanthomonas campestris*, and today it is the most important microbial polysaccharide. Xanthan gum is also regarded as a safe food additive, and applied in EOR and drug delivery (Katzbauer, 1998).

1.3.1 *Xanthomonas campestris*

Xanthomonas campestris is a *γ-proteobacteria* of the *Pseudomonaceae* family, and a plant pathogen; it inhabits host plants and initiates infections. The cells of *Xanthomonas* are straight rods, motile, Gram-negative, and possess a single polar flagellum. The bacteria are chemoorganotrophs, obligate aerobe, and can not denitrify (Bergey and Holt, 1994). *X. campestris* infects plants such as cabbage, alfalfa and beans, but strains of the bacteria are also shown to be good producers of xanthan gum. The strain *X. campestris* pv. *campestris* is often used for xanthan production (Bergey and Holt, 1994, Madigan et al., 2010, Rehm, 2009). For production of xanthan by *X. campestris* several nutrients such as carbon, nitrogen, potassim and calcium salts are needed (Garcıa-Ochoa et al., 2000).

1.3.2 Structure of Xanthan

The chemical structure of the repeating unit of xanthan as proposed by Jansson et al. (1975) is shown in Figure 1.3.1.

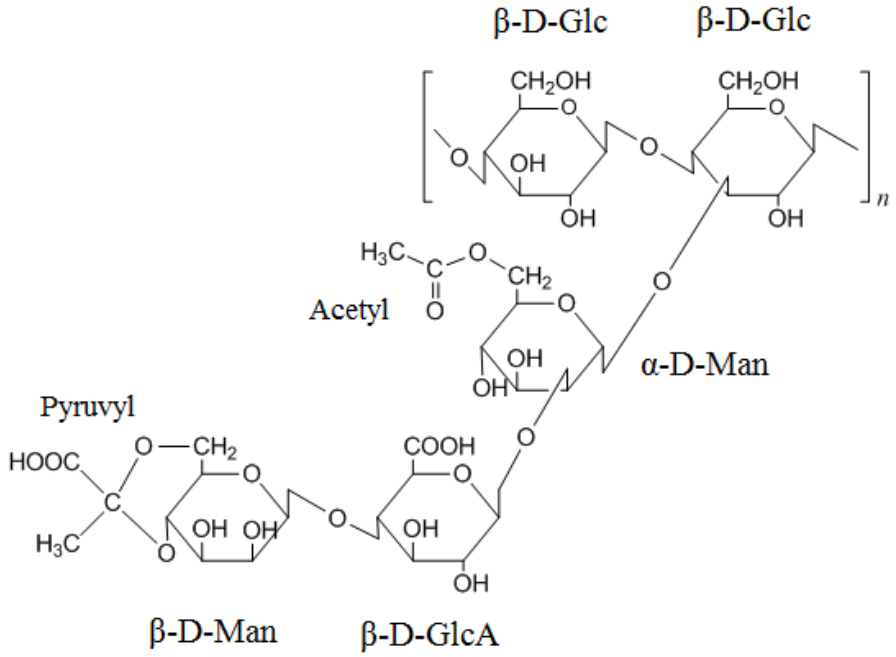

Figure 1.3.1: The chemical structure of the repeating unit of xanthan.

The repeating unit of xanthan consists of a backbone chain of β-1,4-linked D-glucose units, with a trisaccharide side chain attached to every other glucose unit of the backbone. The side chains consist of α-D-mannose, β-D-glucuronic acid, and β-D-mannose. The α-D-mannose is 1,4-linked to the glucose unit in the backbone, and may contain an *O*-acetyl group on O-6. The glucuronic acid is 1,2-linked to the α-D-mannose, and lies between the two mannoses. The outer mannose, β-D-mannose, is 1,4-linked to the glucuronic acid, and may contain an acetal-linked pyruvyl group (Jansson et al., 1975, Melton et al., 1976). The degree of substitution of acetyl and pyruvyl is determined by the strain of *X. campestris* and the fermentation conditions (Papagianni et al., 2001).

The xanthan polymer may exist as single, double, or triple stranded stiff chain, as a consequence of the side chains aligning close to the backbone. The molecular weight of xanthan depends on the chain association, and ranges from $2 \cdot 10^6$ to $20 \cdot 10^6$ Da (Garcıa-Ochoa et al., 2000, Milas and Rinaudo, 1979).

1.3.3 Properties of Xanthan

Xanthan is a polyelectrolyte, and soluble in both hot and cold water. Xanthan provides high viscosity of solutions, even at low concentrations. The viscosity depends highly on the shear rate, due to the shear thinning, or pseudoplastic, properties of xanthan; at low shear rates xanthan is highly viscous, while at high shear rates the viscosity decreases.

Other factors influencing the viscosity are temperature, polymer and salt concentrations, and pH.

The viscosity of xanthan solutions decreases with increasing measurement temperature. However, the viscosity also depends on the dissolution temperature. If the dissolution temperature of the solution is increased to 40 °C the viscosity decreases with increasing measurement temperature. If the dissolution temperature is between 40 and 60 °C the viscosity increases with increasing temperature, and above 60 °C the viscosity decreases with increasing temperature. This phenomenon can be explained by the conformational transitions of the xanthan chains (see Section 1.3.4) (Garcıa-Ochoa et al., 2000, Milas and Rinaudo, 1979).

Increased concentration of the xanthan causes an increase of the solution viscosity, due to intermolecular interactions, thus increasing the effective molecular size. Low salt concentrations in solutions with low polymer concentration leads to reduced ionic interactions, and thus decreased viscosity, while the viscosity of solutions with high concentrations of polymer and salt increases, due to interactions between the polymer molecules (Milas et al., 1985, Smith and Pace, 1982). If the salt concentration is above 0.1 % w/v, the viscosity does not depend on the salinity (Kang and Pettit, 1993).

At high pH (pH>9) xanthan will undergo gradually deacetylation, while at low pH (pH<3) the pyruvyl groups are lost. Loss of these groups will not influence the rheological properties of the xanthan solution significantly (Bradshaw et al., 1983, Tako and Nakamura, 1984).

Acetyl and Pyruvyl Free Xanthan

The acetyl group found at the inner α-D-mannose and the pyruvyl group at the outer β-D-mannose may be removed by mild alkaline and acid hydrolysis, respectively (Christensen et al., 1996).

The structure of xanthan without acetyl and pyruvyl groups is shown in Figure 1.3.2.

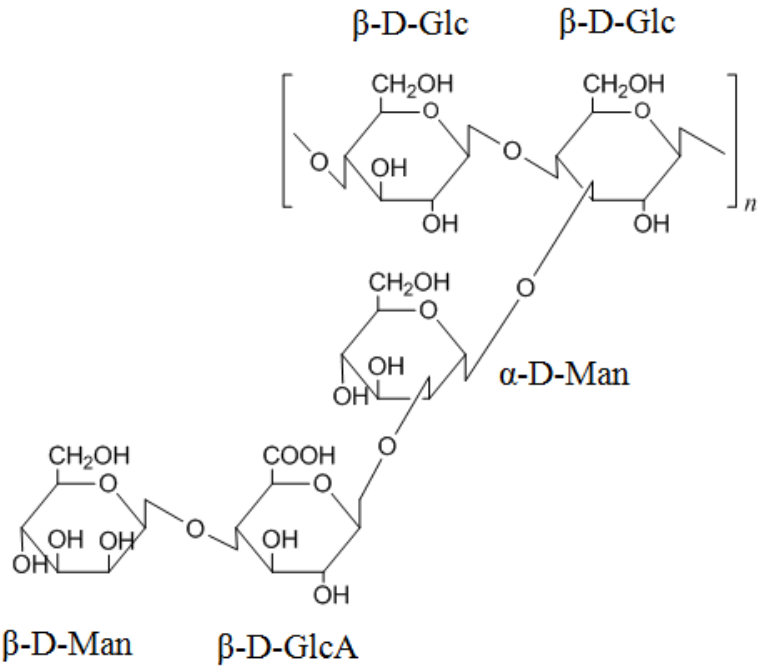

Figure 1.3.2: The chemical structure of the repeating unit of acetyl and pyruvyl free xanthan.

Xanthan that does not contain acetyl or pyruvyl groups has similar rheological properties as native xanthan (Bradshaw et al., 1983). The differences are largest at low shear rates, while at high shear rates the viscosities converge, this occurs because the molecular interactions decrease with increasing shear rate (Garcıa-Ochoa et al., 2000).

1.3.4 Conformational Transitions of Xanthan

At low salt concentrations xanthan will have a disordered conformation; in this conformation the xanthan chains will have structure as single stranded flexible coils. In solutions with higher salt concentrations xanthan will undergo a reversibel conformational transition to an ordered conformation. In this conformation the chain obtains a rigid double helix structure. The conformational transition of a polysacharide is determined by the transition temperature, T_m. For xanthan T_m is dependent on the acetyl and pyruvyl content, ionic strengt, and pH. When this temperature is reached, the rheological properties of the xanthan decrease (Christensen and Smidsrød, 1991, Milas and Rinaudo, 1979, Paoletti et al., 1983, Roy et al., 2014). The transition temperature can easily be detected by use of optical rotation, circular dichroism, or calorimetry (Christensen, 1996). An example of the assignment of the conformational transition of xanthan is presented in Figure 1.3.3.

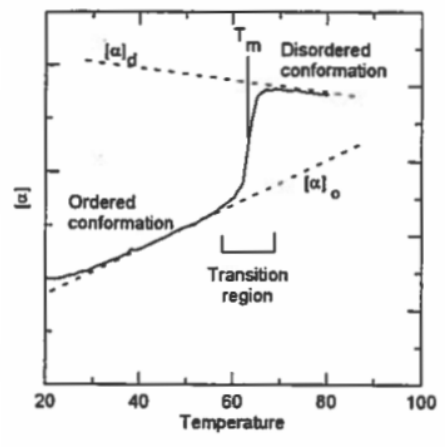

Figure 1.3.3: Transition from ordered to disordered conformation, based on optical rotation measurements. $[\alpha]$ is the observed specific rotation at a given temperature. $[\alpha]_0$ and $[\alpha]_d$ are the specific rotations assigned to ordered and disordered conformation, respectively, and T_m is the transition temperature (Christensen, 1996).

The conformational transition of xanthan from order to disorder has previously been observed by electron microscopy (Stokke et al., 1986). An electron micrograph of the conformational transition between order and disorder is shown in Figure 1.3.4.

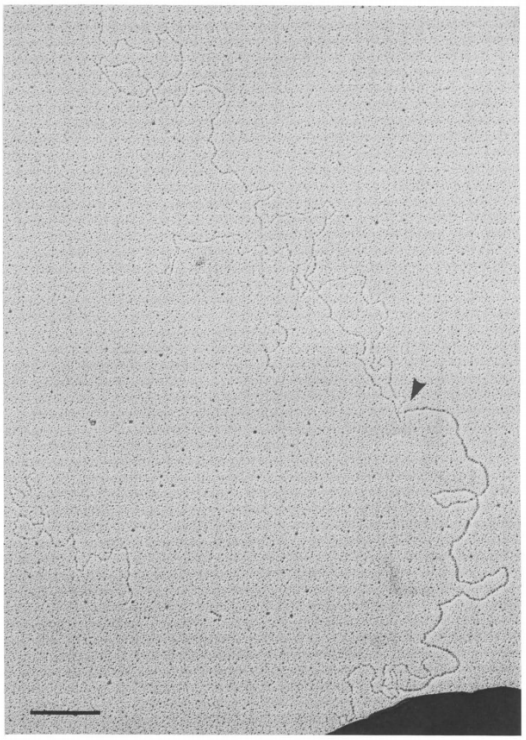

Figure 1.3.4: Electron micrograph of conformational transition of xanthan from double stranded to single stranded. The arrow show where the chain is divided (Stokke et al., 1986).

1.3.5 Applications of Xanthan

Xanthan is widely used as a food additive, in cosmetics and pharmaceutical applications, but also technical applications such as enhanced oil recovery is of importance.

In food xanthan is used as a stabiliser and thickener. Addition of xanthan prevents oiling off and separation of insoluble particles. Another application in food is increase of the mixability and pourability, due to the shear thinning properties. In cosmetics xanthan is mostly used in tooth pastes, because of the shear thinning properties, but it is also used as a stabiliser and thickener in personal care products, in addition to prevent separation of immiscible ingredients. Technical applications of xanthan involves use in agricultural chemicals in order to increase sprayability, in cleaners in order to improve tolerance towards acid and alkali, and in enhanced oil recovery, to stabilise suspension and water under extreme conditions (Katzbauer, 1998). The latter application was the main basis for this master thesis.

1.4 Hydrophobically Modified Polysaccharides

Hydrophobically modified associative polysaccharides are shown to have unusual rheological properties and high solubility in aqueous solutions. This is explained by the inter- and intramolecular interactions between the hydrophobic groups (Esquenet and Buhler, 2001). As a result of these unique properties, water-soluble hydrophobically modified polysaccharides have various applications, such as thickening agents and viscosity modifiers in food, drug delivery, and enhanced oil recovery. Over the last three decades such modified polysaccharides have been thoroughly studied (Roy et al., 2014, Taylor and Nasr-El-Din, 1998).

Hydrophobic associative polymers may contain hydrophobic units randomly distributed throughout the polymer chain (random co-polymer), in an organised manner (block co-polymer), or grafted onto the main chain (graft co-polymer). Grafted polymers are often obtained by chemical modification of polysaccharides. The benefits of polysaccharides are easily accessible raw materials of low costs, and properties such as biocompatibility and biodegradability (Biswas et al., 2013, Roy et al., 2014).

Chemical modification of several polysaccharides, such as cellulose, alginate, pullulan, and chitosan, has previously been studied. In general, the motive of modified polysaccharides has been in drug delivery and biomedical applications. Also, most of the previously studied modified polysaccharides have a simple structure. More advanced polysaccharides, such as xanthan, has not been studied to the same extent (Colinet et al., 2009, Dulong et al., 2006, 2012, Esquenet and Buhler, 2001, Souguir et al., 2007, Yang et al., 2007,

Zhang, 2001)

For hydrophobically modified associative polysaccharides the intrinsic viscosity will typically be lower than for non-modified polysaccharides (Peiffer et al., 1986). However, it is shown that over a critical concentration the intrinsic viscosity of a modified polysaccharide may exceed the viscosity of the non-modified polysaccharide (Wang et al., 1988). The increase of viscosity can be explained by interactions of cross-linking between the polymer chains.

Some hydrophobically modified polysaccharides are shown to have low viscosity even at high polymer concentrations. This phenomenon is explained by intramolecular aggregation of an important number of hydrophobic side groups, thus the hydrodynamic radius is kept low, hence the viscosity of the solution is low (Colinet et al., 2009).

1.5 Chemical Modification of Xanthan

There are not found many examples of hydrophobically modified xanthan in the literature, and most of the examples describes modification in order to obtain xanthan derivatives and xanthan hydrogels for drug delivery (Hamcerencu et al., 2009, Kumar et al., 2009, Roy et al., 2014), or for encapsulation of cells (Mendes et al., 2011).

These examples of modified xanthan involves an esterification reaction, which results in low regioselectivity and may cause crosslinkages between xanthan chains (Roy et al., 2014). To overcome this problem, the hydrophobic groups may be coupled to the carboxylic acid groups by carbodiimide chemistry (Bejenariu et al., 2009). In this project octylamine will be grafted onto the carboxylic acid groups of xanthan by using a carbodiimide as a coupling agent, for formation of amide bonds.

By chemical modification of xanthan the rigid double-stranded helical conformation will ideally not be changed, since the helical conformation depends on the hydrogen bonds of the carboxylic acid groups (Milas and Rinaudo, 1986, Roy et al., 2014). Amide groups possess similar ability to form hydrogen bonds as the carboxylic acid groups. The properties of the xanthan is thus only affected by presence of alkyl chains.

1.5.1 Formation of Amide-Bond by Carbodiimide-Mediated Reaction

The most common method for formation of amide bonds is the carbodiimide method. The reaction mechanism of formation of an amide bond from a cabrodiimide-mediated reaction is shown in Figure 1.5.1.

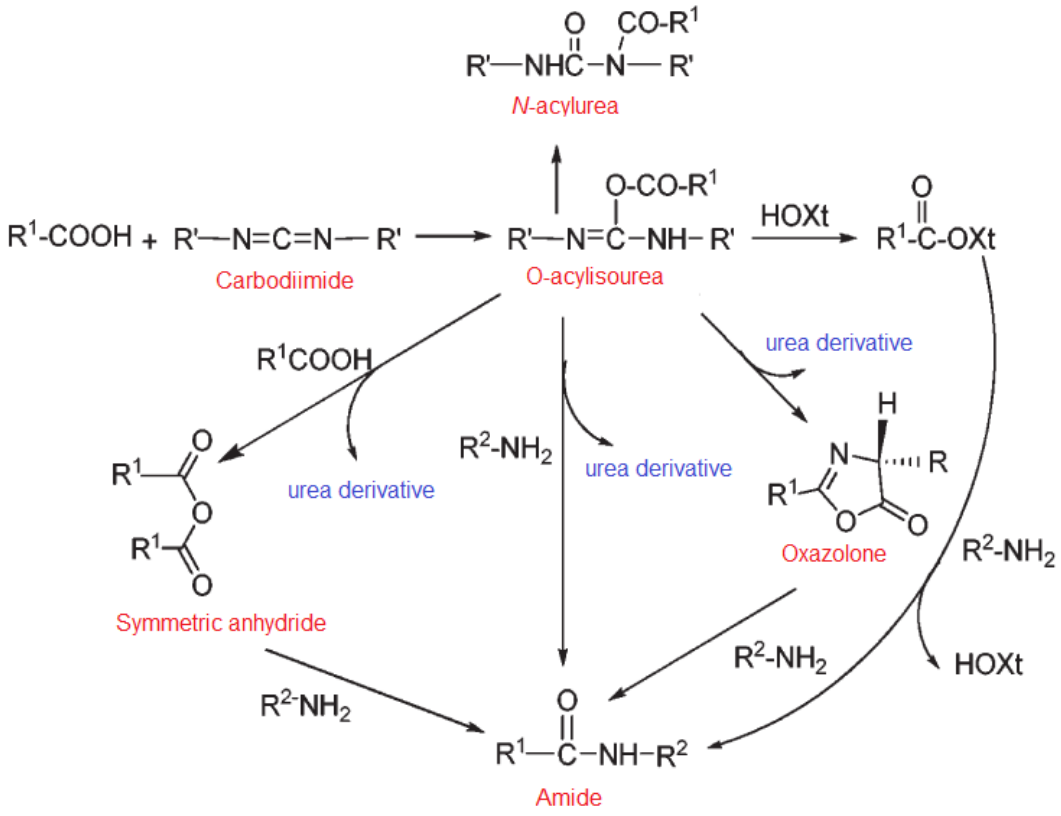

Figure 1.5.1: Mechanism of formation of amide bond from a carbodiimide-mediated reaction (El-Faham and Albericio, 2011).

Carbodiimides contain two nitrogen atoms, which causes a weak negative charge that triggers reaction between carbodiimide and an acid, forming *O*-acylisourea (Benoiton and Chen, 1981, Rebek and Feitler, 1974, Sheehan and Hess, 1955). *O*-Acylisourea is very reactive and will rapidly undergo aminolysis in the presence of the amine component and forms the peptide. If there is not sufficiently enough carboxylic acid, a second molecule will attack the acid and *O*-acylisourea forms a symmetrical anhydride, which is aminolysed to form the peptide. The third pathway is formation of oxazolone, which also is aminolysed to form the peptide. The last option is an irreversible racemisation of *O*-acylisourea to *N*-acylurea, which is an inert form of the incoming acid (El-Faham and Albericio, 2011).

Traditionally, dicyclohexylcarbodiimide (DCC) was used in carbodiimide-mediated reactions. However, use of DCC causes formation of a precipitate of *N,N'*-dicyclohexylurea (DCU), which is difficult to remove (Han and Kim, 2004). Thus, DCC has been replaced with other carbodiimides such as diisopropylcarbodiimide (DIC), *N*-ethyl-*N'*-(3-dimethylaminopropyl) carbodiimide hydrochloride (EDC/EDAC), and *N*-cyclohexyl-*N'*-isopropyl carbodiimide (CIC) (Izdebski et al., 1994). EDAC is especially suited for use in solutions, since both the reagent and the urea compound are soluble in aqueous solutions,

thus they may easily be removed (El-Faham and Albericio, 2011).

1.5.2 Grafting of Octylamine onto Xanthan

Hydrophobically modified xanthan may be obtained by grafting of octylamine. By applying *N*-ethyl-*N'*-(3-dimethylaminopropyl) carbodiimide hydrochloride (EDAC) and N-hydroxysuccinimide (NHS) as activating agents the carboxylic acid groups are activated. Octylamine may be grafted onto the carboxylic acid groups of both the glucuronic acid and the pyruvyl group of the outer β-D-mannose (Roy et al., 2014). The chemical structures of EDAC and NHS are shown in Figure 1.5.2 (a) and (b), respectively.

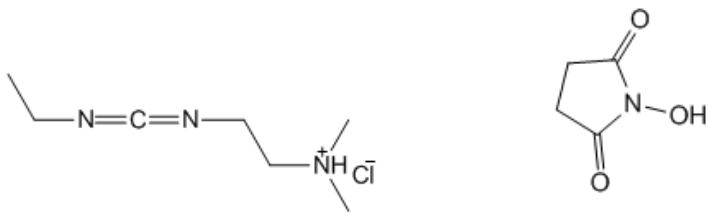

(a) EDAC (b) NHS

Figure 1.5.2: Chemical structure of the activating agents used in grafting of octylamine onto xanthan; (a) *N*-ethyl-*N'*-(3-dimethylaminopropyl) carbodiimide hydrochloride (EDAC) and (b) N-hydroxysuccinimide (NHS).

The octylamine binds to the activated carboxylic acid groups (Roy et al., 2014). The chemical structure of octylamine is shown in Figure 1.5.3.

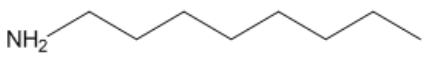

Figure 1.5.3: Chemical structure of octylamine.

The chemical modification of xanthan by grafting of octylamine involves a two step reaction, as shown in Figure 1.5.4.

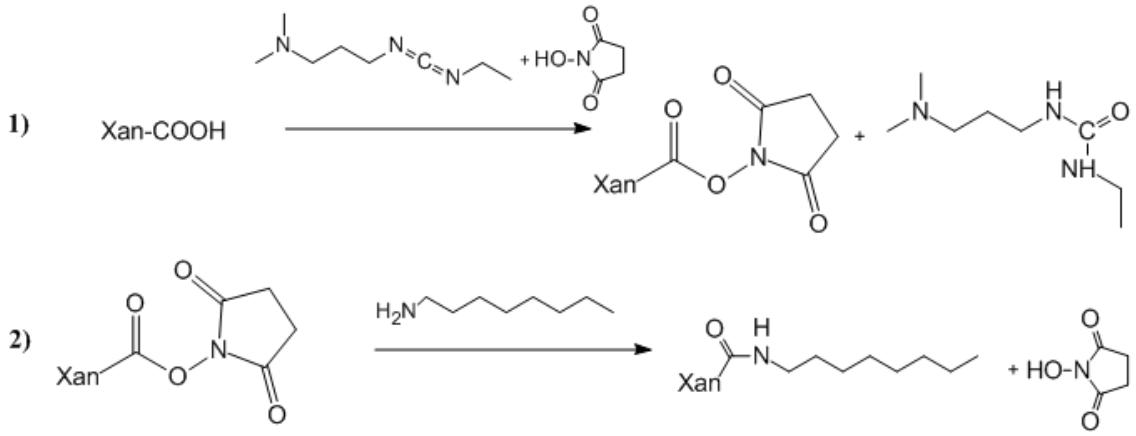

Figure 1.5.4: Modification of xanthan by grafting of octylamine. 1) Addition of activating agents EDAC and NHS. 2) Addition of octylamine.

It is recently found that the reaction is most efficient when the first step (activation of carboxylic acid groups by EDAC and NHS) is performed at pH 4.5, and the second step (grafting of octylamine) at pH 10. At pH 4.5 the nitrogen of the octylamine is protonated, thus no reaction with the carboxylic acid groups will take place. Therefore, the pH must be increased. At pH 10 octylamine has its nucleophilic function intact, which is explained by its pKa value of 10.56 (Roy et al., 2014).

A detailed illustration of the grafting reaction is shown in Figure 1.5.5.

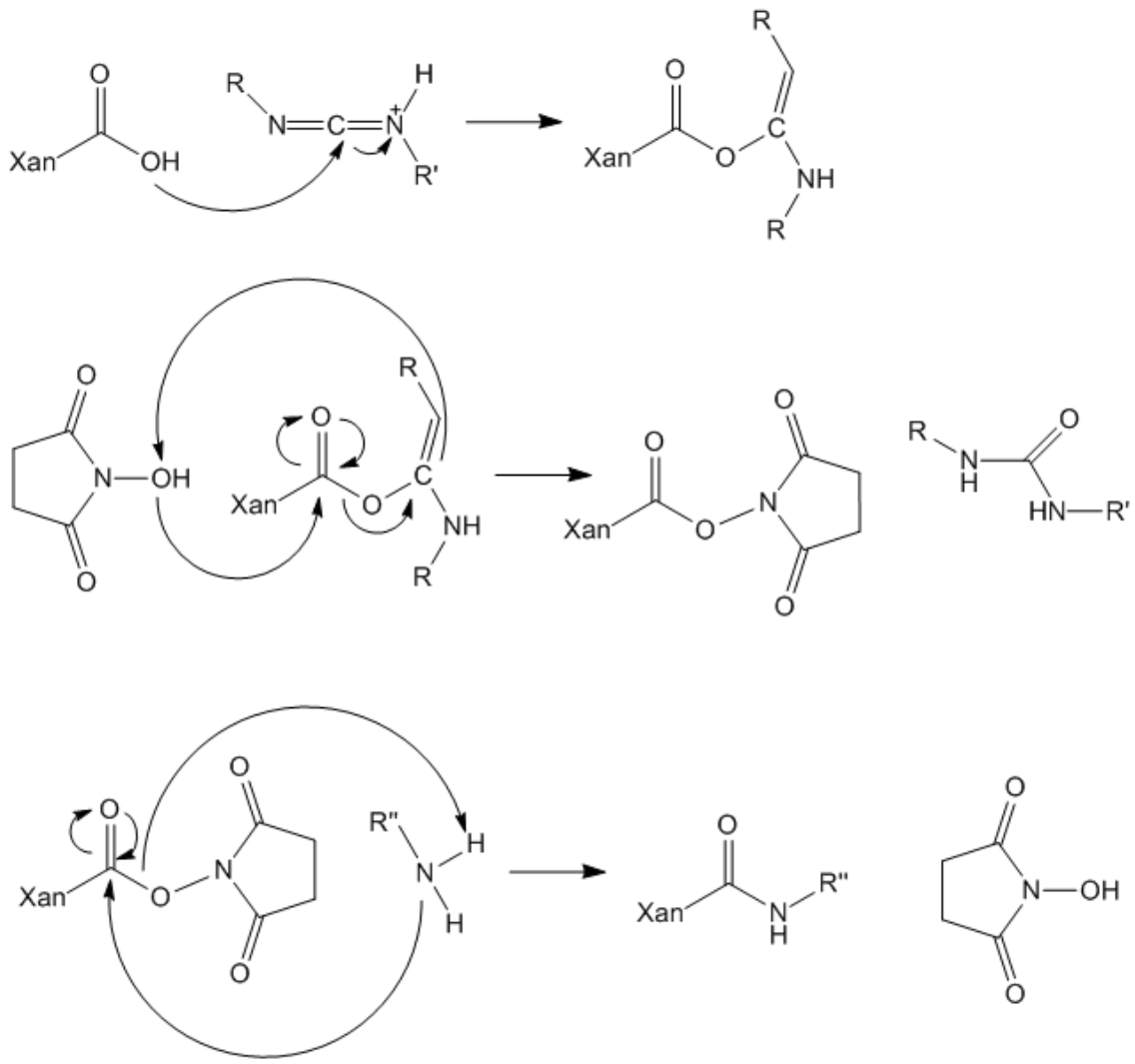

Figure 1.5.5: Detailed reaction mechanism of modification of xanthan by grafting of octylamine (Roy, 2014).

The carboxylic acid groups of xanthan reacts with the EDAC to form a *O*-acylisourea intermediate, which reacts with the NHS, forming an intermediate that reacts with the octylamine by a nucleophilic attack, forming an amide bond.

1.6 Sonication of Xanthan

Sonication with ultrasound is previously proved to have a decreasing effect on the molecular weight and intrinsic viscosity of xanthan, due to depolymerisation caused by high mechanical and chemical effects (Sato et al., 1984). The chemical effects are derived from cavitation, which causes formation of voids at weak points. These cavities will grow, and collapse when it no longer is able to sustain itself with respect to surface tension and static pressure forces. The cavitation phenomenon may cause release of free radicals,

which may react with the sonicated polysaccharide (Cains et al., 1998, Tiwari et al., 2010).

1.7 Viscosity

Viscosity is defined as a measure of the resistance to flow, and is given by equation (1.7.1) (Smidsrød and Moe, 2008).

$$\eta = \frac{F/A}{dv/dz} = \frac{\sigma}{\dot{\gamma}} \tag{1.7.1}$$

Here σ is the shear stress and $\dot{\gamma}$ is the shear rate. For Newtonian fluids this relationship is constant. The shear stress is the ratio between the force, F, that causes flow of the liquid, and the area, A, at which the force works. The shear rate is the velocity gradient, dv/dz, perpendicular to the flow direction.

The specific viscosity of a solution can be calculated by equation (1.7.2).

$$\eta_{sp} = \frac{\eta_s - \eta_0}{\eta_0} = \frac{t_s - t_0}{t_0} \tag{1.7.2}$$

Here η_s is the viscosity of the solution, η_0 is the viscosity of the solvent, and t_s and t_0 is the flow-through time of the solution and the solvent, respectively.

1.7.1 Intrinsic Viscosity

Intrinsic viscosity is defined as the ability of a substance to provide viscosity to a solution, and is given by equation (1.7.3)

$$[\eta] = \lim_{c \to 0} \frac{\eta_{sp}}{c} \tag{1.7.3}$$

Here c is the concentration of the solution.

The intrinsic viscosity is characteristic for a certain polymer in a given solvent at a given temperature, and can be determined by measuring η_r at different polymer concentrations, and plotting η_{sp}/c against the concentrations, c. Then the intrinsic viscosity, $[\eta]$ is found by extrapolation to zero concentration. This is called the Huggins' plot. The Huggin's equation is given in equation (1.7.4) (Huggins, 1942, Smidsrød and Moe, 2008).

$$\eta_{sp} = [\eta] \cdot c + k'[\eta]^2 \cdot c^2 \tag{1.7.4}$$

If the polymer is non-Newtonian it is important that the measurements are done within the Newtonian range or extrapolate to zero shear rate, $\dot{\gamma} = 0$.

When the concentrations and the intrinsic viscosity are very high, a plot of η_{sp}/c against c may become non-linear. Then a semi-logarithmic plot, called Hermann plot, can be used to achieve a linear line. The Hermann equation is given by equation (1.7.5).

$$\log\frac{\eta_{sp}}{c} = \log[\eta] + A\log[\eta] \cdot c \tag{1.7.5}$$

Here A is a constant without any known theoretical value.

Another method for determining the intrinsic viscosity is use of an equation derived by Fuoss and Mead, see equation (1.7.6) (Mead and Fuoss, 1942).

$$\ln\frac{\eta_r}{c} = [\eta] - B[\eta]^2 c \tag{1.7.6}$$

By combining the Huggins and Fuoss-Mead equations, Billmeyer derived an equation for calculation of the intrinsic viscosity, see equation (1.7.7) (Billmeyer, 1949, Shirai et al., 2006).

$$[\eta] = \frac{2(\eta_{sp} - \ln\eta_r)^{1/2}}{c} \tag{1.7.7}$$

By plotting $\frac{2(\eta_{sp}-\ln\eta_r)^{1/2}}{c}$ againt c, the intrinsic viscosity can be found as the intersect at the y-axis.

The molecular weight of a polymer is dependent on the intrinsic viscosity. The relationship is given by the Mark-Houwink-Sakurada (MHS) relationship, shown in equation (1.7.8)

$$[\eta] = K \cdot M^a \tag{1.7.8}$$

Here K and a are MHS parameters depending on the polymer, and M is the molecular weight. The exponent a depends of the type of the polymer, and can be summarised by Haug's triangle, see Figure 1.7.1 (Smidsrød and Moe, 2008).

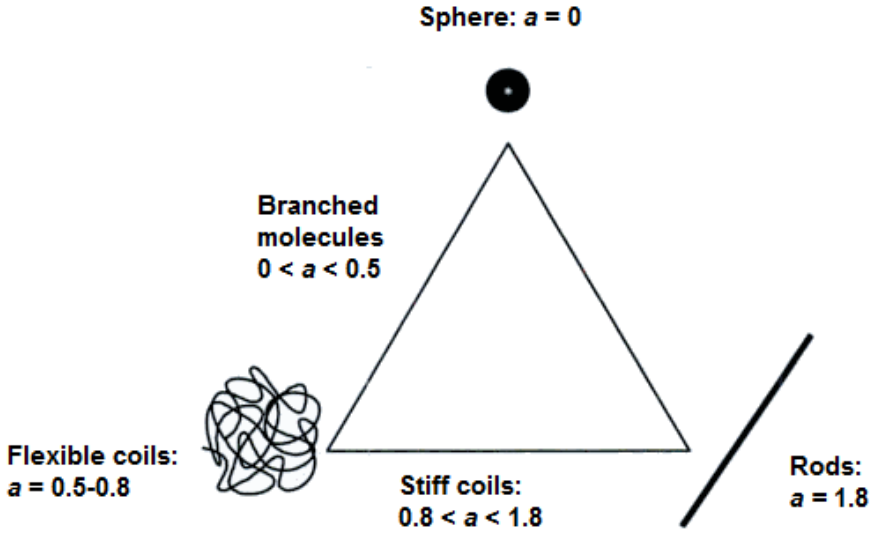

Figure 1.7.1: Haug's triangle, the exponent a in the Mark-Houwink-Sakurada equation for the three idealised conformations of polymers (Smidsrød and Moe, 2008).

1.8 SEC-MALLS

SEC-MALLS is a combination of size exclusion chromatography (SEC) and multi-angle laser light scattering (MALLS), and may be applied for determination of for example molecular weight and size of molecules.

1.8.1 Size Exclusion Chromatography (SEC)

Size exclusion chromatography is driven by entropy (Podzimek, 2011), and is used as an analytical method to determine molecular weight and molecular weight distribution of a sample. The stationary phase of the column consists of gel particles or macro porous polymer particles. The solvent, which flows between the particles, is the mobile phase (Smidsrød and Moe, 2008). Ideally, there are no interactions between the stationary phase and the solution that is analysed, thus the compounds are separated according to their size in the solution. An illustration of separation of the molecules in a SEC column is shown in Figure 1.8.1.

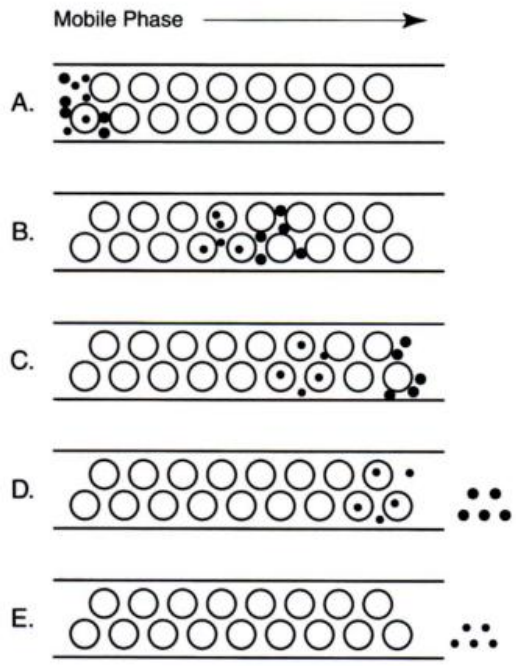

Figure 1.8.1: Overview over the principles of size exclusion chromatography. A. Start of separation; B. Smaller molecules diffuse into particles, larger molecules elute in the interstitial regions of the column; C. Separation is completed; D. Large molecules elute first; E. Small molecules elute last (Mori and Barth, 1999).

The sample to be analysed is dissolved in a small amount of solvent and placed at the top of the columns. When analysing a solution, the molecules permeate into the pores. The smaller molecules permeate deeper into pores, and may also permeate into small pores, while the larger molecules are excluded from the pores with effective size smaller than the molecules. As a result of this, large molecules will elute from the column first, followed by molecules with decreasing size. This principle is known as *steric exclusion* (Podzimek, 2011).

Several methods, such as UV-absorption, refractive index measurements, and chemical methods, may be used to determine the concentration of the sample leaving the column.

The relationship between concentrations in the stationary and the mobile phase at equilibrium can be described by the partition coefficient, k, which depends on the ratio between the radius of gyration and the average diameter of the pores. The retention volume, V_R, which is the volume necessary for bringing a certain molecule through the column is defined by equation (1.8.1) (Smidsrød and Moe, 2008).

$$V_R = V_m + k \cdot V_s \tag{1.8.1}$$

Here V_m and V_s are the volumes of the mobile and the stationary phase, respectively.

The minimum retention volume is $V_R = V_m$, the *void volume*, is obtained when the molecules are much larger than the pores. The maximum retention volume is reached when molecules are so small that they can enter the pores without restrictions.

Detectors

Detectors are used for monitoring of the molecules in the solute eluting from the SEC system. The change of the mobile-phase composition is monitored and converted into an electrical signal, which is processed by a computer software. The most important detectors are refractive index (RI) detector, ultraviolet (UV) detector, light scattering photometer, viscometer, infrared (IR) photometer, and the evaporative light scattering detector (ELSD) (Podzimek, 2011).

The RI and UV have signals proportional to the concentration of the eluated sample. The light scattering detector has a signal that is proportional to the product of molar mass and concentration. The signal of the viscometer is proportional to the product of concentration and molar mass to the power of the Mark-Houwink exponent (Podzimek, 2011).

1.8.2 Light Scattering

Light scattering is one of few methods for determination of molecular weights of polymers. By light scattering, also information about the macromolecular size and the interactions between macromolecules, and macromolecules and solvent, may be obtained. Light scattering can be applied over a broad range of molar masses, and is a result of interaction between light and polymer, where the light consists of electric and magnetic parts, thus making a oscillating field that interacts with the molecule. The molecule creates dipoles and oscillates, thus releases radiation. The ability of a molecule to scatter light, the polarizability, is dependent on that the electron cloud of the molecule is displaced from its normal shape by an external electrical field. The polarizability is proportional to the specific refractive index increment, dn/dc (Podzimek, 2011).

Large perfect crystals do not scatter light. This is explained by the fact that in any direction of observation there can be found two identical volume elements with a distance such that the light beams scattered from these two elements reach the detector phase shifted by $\lambda/2$ (a half wavelength). In a perfect crystal identical volume elements have identical number of molecules, and the intensities of the scattered light are identical. Two light beams with identical intensities, shifted by $\lambda/2$ will cancel each other due to interference. Light scattering caused by pure liquids will be more intensive than for

crystals, this is caused by the fact that the number of molecules in a volume element of a liquid varies with time, because of microscopic density fluctuations. For a liquid polymer solution both the intensity of the light scattered by the polymer itself, and the light scattered by the solvent will contribute to the intensity of the scattered light of the solution.

There are three types of light scattering; *Static light scattering*, *Dynamic light scattering*, and *Raman scattering*. In static light scattering, also called Rayleigh or classical light scattering, the light intensity is determined at a given scattering angle by averaging the fluctuating intensity over a long time. From this type of light scattering the molar mass, molecular size expressed as RMS (root mean square) radius and the second viral coefficient, A_2, can be obtained. In dynamic light scattering the fluctuations of the scattered light intensity, due to Brownian motion of the scattering molecules, are studied instead of the average intensity. From the dynamic light scattering information about the diffusion coefficient and hydrodynamic radius of the scattering molecules can be achieved. Raman scattering gives information about the structure of the scattering molecules. (Podzimek, 2011)

Multi-Angle Laser Light Scattering (MALLS)

For multi-angle laser light scattering (MALLS), static light scattering is applied. An illustration of a multidetector light scattering photometer is shown in Figure 1.8.2.

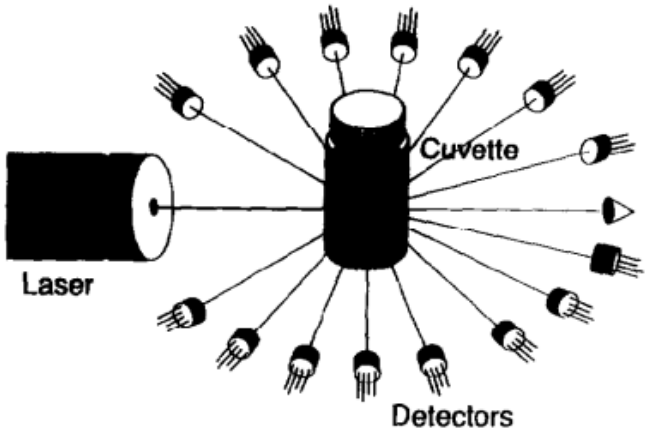

Figure 1.8.2: Schematic overview of a multidetector light scattering photometer (Wyatt, 1993).

The relationship between the scattered light intensity and the properties of the analysed

polymer solution is described by equation (1.8.2) (Podzimek, 2011, Zimm, 1948).

$$\frac{R_\theta}{K^* c} = MP(\theta) - 2A_2 cM^2 P^2(\theta) + ... \tag{1.8.2}$$

Here R_θ is the excess Rayleigh ratio, c is the polymer concentration, M is the molar mass, A_2 is the second viral coefficient, K^* is the optical constant, and $P(\theta)$ is the particle scattering function.

By using a software, like ASTRA, equation (1.8.2) can be used for determination of molecular weight and size parameters for each "eluant slice" directly following chromatographic separations when the concentration c is fixed (Wyatt, 1993).

1.9 ^{1}H Nuclear Magnetic Resonance Spectroscopy

The basis of nuclear magnetic resonance (NMR) spectroscopy is the magnetic properties of the atomic nuclei, and the absorption of energy when the nucleus is excited from its spin state with the lowest energy to the next higher energy state. The spin quantum number of a proton is $I = \frac{1}{2}$, thus the magnetic quantum numbers for a proton are $m_I = +\frac{1}{2}$ and $m_I = -\frac{1}{2}$. Electromagnetic radiation can only be absorbed when the two spin states have different energies, which may be achieved by applying a magnetic field to the sample (Carey, 2008). The alignments of protons in a magnetic field are illustrated in Figure 1.9.1.

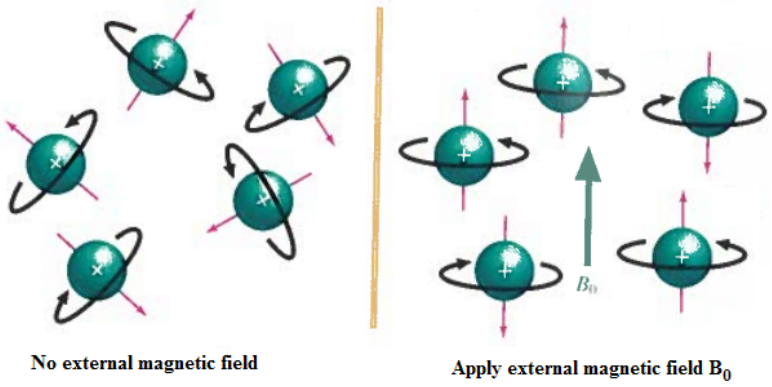

Figure 1.9.1: Illustration of alignment of nucleus magnetic moment when a magnetic field B_0 is applied (Carey, 2008).

A spinning proton can be compared to a small magnet, and has a magnetic momentum. When a magnetic field B_0 is applied, the spin state of a proton that is aligned with the field has lower energy than the spin state of a proton that is aligned opposite to the field.

The energy difference between the upper and lower spin state, ΔE is proportional to the magnetic field B_0, as shown in Figure 1.9.2.

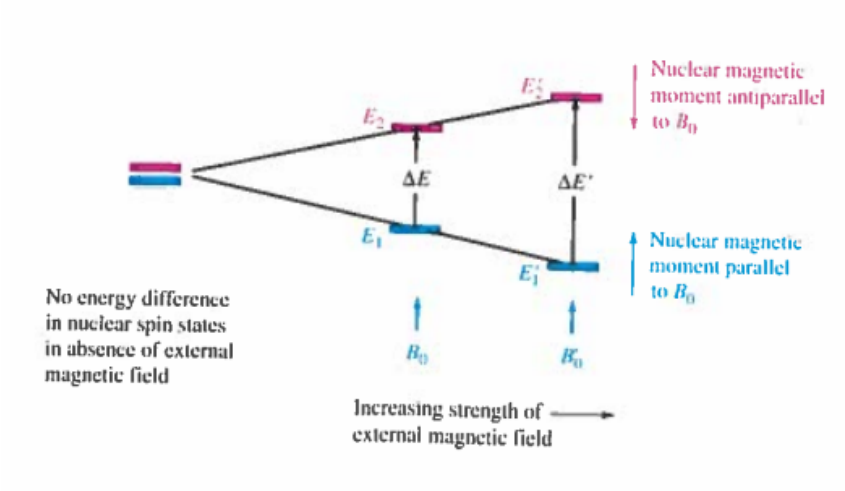

Figure 1.9.2: Illustration of energy difference, ΔE, as the magnetic field, B_0, increases (Carey, 2008).

The distribution of nuclei with different spin states is given by Boltzmann's equation (1.9.1).

$$\frac{N_\beta}{N_\alpha} = e^{\frac{-\Delta E}{kt}} = e^{\frac{-\gamma h B_0}{2\pi k T}} \approx 1 - \frac{\gamma h B_0}{2\pi k T} \tag{1.9.1}$$

The energy difference is given by Planck's equation, see equation (1.9.2) (Günther, 2013).

$$\Delta E = hv \tag{1.9.2}$$

Here h is Planck's constant and v is the frequency of the radiation.

In molecules, protones are bound to other atoms and will therefore be shielded, thus the magnetic field felt by a proton will be less than the actual applied field. Hence, different protons give signals at different field strengths. This phenomenon gives a chemical shift, which is provides information of the structure of the analysed sample.

1.9.1 Applications of ^{1}H-NMR in Biopolymers

Nuclear magnetic resonance spectroscopy allows analysis of biopolymers in solution, in contrast to methods like X-ray and neutron diffraction. This is an advantage, since parameters such as solvent, pH, ionic strength, and temperature, may be studied when the biopolymer is in solution (Finley et al., 1990).

1.9.2 ^{1}H-NMR Spectra of Xanthan

Xanthan has previously been characterised by ^{1}H-NMR. The peaks of the pyruvyl and acetyl groups can be found at 1.4 and 2.09 ppm, respectively. The peak of hydrogen on carbon 1 of the inner α-D-mannose, which is less shielded (i.e. more deshielded) is found at approximately 5.2 ppm (Rinaudo et al., 1983). A ^{1}H-NMR spectrum for xanthan is shown in Figure 1.9.3.

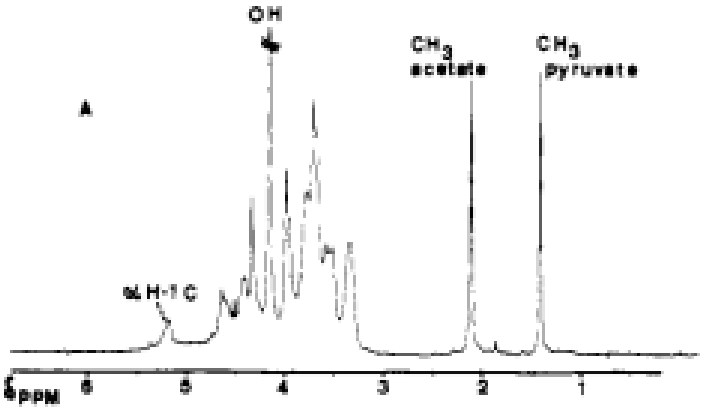

Figure 1.9.3: ^{1}H-NMR spectrum of xanthan (Rinaudo et al., 1983).

1.9.3 Determination of Grafting Density

The grafting density, $\%octyl$, can be calculated by equation (1.9.3).

$$\%octyl = \frac{n_{octyl}}{n'_{RU}} \tag{1.9.3}$$

Here n_{octyl} and n'_{RU} is the number of moles octylamine and repeating units of xanthan, respectively.

When octylamine is grafted onto xanthan, one molecule of H_2O is lost for each molecule of octylamine attached. Hence, equation (1.9.4) is obtained, for calculation of the molecular weight of repeating unit after modification.

$$M'_{RU} = M_{RU} + \%octyl \cdot M_{octyl} - \%octyl \cdot M_{H_2O} \tag{1.9.4}$$

Here M_{RU}, M_{octyl} and M_{H_2O} are the molecular weights of repeating unit before modification, octylamine and water, respectively.

Since equation (1.9.3) and (1.9.4) is dependent on each other, iterative calculations is must be performed in order to determine $\%octyl$ and M'_{RU}.

1.10 Scope of this Master Thesis

The aim of this master thesis is to depolymerise xanthan samples using sonication in order to achieve molecular sizes suitable for analysis methods as SEC-MALLS, ^{1}H-NMR, and intrinsic viscosity measurements, and study the effect of the sonication on molecular weight, intrinsic viscosity, and conformation of the xanthan molecules.

Octylamine is to be grafted onto xanthan molecules in order to obtain hydrophobically modified xanthan, by using a method adopted from the University of Le Havre, France. The effect of the modification will be studied by comparing molecular weight, intrinsic viscosity, and conformation, of the non-modified and modified xanthan samples. Also, a goal is to remove the acetyl and pyruvyl groups from xanthan and from this determine whether the octylamine binds to the carboxylic acid group of the pyruvyl.

Chapter 2

Materials and Methods

2.1 Xanthan Samples

Two different xanthans were studied in this project:

- Kelzan XCD (CP Kelco)
- Xanthan from Statoil

The Kelzan XCD was a commercial xanthan in powder form, provided from the NTNU biopolymer laboratory. The xanthan provided from Statoil was originally obtained in 1989, precipitated from a fermentation broth in the NTNU biopolymer laboratory. This xanthan has never been exposed to any disordering circumstances, and is assumed to be pure.

2.2 Flow Chart

An overview of the experimental work performed in this project is presented as a flow chart in Figure 2.2.1. In addition there was performed a test sonication and test modifications, which are not included in the flow chart. The different experiments and procedures are explained throughout the chapter.

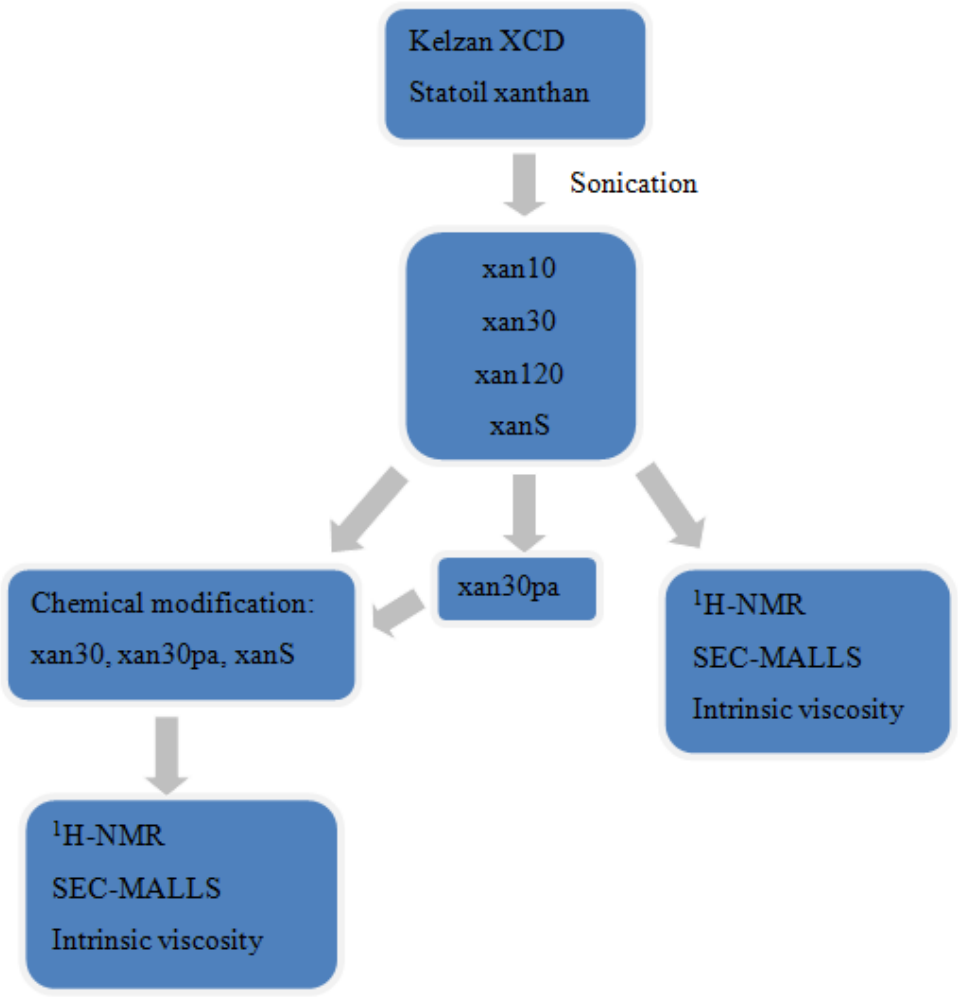

Figure 2.2.1: Flow chart of experimental work.

2.3 Preparation of Xanthan Solutions

2.3.1 Materials

- Magnetic stirrer
- Ultraturrax (VWR VDI 12)
- Blender
- NaCl (Merck KGaA)
- Isopropanol

2.3.2 Kelzan Test Sample for Sonication

There was prepared a solution from the Kelzan XCD with concentration 10 mg/mL for test of the sonication and viscosity measurements. The xanthan powder was dissolved by mixing with ultrapure (MQ) water by ultraturrax. Table 2.3.1 shows the applied amounts of Kelzan XCD and MQ water.

Table 2.3.1: Overview of weighed out amounts of Kelzan XCD and MQ water for stock solution, $m_{xanthan}$ and m_{MQ}, respectively, for test sample used for sonication.

Start xanthan	$\boldsymbol{m_{xanthan}}$ [g]	$\boldsymbol{m_{MQ}}$ [g]
Kelzan XCD	0.9998	99.25

This stock solution was diluted to a concentration of 1 mg/mL with MQ water and NaCl. The concentration of NaCl in the diluted solution was 0.01 M.

It was assumed that 1 g of the diluted solution equals 1 mL. An overview of all the amounts, dilutions, and concentrations can be found in Table A.1.1 in Appendix A.

2.3.3 Pure Xanthan Samples for Sonication and Modification

From the Kelzan XCD there was prepared a stock solution of 10 mg/mL, and from the Statoil xanthan a solution of 5 mg/mL, by dissolving xanthan (solid) in MQ water. The Kelzan XCD was dissolved by adding a few drops of isopropanol to the powder and letting it moisten for 10 minutes, then mixing with MQ water by a blender until a homogeneous solution was achieved. The Statoil xanthan was also moistened with isopropanol, but this solution was mixed with ultraturrax, due to a smaller volume which was inconvenient for dissolving with the blender. The stock solutions was diluted to 1 mg/mL with a solution of MQ water and NaCl. The concentration of NaCl in the diluted solutions was 0.1 M.

The exact amounts of xanthan, $m_{xanthan}$, MQ water, m_{MQ}, weighed out are presented in Table 2.3.2.

Table 2.3.2: Overview of weighed out amounts of xanthan and MQ water for stock solutions, $m_{xanthan}$ and m_{MQ}, respectively.

Start xanthan	$\boldsymbol{m_{xanthan}}$ [g]	$\boldsymbol{m_{MQ}}$ [g]
Kelzan XCD	4.9974	499.97
Statoil xanthan	0.2029	40.0016

It is assumed that 1 g of the diluted solutions equals 1 mL. An overview of all the amounts, dilutions, and concentrations can be found in Tables A.2.1 and A.2.2 for the Kelzan samples and the Statoil sample, respectively, in Appendix A.

2.3.4 Test Samples for Modification

From Kelzan XCD there was prepared solutions of 5 mg/mL for test modifications. The xanthan powder was dissolved by adding a few drops of isopropanol, then mixing by ultraturrax until a homogeneous solution was obtained. The solutions were not sonicated, purified, or added any salt. There was prepared two solutions for test modification; these samples were named with the prefix test1 and test2.

2.3.5 Determination of Water Content

The water content of the Kelzan XCD was determined by drying a known amount of powder in a heat cabinet at 60 °C overnight. The sample was weighed before and after drying. The xanthan provided from Statoil was assumed to have the same water content as the Kelzan XCD. For exact amounts and calculations, see Appendix A.3.

2.4 Sonication and Purification of Xanthan Samples

2.4.1 Materials

- Sonicator (Labsonic 1510 Ultrasound generator)
- Beaker for sonication, 200 mL
- Micropipette, 1-5 mL
- Thermometer
- Centrifuge (Sorvall instruments RC5C)
- Rotary evaporator (Büchi Rotavapor - R)

- Filter, 1.2 µm and 0.45 µm (Millipore)
- Dialysis tubes (Spectra/Por molecularporous membrane tubing, MWCO 12-14 kDa)
- pH meter
- Acetone (VWR Prolabo Chemicals)
- EDTA (Merck KGaA)
- $NaNO_3$ (Merck KGaA)
- Hydrochloric acid (Merck KGaA)
- Sodium hydroxide (Merck KGaA)

2.4.2 Sonication of Kelzan Test Sample

For the test sample prepared from Kelzan, 200 mL was sonicated at 200 W for 10 minutes. The temperature in the xanthan solutions during sonication was held below 40 °C by keeping the beaker with the solution in an ice bath. After sonication the solution was centrifuged at 10 000 rpm for 1 hour and filtrated with a 1.2 µm filter, before measuring the intrinsic viscosity, see section 2.11.

2.4.3 Sonication and Purification of Xanthan Samples

From the xanthan solution prepared from Kelzan, there was taken out 3 samples of 200 mL. These were sonicated at three different sonication times; 10, 30, and 120 minutes, respectively, to obtain the samples *xan10*, *xan30*, xan *xan120*. The sample prepared from the Statoil xanthan was sonicated for 60 minutes, and named *xanS*. An overview of the samples and their sonication times is given in Table 2.4.1. Before sonication each solution were added 2 mL acetone, which gave an acetone concentration of 1 v%. The temperature during sonication in these xanthan solutions was also held below 40 °C by keeping the beaker with the solution in an ice bath. The samples were sonicated only 10 minutes at a time, with 10-15 minutes break between each "sonication round", in order to prevent overheating of the xanthan.

Table 2.4.1: Overview over sonicated xanthan samples and their respective sonication times.

Sample	**Sonication time [min]**
xan10	10
xan30	30
xan120	120
xanS	60

After sonication the xanthan solutions were centrifuged at 10 000 rpm for 60 minutes, then filtrated with a 0.45 µm filter.

After filtration, the xanthan solutions were dialysed against a solution of 0.15 M $NaNO_3$ and 0.01 M EDTA at pH 7. The sonicator probe releases titanium ions, which will bind to the EDTA. This dialysis was performed two times for 3-4 hours at room temperature, then one time overnight at 4 °C, with continuously stirring. The solutions were further dialysed towards 20 mM $NaNO_3$, two times for 3-4 hours at room temperature, and one time overnight at 4 °C, then upconcentrated to approximately 5 mg/mL by damping in at 40 °C with a rotary evaporator. Then the solutions were dialysed against MQ-water two times for 3-4 hours at room temperature and one time overnight at 4 °C. The concentration of the solutions after dialysis towards MQ-water were determined by phenol-sulfuric acid analysis (see section 2.5), before they were freeze dried.

After dialysis towards MQ-water, the solutions were analysed by SEC-MALLS, and the intrinsic viscosities were measured. A description of SEC-MALLS and intrinsic viscosity measurements is given in section 2.10 and 2.11, respectively.

2.5 Phenol-Sulfuric Acid Analysis

2.5.1 Materials

- Spectrophotometer (Shimadzu Double Beam Spectrophotometer UB-150-01)
- Micropipettes, 20-200 µL and 1-5 mL
- Test tubes
- Cuvettes
- Sulfuric acid, concentrated
- Phenol, 3 %

2.5.2 Procedure

The phenol sulfuric acid analysis was performed for the four sonicated, non-modified, samples xan10, xan30, xan120, and xanS, in order to determine the concentration of the solutions before SEC-MALLS and intrinsic viscosity measurements.

A stock solution of 0.1 mg/mL was prepared from the commercial xanthan Kelzan XCD. The xanthan was moistened with isopropanol for 10 minutes, then dissolved in MQ-water and homogenised with an ultraturrax. From the stock solution it was pipetted out different amounts to test tubes. MQ-water was added to give a total volume of 2 mL in each tube. An overview is given in Appendix B. Then 0.5 mL 3 % phenol and 5 mL concentrated sulfuric acid (H_2SO_4) was added to the tubes. The reaction was left for 30 minutes, then the test tubes were cooled in water, and the absorbance was

measured by a spectrophotometer, at 485 nm. From the absorbance values determined from measurements of the samples with known concentrations a standard curve was obtained. By analysing the xanthan solutions xan10, xan30, xan120, and xanS, with unknown concentrations and plotting the results in the standard curve, the concentrations were determined.

2.6 Chemical Modification of Xanthan

Three sets of the chemical modification of xanthan were performed. The first two with non-sonicated and non-purified xanthan (Kelzan XCD), named with prefix test1 and test2 for the two sets, respectively, then with the sonicated and purified samples xan30 and xanS, and an acetyl and pyruvyl free sample, xan30pa. The modification method was adopted from an article by a group at the University of Le Havre, France (Roy et al., 2014). However, some justifications were done, such as performing the grafting reaction at both 4 °C and room temperature, and preparation and modification of an acetyl and pyruvyl free xanthan.

2.6.1 Materials

- pH meter
- Micropipettes, 20-200 µL and 2-10 mL
- Rotary evaporator (Büchi Rotavapor - R)
- Dialysis tubes (Spectra/Por molecularporous membrame tubing, MWCO 12-14 kDa)
- Octylamine, 99 % (Sigma Aldrich)
- N-(3-Dimethylaminopropyl)-N'-ethyl-carbodiimide, $\geq$ 99 % (Fluka Analytical)
- N-Hydroxysuccinimide, 98 % (Sigma Aldrich)
- Hydrochloric acid, concentrated (Merck KGaA)
- NaCl (Merck KGaA)
- Sodium hydroxide, 1 M
- Hydrochloric acid, 1 M

2.6.2 Modification of Non-Sonicated Kelzan XCD

The chemical modification of non-sonicated xanthan was performed for Kelzan XCD as a test of the modification method, and to determine whether the temperature has influence on the grafting reaction or not. There was performed two test-modifications in order to

determine the reproducibility of the modification method. The chemical modification of xanthan consisted of two steps. In the first step a xanthan solution with concentration 5 mg/mL was dialysed towards MQ water with pH 3 for 24 hours. The pH was adjusted by adding 1 M HCl. After dialysis the temperature was decreased to 4 °C, and the solution was diluted to 1 mg/mL and stirred until complete homogenization, before addition of EDAC (*N*-ethyl-*N'*-(3-dimethylaminopropyl) carbodiimide hydrochloride) and NHS (N-hydroxysuccinimide). The amounts of EDAC, NHS and octylamine added were equal to 3 equivalents of the carboxylic acid groups of the xanthan. The exact amounts of xanthan solutions, NHS, EDAC and octylamine can be found in Table C.1.1 in Appendix C. The pH was adjusted to 4.5 with 1 M HCl, and the solution was stirred for 24 hours at 4 °C.

In the second step of the modification reaction aqueous solution of octylamine was added, and the pH was adjusted to 10 with 1 M NaOH. For the samples test1 and test2, the solution was split in two; one part was stirred at 4 °C and the other at room temperature. Both solutions were left overnight, obtaining the samples test1mod1, test1mod2, test2mod1, and test2mod2. The suffix mod1 and mod2 indicates that the grafting reaction (second step) was performed at 4 °C and room temperature, respectively.

To purify the modified xanthan solution, there was performed dialysis against HCl, pH 3, for 24 hours, then towards 0.1 M NaCl for 24 hours. The solutions were upconcentrated at a rotavapor to approximately 5 mg/mL and dialysed towards MQ-water for 6-8 days, until approximately zero conductivity. The purification was performed at approximately 4 °C, and the dialysate was changed two times a day. After purification the samples were freeze dried.

2.6.3 Modification of Purified Sonicated Xanthan

The purified sonicated xanthan samples that were modified were xan30, xan30pa and xanS. xan30pa was an acetyl and pyruvyl free sample prepared from xan30. The procedure for removal of acetyl and pyruvyl is described in the following section.

The modification of the sonicated xanthan samples was performed exactly as for the non-sonicated samples, described in the previous section, except the solutions were not split in two after addition of octylamine. The second step, addition of octylamine, was performed only at 4 °C. The amounts of NHS, EDAC and octylamine was equal to 3 equivalents of the carboxylic acid groups of the xanthan. An overview of the amount xanthan and added amounts of EDAC, NHS and octylamine is shown in Table C.1.1 in Appendix C.

2.7 Removal of Acetyl and Pyruvyl Groups

2.7.1 Materials

- pH meter
- Heat cabinet
- Hydrochloric acid, 5 M
- Sodium hydroxide, 5 M

2.7.2 Procedure

From the sample xan30 an acetyl and pyruvyl free xanthan sample, xan30pa, was prepared. The method for removal of acetyl and pyruvyl groups was based on an article by Christensen et al. (1996). A freeze dried sample was dissolved in MQ-water, to a concentration of 5 mg/mL. HCl was added to obtain a concentration of 0.1 M, and the solution was placed in a heat cabinet at 80 °C for 3 hours. Then the solution was cooled to room temperature, NaOH was added to a concentration of 0.025 M, the solution was bubbled with N_2, and left for 3 hours in room temperature. The pH was adjusted to 6, and the solution was dialysed towards MQ-water for 24 hours, then freeze dried.

2.8 Depolymerisation by H_2O_2 and NaOH for ^{1}H-NMR

2.8.1 Materials

- Heat cabinet
- Hydrogen peroxide, 10 % (Ås produksjonslab AS)
- Sodium hydroxide, 1 M

2.8.2 Procedure

Xanthan samples were dissolved in 1.5 mL MQ water, to a concentration of 6 mg/mL, and 7.4 µL of 1 M NaOH and 25 µL of H_2O_2 were added, before the samples were left for 1 hour at 80 °C. Then the samples were cooled in an ice bath for 30 minutes, and freeze dried.

2.8.3 Depolymerisation of xan-3-94-2 and xan-3-94-14, Kelzan XCD, and xanS

Two samples xan-3-94-2 and xan-3-94-14, kindly provided by Professor Bjørn E. Christensen. The samples were originally prepared in conjunction with experimental work that resulted in an article on depolymerisation of double-stranded xanthan (Christensen et al., 1993). The samples had known contents of α-D-mannose, thus by calculating the α-D-mannose content by using TSP as an external reference (see section 2.9), and comparing with the given values, it was possible to determine whether the α-man H-1 peak in the ^{1}H-NMR spectra could be used for calculations of the degree of substitutions of acetyl and pyruvyl groups, and of the grafting densities of the modified xanthan samples.

In addition, there was performed a depolymerisation series both for non-sonicated, non-purified Kelzan XCD, and for the xanS which was sonicated for 60 minutes. The samples were analysed by SEC-MALLS, in order to determine their molecular weights, and hence obtain information about the behaviour of the xanthan molecules during the depolymerisation reaction for NMR preparation. An overview of the not sonicated xanthan and the xanS samples, and their respective reaction times is given in Table F.2.2 in Appendix F.

2.9 ^{1}H-NMR

2.9.1 Materials

- Bruker Avance DPX 300MHz
- Bruker Avance DPX 400MHz
- NMR tubes
- D_2O
- TSP, 1 %

2.9.2 Procedure

Depolymerised freeze dried xanthan samples were dissolved in D_2O and added 5 µL of a 1% TSP (2,2,3,3-d(4)-3(trimethylsilyl)propionic acid) solution. The ^{1}H-NMR was run at 80 °C and 300 MHz for the test-modifications, and at 400 MHz for the non-modified and modified purified sonicated samples. The amounts of each xanthan sample used for ^{1}H-NMR analysis are given in Appendix H in Table H.1.1 and H.1.3 for the test modifications and the modification of the pure sonicated samples, respectively. All NMR measurements were performed by Wenche I. Strand at the biopolymer laboratory at the Department of

Biotechnology.

2.10 SEC-MALLS

2.10.1 Materials

- Small glass tubes (Supelco Clear Vials, Screw Top, 4 mL)
- Filter, 0.8 µm (Millipore)
- SEC-MALLS buffer, 0.15 M $NaNO_3$ + 0.01 M EDTA
- SEC-MALLS buffer, 0.15 M $NaNO_3$ + 0.01 M EDTA + 20 % acetonitrile

An overview of the equipment used when running SEC-MALLS analyses is presented in Table 2.10.1

Table 2.10.1: Overview over SEC-MALLS equipment.

Part	**Producer**	**Specification**
Degasser	Biotech	Degasi Classic
Pump	Shimadzu	LC-10AD
Autoinjector	Shimadzu	SCL-10A VP
LS-detector	WTC*	Dawn Heleos II
RI-detector	WTC*	Optilab T-rEx
Columns	Toso Haas	TSK G-6000/5000/4000/3000 PWXL**
Viscositydetector	WTC*	Viscostar II

* WTC=Wyatt Technology Corporation
** TSK G-4000-3000PWXL used before April 4th, TSK G-6000-5000PWXL used after April 4th

SEC-MALLS columns optimal for the low molecular weight xanthan samples analysed in this project were TSK G-4000-3000PWXL, but due to parallel experiments in the laboratory, SEC-MALLS columns TSK G-6000-5000PWXL were used after April 4th. The SEC-MALLS columns were serially connected.

2.10.2 Procedure

Samples for SEC-MALLS analyses was performed by preparing a xanthan solution of 0.3 - 0.5 mg/mL. The buffer used was a solution of 0.15 M $NaNO_3$ and 0.01 M EDTA. For the modified xanthan samples a buffer of 0.15 M $NaNO_3$, 0.01 M EDTA, and 20 % acetonitrile was also used. The samples were filtrated with a 0.8 µm filter into 4 mL glass

tubes. All of the SEC-MALLS analyses were performed by Ann-Sissel T. Ulset at the biopolymer laboratory at the Department of Biotechnology. In Tables F.1.1 to F.2.2 in Appendix F overviews of the samples analysed by SEC-MALLS are given.

ASTRA Processing

The flow rate was 0.5 mL/min. Columns and detector temperature was room temperature, except for the RI detector temperature, which was 40 °C. The specific refractive index increment, dn/dc, was 0.150, the second viral coefficient, A_2, was set to $1 \cdot 10^{-3}$ mL mol/g^2, and the angular fitting was 2nd order Zimm. Pullulan 16.2 was used for normalisation. The wave length of the light scattering instrument was 658 nm. All SEC-MALLS data were processed with assistance from Ann-Sissel T. Ulset and Professor Bjørn E. Christensen.

2.11 Intrinsic Viscosity Measurements

2.11.1 Materials

- Single capillary viscometer
- Cannon four-bulb shear dilution viscometer
- Schott Gerate AVS 310
- Radiometer Copenhagen ABU91 Autoburette
- Filter, 5 µm (Millipore)

The shear rate at the wall of the single capillary viscometer was calculated during a specialisation project in the fall of 2013 to be 2500 s^{-1} (Driveklepp, 2013).

The shear rate constants for the four-bulb shear dilution viscometer are given in Table 2.11.1.

Table 2.11.1: Shear rate constant for Cannon four-bulb shear dilution viscometer.

Bulb no.	Shear rate constant
1	170944
2	95949
3	60657
4	34188

2.11.2 Procedure

Intrinsic viscosity was determined with single capillary viscometer for the Kelzan test sample for sonication, the purified sonicated non-modified samples xan10, xan30, xan120, and xanS, the acetyl and pyruvyl free sample xan30pa, and the modified samples of xan30, xanS, and xan30pa. In addition, the intrinsic viscosity of non-modified and modified xan30 at different shear rates was determined by four-buld shear dilution viscometer.

For viscosity measurements there was prepared solutions with concentration approximately 1 mg/mL. The solvent used for all viscosity measurements was 0.1 M NaCl, and the measurement temperature was 20.0 °C. Before transferring to the ubbelohde, the solutions were filtrated with a 5 µm filter, in order to exclude particles that may have got into the solutions.

For viscosity measurements by the single capillary viscometer a Schott Gerate AVS 310 was used to measure the flow-through time, and a Radiometer Copenhagen ABU91 Autoburette was used for automatic dilution of the xanthan solutions during measurements. The softwares IntrinsicControl and IntrinsicRun were used for controlling the dilution volumes and recording the flow-through times for automatic viscosity measurements with single capillary viscometer.

For the four-bulb shear dilution viscometer the flow-through time for each bulb was measured manually by a stopwatch.

Chapter 3

Results and Discussion

This chapter is presented in three parts; Preparation of Sonicated Xanthan Samples, Characterisation of Modified Xanthan Samples, and Comparison of Non-modified and Modified Xanthan Samples. For a further, general discussion of the results, please see Chapter 4.

3.1 Preparation of Sonicated Xanthan Samples

Sonication was performed in order to depolymerise the xanthan chains into smaller molecules and obtain lower molecular weights, suitable for SEC-MALLS, intrinsic viscosity measurements, and ^{1}H-NMR analyses.

3.1.1 Intrinsic Viscosity of Non-Purified Sonicated Kelzan Test Sample

The intrinsic viscosity of the sonicated non-purified Kelzan test sample was determined by measurements with single capillary viscometer. The shear rate at the wall was 2500 s^{-1}. The viscosity measurements were performed at 20.0 °C. The results are presented in Figure 3.1.1. Raw data, calculations, and standrad deviations are given in Appendix D.1.

The intrinsic viscosity was calculated as an average of the intrinsic viscosity determined by the Huggins, Fuoss-Mead, Billmeyer and the Hermann equations, and determined to be 195 mL/g, which is lower than expected. Kelzan XCD is a high molecular weight xanthan (Kelco Oil Field Group, 2001), and with the sonication time being 10 minutes, a higher intrinsic viscosity would be expected (Sato et al., 1984). The Huggins' plot is shown in Figure 3.1.1.

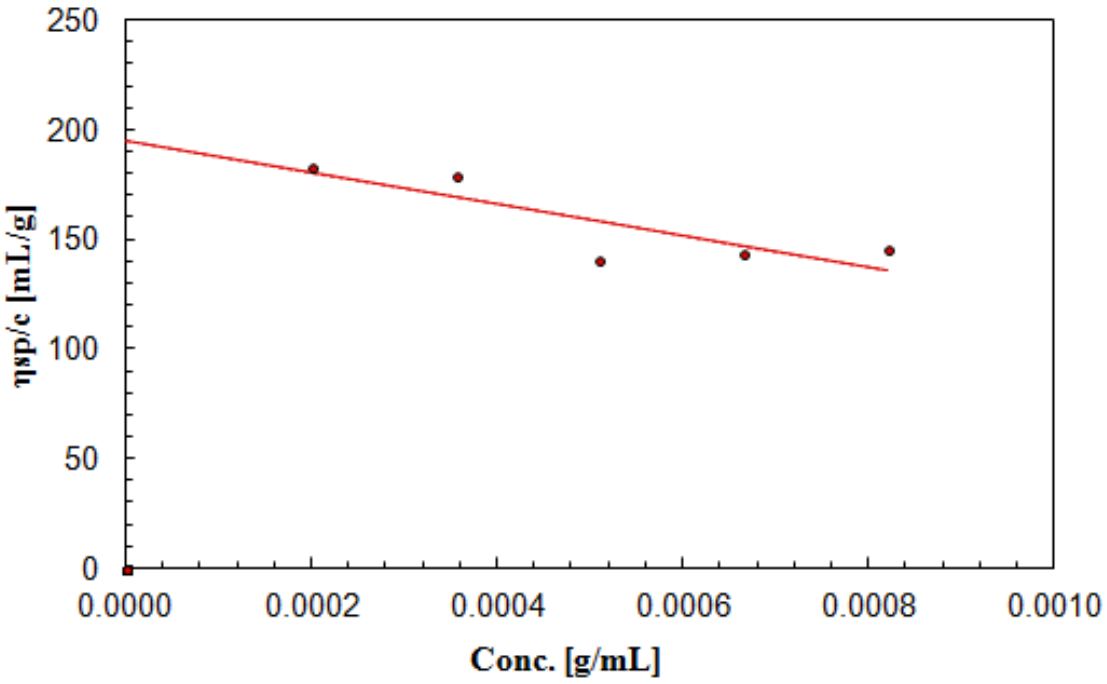

Figure 3.1.1: Huggins plot of the Kelzan test sample, sonicated for 10 minutes, and not purified. The viscosity measurements were performed by single capillary viscometer with wall shear rate 2500 s^{-1}. The measurement temperature was 20.0 °C, and the solvent was 0.1 M NaCl.

From the Huggins' plot it is seen that the a linear regression provides a decreasing trend of the specific viscosity over concentration as the concentration increases. There is observed a drop in specific viscosity over concentration after the two lowest concentrations. The reason for this may be that these two concentrations were too low for reliable measurements. If these two concentrations are ignored, the intrinsic viscosity lies within the range of 100 - 150 mL/g, which is even lower than the calculated value. One reason for the varying viscosities may be presence of particles in the solution, since it was not purified after sonication. The sonicator probe may release titanium ions which could cause aggregates of the xanthan chains in the solution. Since this samples was not purified, this aggregation may explain the apparent low viscosity of the sample.

Overall, there is no reliable trend in these results. Hence, in order to achieve reliable results, it was necessary to obtain a purified xanthan with lower molecular weight. This was achieved by longer sonication times and purification, of which the results are presented in the following sections.

3.1.2 SEC-MALLS of Purified Sonicated Xanthan Samples

Molecular Weight

Solutions of 1 mg/mL xanthan containing 0.1 M NaCl, prepared from Kelzan XCD, were sonicated for 10, 30 and 120 minutes, in order to obtain the samples xan10, xan30 and xan120, respectively. The sample xanS was obtained from the xanthan provided by Statoil, and was sonicated for 60 minutes. An overview of the SEC-MALLS results for these samples can be found in Table F.1.1 in Appendix F.

All molecular weights presented in this chapter were found from SEC-MALLS analyses of the xanthan samples with serially connected columns TSK G-4000-3000PWXL or TSK G-6000-5000PWXL, depending on the date of SEC-MALLS analysis. The latter was applied due to a parallel experiment in the laboratory demanding high molecular weight columns, this was not ideal concerning the xanthan samples in this project, and may have caused some uncertainties of the results. SEC-MALLS buffer used was a solution of 0.15 M $NaNO_3$ and 0.01 M EDTA. The SEC-MALLS data were processed by the software ASTRA, with assistance from Ann-Sissel T. Ulset and Professor Bjørn E. Christensen.

The molecular weight distributions, as a plot of molecular weight against elution volume, and the concentration profiles by the differential refractive index (dRI) signal, for the sonicated xanthan samples xan10, xan30, xan120, and xanS are presented in Figure 3.1.2.

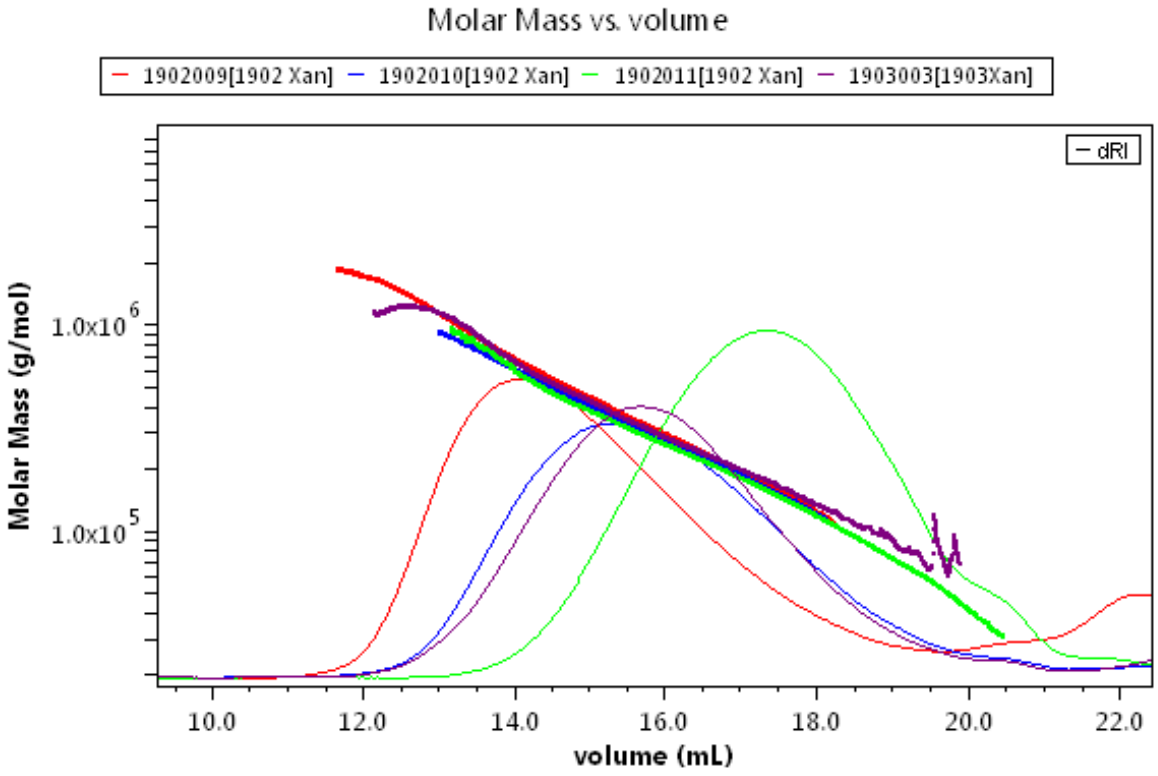

Figure 3.1.2: Concentration profiles from differental refractive index signal seen by the curved lines, and molecular weight distributions seen by the crossing, neraly straight lines, of the sonicated samples xan10 (red line), xan30 (blue line), xan120 (green line), and xanS (purple line). The plot was obtained by processing SEC-MALLS results with ASTRA. SEC-MALLS columns were TSK G-4000-3000PWXL, and buffer was 0.15 M $NaNO_3$ and 0.01 M EDTA.

The red, blue, green, and purple lines in the figure represent xan10, xan30, 120, and xanS, respectively. The concentration profiles is shown by the differential refractive index (dRI), the curved lines, while the molecular weight distributions are shown by the crossing, nearly straight lines. It is seen that the concentration profiles are shifted to the right, towards higher elution volume, as the sonication time increases. Since the RI detector analyses the solution eluted from the column, the fact that the curves are shifted to the right indicates that the molecular weight decreases, since large molecules will leave the column at an earlier stage than smaller molecules. Large molecules will not permeate into the porous material of the columns, hence they will be eluted faster than smaller molecules, which permeates into the pores of the column material. xan10 is least shifted, thus it is earliest eluted from the column, which indicates that it has the highest molecular weight. Next is xan30 (blue) and xanS (purple), while xan120 uses the longest time through the column, thus has the lowest molecular weight.

The curves also show that these xanthan samples are quite pure, as the curves are smooth, and do not show many irregular tendencies or peaks. There is, however, observed some irregularities of the dRI signal around 20 - 22 mL, which may indicate that there are

some impurities in the solutions. The molecular weight distributions of the analysed xanthan samples are not entirely overlapping, which also indicates that the samples are not perfectly pure. Nevertheless, SEC-MALLS analyses gave better results than expected for a complex polysaccharide like xanthan.

An overview of the sonicated samples and their molecular weights, M_w, is shown in Table 3.1.1. The molecular weight for each sample was calculated as the average of the molecular weights determined by several injections for SEC-MALLS. These are presented, together with their respective uncertainties, in Table F.1.1 in Appendix F.

Table 3.1.1: Molecular weight, M_w, for the sonicated xanthan samples, obtained from processing SEC-MALLS result with ASTRA. The buffer was 0.15 M $NaNO_3$ and 0.01 M EDTA, and columns were TSK G-4000-3000PWXL.

Sample	$\boldsymbol{M_w}$ **[kDa]**
xan10	604
xan30	369
xan120	182
xanS	361

The relationship between the molecular weight of xanthan and sonication time is shown in Figure 3.1.3.

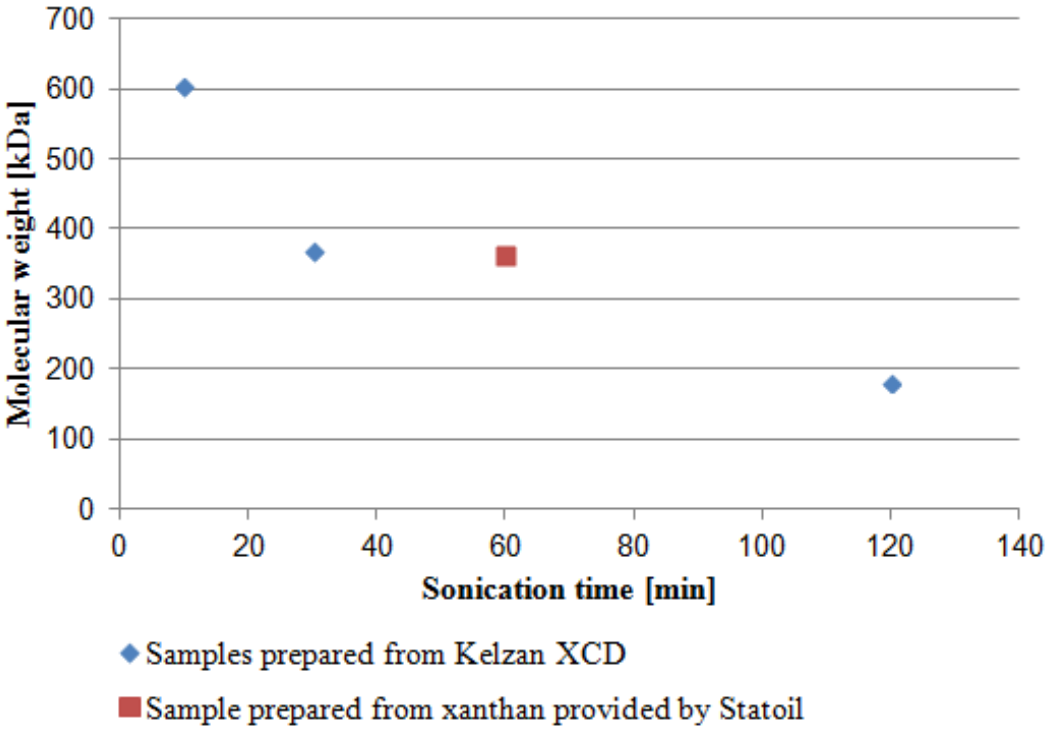

Figure 3.1.3: Molecular weight of xanthan as a function of sonication time. The blue marks represent the purified sonicated samples xan10, xan30 and xan120, while the red mark represents the purified sonicated sample xanS. The molecular weights were determined by SEC-MALLS, with columns TSK G-4000-3000PWXL and buffer was 0.15 M $NaNO_3$ and 0.01 M EDTA.

Figure 3.1.3 shows the molecular weight of the sonicated samples plotted against the sonication time. As seen from the figure, the molecular weight decreases with increasing sonication time. This trend is expected, due to splitting of the long xanthan chains into shorter chains. The blue marks in the plot represent the purifed sonicated samples xan10, xan30, and xan120, while the red mark represents the purified sonicated xanS sample. It is observed that the xanS sample appear to have a higher molecular weight relative to the sonication time compared to the samples xan10, xan30, and xan120, that were prepared from the Kelzan XCD. The reason for this may be that xanS was prepared from a different start xanthan than the three others and the molecular weight before sonication may have been higher. Thus, longer sonication times are necessary to provide lower molecular weights.

From the figure it is also observed that the molecular weight is most decreasing in the start, then the decrease trend appears to flatten out. This is most likely because long molecules are easier to break, and as the molecules become shorter, depolymerisation by applying mechanical force will become more difficult since the shorter xanthan chains will be more rigid and resistant towards breakages.

RMS Conformation Plot

From processing SEC-MALLS results in ASTRA there was obtained a RMS (root mean square) conformation plot, of the RMS radius against molecular weight, which provides information about the xanthan conformations. The plot is shown in Figure 3.1.4.

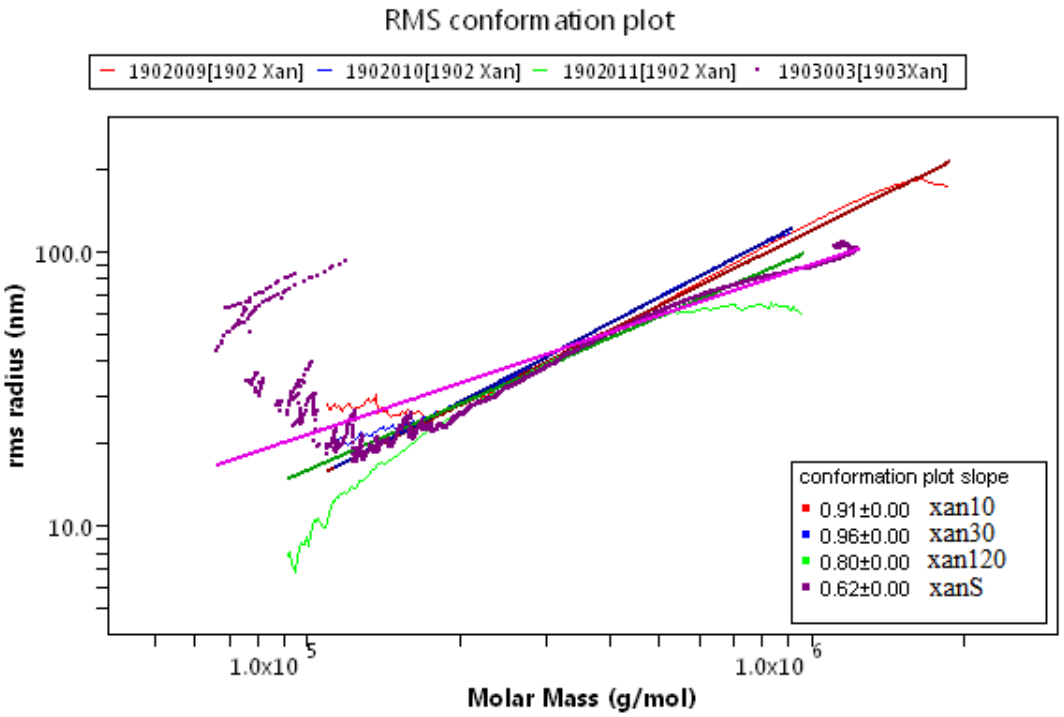

Figure 3.1.4: RMS conformation plot for the purified sonicated samples xan10 (red line), xan30 (blue line), xan120 (green line) and xanS (purple line), obtained from ASTRA. Molecular weight is plotted against molar mass, both determined by SEC-MALLS. Buffer used for SEC-MALLS was 0.15 M $NaNO_3$ and 0.01 M EDTA and columns applied were TSK G-4000-3000PWXL.

The slopes of the linear regression lines for each sample, obtained from the RMS conformation plot in Figure 3.1.4, are presented in Table 3.1.2.

Table 3.1.2: Slopes obtained from RMS conformation plot in Figure 3.1.4 for the purified sonicated samples xan10, xan30, xan120 and xanS.

Sample	Slope
xan10	0.91 ± 0.00
xan30	0.96 ± 0.00
xan120	0.80 ± 0.00
xanS	0.62 ± 0.00

The slopes of the RMS conformation plots provide information about the conformations of the analysed xanthan samples. The samples xan10 and xan30 have slopes near 1,

which indicates that the xanthan chains are rigid rods (Wyatt Technology Corporation, 2014). Thus, low sonication times, 10 and 30 minutes, do not seem to have any effect on the conformation of the xanthan chains, if they are assumed to be rigid before sonication. This assumption should be valid, as xanthan will have an ordered conformation in solutions containing salt. The slope for xan120, which was sonicated for 120 minutes are somewhat lower than for the two mentioned samples. This may indicate that longer sonication times could have an impact on the xanthan chain conformation. However, it is previously shown that the xanthan chains achieve a more rigid structure as the sonication time increases, since the length of the chains decreases (Sato et al., 1984). This would also be expected, as mentioned in the previous section, because it would theoretically be harder to depolymerise shorter chains as they should be rigid. The reason for the change in conformation after longer sonication times may be that the mechanical and chemical effects on the chains are high enough to influence the chain conformation, even of short xanthan molecules. Another reason may be that even if the temperature during sonication was held below 40 °C, it may in parts of the xanthan solution have exceeded the conformational transition temperature, hence causing a conformational transition from an ordered to a more disordered, flexible conformation.

The slope for sample xanS is even less than for xan120. The reason for this is probably that this sample was prepared from another start xanthan than the other three samples. The lower value implies that the xanthan chain is more flexible than the other samples. As for xan120, the reason for the flexible conformation may be too high temperature during the sonication, causing a conformation transition from order to disorder.

Mark-Houwink-Sakurada Plot

By plotting intrinsic viscosity against molecular weight, both determined by SEC-MALLS, Mark-Houwink-Sakurada (MHS) plots for the purified sonicated samples xan30 and xanS were obtained by ASTRA. MHS plots for xan10 and xan120 could not be obtained, because the viscdetector of the SEC-MALLS apparatus was out of order at the time the purified sonicated samples were analysed. The reason MHS plots for xan30 and xanS were obtained was that these samples were analysed over again in conjunction with analyses of the modified xanthan samples. The MHS plots are presented in Figure 3.1.5, also, the acetyl and pyruvyl free sample xan30pa, prepared from xan30, and further studied in section 3.1.4 is included. SEC-MALLS columns used were TSK G-6000-5000PWXL, and the buffer was 0.15 M $NaNO_3$ and 0.01 M EDTA.

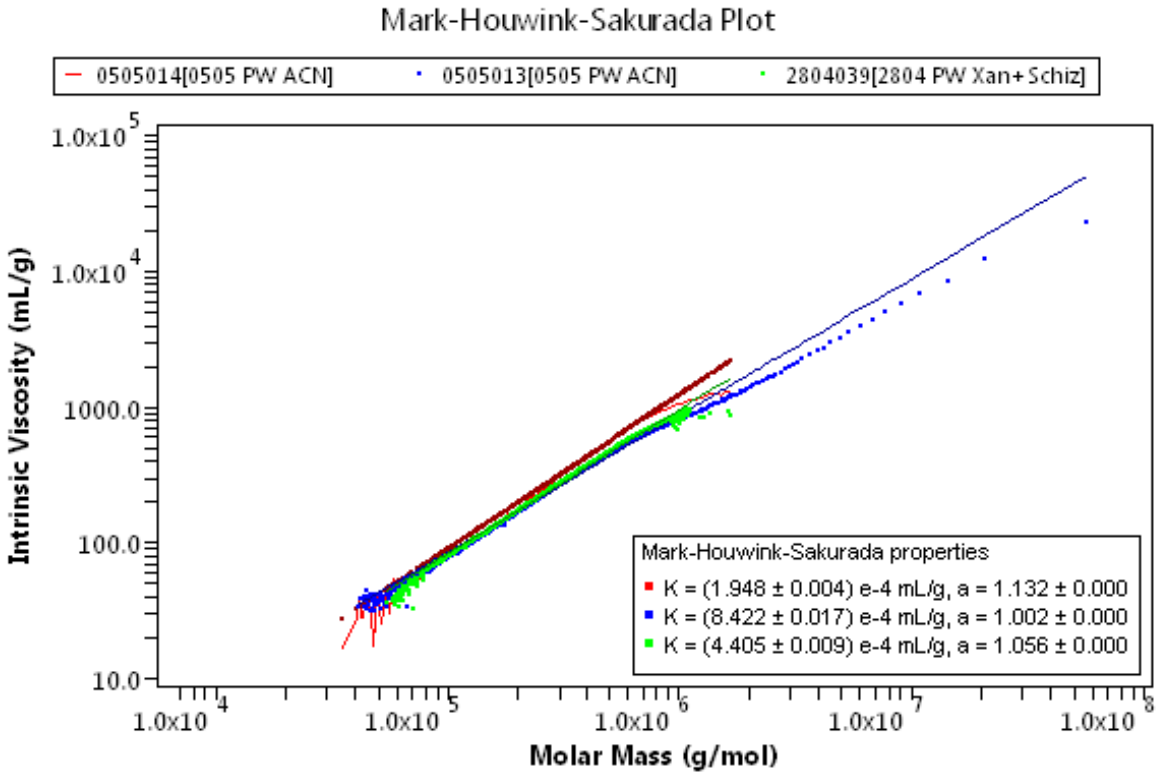

Figure 3.1.5: Mark-Houwink-Sakurada plots for xan30 (red line), xanS (blue line), and xan30pa (green line), obtained from processing SEC-MALLS results with ASTRA. Both intrinsic viscosity and molecular weights are determined by SEC-MALLS. Buffer used for SEC-MALLS was 0.15 M $NaNO_3$ and 0.01 M EDTA, and columns were TSK G-6000-5000PWXL.

The MHS parameters, K and a, with standard deviations, for the purified sonicated samples xan30, xanS, and xan30pa are presented in Table 3.1.3.

Table 3.1.3: Mark-Houwink-Sakurada parameters, K and a, for the purified sonicated samples xan30 and xanS, and the acetyl and pyruvyl free sample xan30pa.

Sample	$\boldsymbol{K}$ **[mL/g]**	$\boldsymbol{a}$
xan30	$(1.984 \pm 0.004) \cdot 10^{-4}$	1.132 ± 0.000
xanS	$(8.422 \pm 0.017) \cdot 10^{-4}$	1.002 ± 0.000
xan30pa	$(4.405 \pm 0.009) \cdot 10^{-4}$	1.056 ± 0.000

The MHS exponent, a, from the MHS plots in Figure 3.1.5 show the same tendencies for the conformations xan30 and xanS as the RMS conformation plot in Figure 3.1.4. The xan30 sample appears to be more rigid than xanS, due to a higher MHS exponent. The MHS exponent implies that all the samples are stiff coils, near rigid rods (Smidsrød and Moe, 2008). For the acetyl and pyruvyl free sample xan30pa it is seen that the MHS exponent is lower than that for xan30, which implies a more flexible conformation. This is probably due to removal of the acetyl and pyruvyl groups. The xan30pa samples is discussed more in detail in section 3.1.4.

3.1.3 Intrinsic Viscosity of Non-Modified Purified Sonicated Xanthan Samples Determined by Single Capillary Viscometer

The intrinsic viscosities were determined by viscosity measurements with single capillary viscometer with wall shear rate 2500 s^{-1} at 20.0 °C with solvent 0.1 M NaCl, and calculated as an average of the intrinsic viscosity determined by the Huggins, Fuoss Mead, Billmeyer, and the Hermann equations. Raw data and calculations, together with standard deviations of the intrinsic viscosities are given in section D.2 in Appendix D. The intrinsic viscosities with standard deviations for the sonicated, purified non-modified xanthan samples xan10, xan30, xan120, and xanS are presented in Table 3.1.4.

Table 3.1.4: Intrinsic viscosity, $[\eta]$, for purified sonicated xanthan samples xan10, xan30, xan120, and xanS. The intrinsic viscosity measurements were performed by a single capillary viscometer with wall shear rate 2500 s^{-1}, at 20.0 °C. The solvent was 0.1 M NaCl.

Sample	$[\eta]$ [mL/g]
xan10	494
xan30	385
xan120	140
xanS	257

The dependency of intrinsic viscosity on sonication time is shown in Figure 3.1.6.

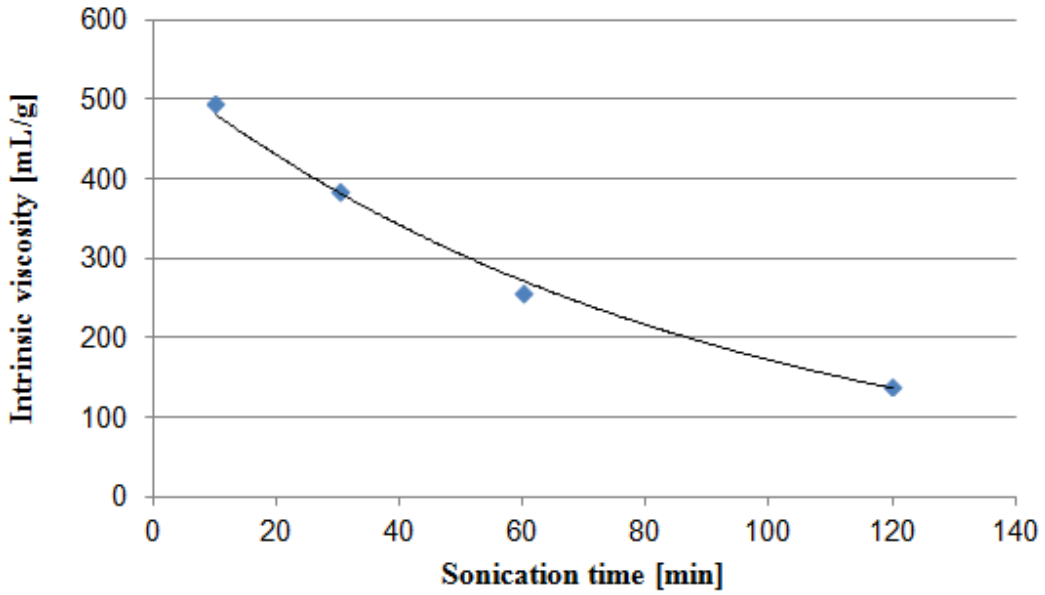

Figure 3.1.6: Intrinsic viscosity of xanthan as a function of sonication time. An expression for the intrinsic viscosity as a function of sonication time was found by exponential regression in Excel. The intrinsic viscosities were determined by measurements with single capillary viscometer, with wall shear rate 2500 s^{-1} at 20.0 °C. The solvent was 0.1 M NaCl.

Figure 3.1.6 shows the intrinsic viscosities of the purified sonicated samples xan10, xan30, xan120, and xanS as a function of their respective sonication times. From the figure it is seen that the intrinsic viscosity of xanthan decreases as the sonication time increases. An exponential regression line was added in Excel, as a guide to the eye. This decrease in intrinsic viscosity is expected, since the sonication of xanthan causes lower molecular weights, as seen from Figure 3.1.3, which provides a lower intrinsic viscosity. In Figure 3.1.6, the intrinsic viscosity of the sample xanS (at 60 minutes) fits nicely with the trend of the others, although the molecular weight did not. The reason for this is unknown, but a possible explanation may be that the samples were prepared from different start xanthans. Another reason may be the difference in conformation, as seen in Figure 3.1.4, in that the sample xanS seems to have a more flexible, not as rigid like, structure than xan10, xan30 and xan120, which may have been caused by to high temperature during sonication.

A plot of the intrinsic viscosity against molecular weight was made, and compared to the literature (Sato et al., 1984), values for molecular weight and intrinsic viscosity can be found in Table D.4.1 in Appendix D. The plot is presented in Figure 3.1.7.

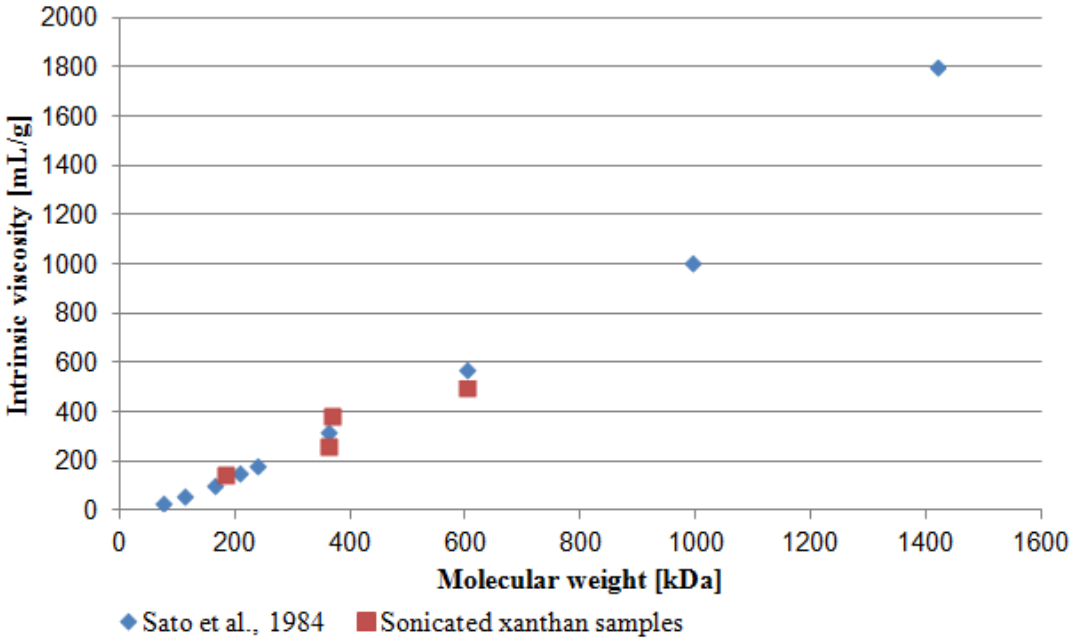

Figure 3.1.7: Intrinsic viscosity as a function of molecular weight. The blue marks represent results from the literature (Sato et al., 1984), while the red marks represent the results from this project. The molecular weights were determined by SEC-MALLS and the intrinsic viscosities were determined by measurements with single capillary viscometer, with wall shear rate 2500 s^{-1}, and solvent 0.1 M NaCl, at 20.0 °C.

From the figure it is observed that the relationship between the intrinsic viscosity and the

molecular weight of xanthan fits nicely with the literature (Sato et al., 1984), although the intrinsic viscosities from Sato et al. (1984) are determined for zero shear rate, and the results for this project were determined for 2500 s^{-1}. This may indicate that the intrinsic viscosity of xanthan with the molecular weights and concentration analysed is this project were not dependent on the shear rate.

The samples used further in this project, for the chemical modification, were xan30 and xanS, in addition to the acetyl and pyruvyl fraa sample, xan30pa, prepared from xan30.

3.1.4 Acetyl and Pyruvyl Free Xanthan

The acetyl and pyruvyl free xanthan sample, xan30pa, was prepared by mild acid and alkaline hydrolysis of xan30. This was performed in order to determine whether the octylamine binds to the pyruvyl group of the β-D-mannose or not, see section 3.2 for further results of the modified samples.

The non-modified xan30pa sample was analysed by SEC-MALLS, and in addition the intrinsic viscosity was determined by single capillary viscometer. A plot of the molecular weight distribution, and the concentration profile from the dRI signal, of xan30pa, obtained by processing SEC-MALLS results with ASTRA, is shown in Figure 3.1.8.

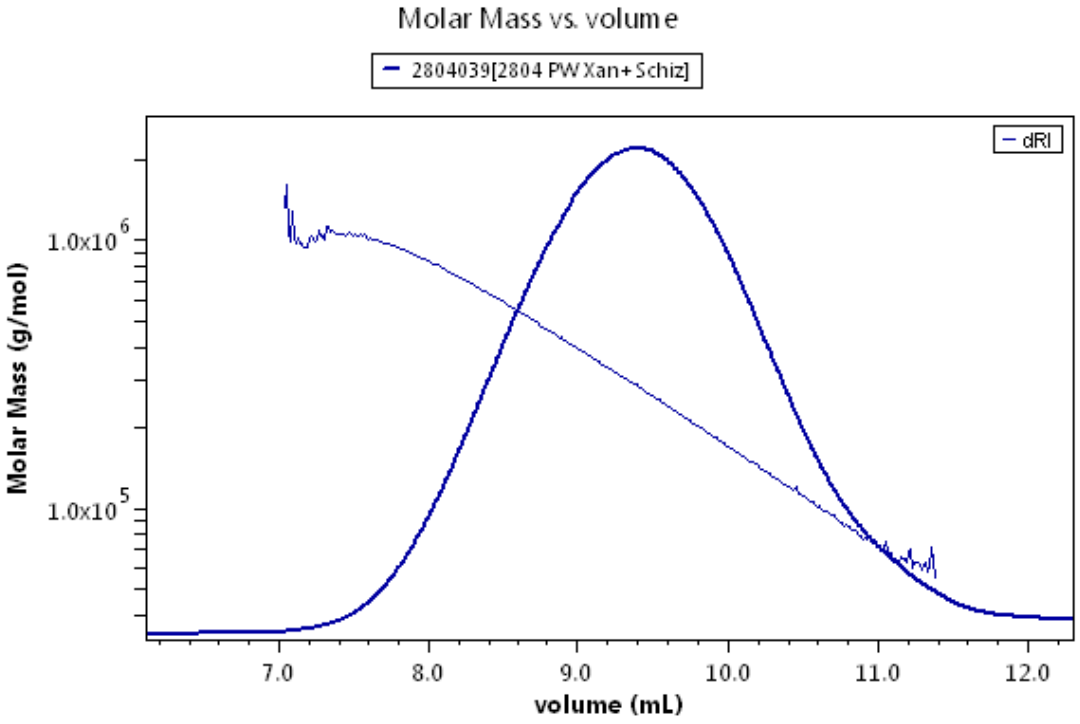

Figure 3.1.8: Concentration profile (curved line) and molecular weight distribution (crossing) of the acetyl and pyruvyl free sample xan30pa. The plot was obtained by processing SEC-MALLS results with ASTRA. SEC-MALLS columns were TSK G-6000-5000PWXL, and the buffer was 0.15 M $NaNO_3$ and 0.01 M EDTA.

The curved line represents the concentration profile of the analysed sample from the differental refractive index (dRI) signal, while the crossing line shows the molecular weight distribution. From the concentration profile it can be seen that the sample is quite pure, since there are not any irregular peaks. Also, the molecular weight distribution provides an almost straight line, but with some irregularities on the outer edges, indicating that the sample is not perfectly pure.

By plotting the root mean square (RMS) radius against molecular weight, an RMS conformation plot was obtained from ASTRA. The plot is shown in Figure 3.1.9.

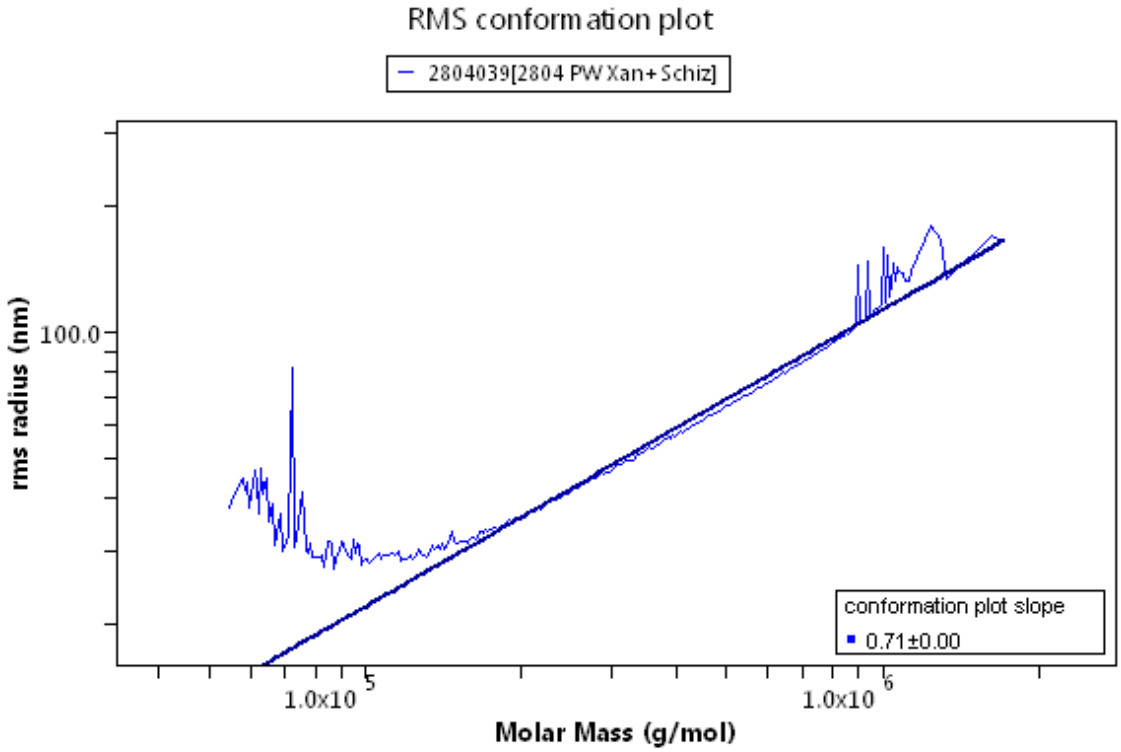

Figure 3.1.9: RMS conformation plot for the acetyl and pyruvyl free xanthan sample xan30pa, prepared from the sonicated sample xan30. The plot is obtained from ASTRA. Buffer used for SEC-MALLS was 0.15 M $NaNO_3$ and 0.01 M EDTA, and columns were TSK G-6000-5000PWXL.

From the figure it is seen that the slope, 0.71 ± 0.00, is lower than that of the xan10, xan30, and xan120, see Table 3.1.2. Since the slope is lower than that for xan30 it implies that the conformation of the xanthan chain is changed when removing the acetyl and pyruvyl groups. By removal of the acetyl and pyruvyl groups there is lost two larger functional groups, which are replaced by -OH groups. The removal of pyruvyl groups also causes removal of an carboxylic acid group, thus an ionic charge is lost. Hence, the ionic interactions will decrease, and the conformation may be changed. A combination of this may have provided a more flexible structure of the xanthan chains.

The intrinsic viscosity of xan30pa was determined by measurements with single capillary viscometer with wall shear rate 2500 s^{-1}, and solvent 0.1 M NaCl. The intrinsic viscosity was calculated as the average of intrinsic viscosities determined by Huggins, Fuoss-Mead, Billmeyer, and Hermann equations, see section D.2 in Appendix D for raw data, calculations, and standard deviations. Both the molecular weight and intrinsic viscosity of xan30pa is presented in Table 3.1.5.

Table 3.1.5: Molecular weight, M_w, and intrinsic viscosity, $[\eta]$, of the pyruvate and acetate free xanthan sample xan30pa. The molecular weight was determined by SEC-MALLS with columns TSK G-6000-5000PWXL, buffer was 0.15 M $NaNO_3$ and 0.01 M EDTA. The intrinsic viscosity was determined by measurements with single capillary viscometer, with wall shear rate 2500 s^{-1}, at 20.0 °C, solvent was 0.1 M NaCl.

Sample	$\mathbf{M_w}$ **[kDa]**	$[\boldsymbol{\eta}]$ **[mL/g]**
xan30pa	337	382

By comparing the molecular weight and intrinsic viscosity of xan30pa to the molecular weight and intrinsic viscosity for xan30 from Tables 3.1.1 and 3.1.4, it can be seen that the xan30pa sample has similar properties regarding molecular weight and intrinsic viscosity, as the xan30. However, by looking at the RMS conformation plots, see Figures 3.1.9 and 3.1.9, it is observed that the slope for xan30pa is not as steep as for xan30, which indicates that removal of acetyl and pyruvyl provides a more flexible conformation of the xanthan chains.

The Mark-Houwink-Sakurada plot, obtained from processing SEC-MALLS results with ASTRA, for the acetyl and pyruvyl free xan30pa was presented earlier, in Figure 3.1.5 together with xan30 and xanS. It was seen that the MHS exponent for xan30pa was less than that for xan30, which implies that xan30pa had a more flexible conformation than xan30. This is in accordance to the RMS conformation plots.

3.1.5 Depolymerisation by H_2O_2 and NaOH for ^{1}H-NMR

Prior to the ^{1}H-NMR analyses, the xanthan samples were depolymerised with H_2O_2 and NaOH in order to obtain the small molecular size necessary to achieve clear NMR spectra. Already in the first test modification, it was made an observation that the samples were still quite viscous after the depolymerisation. The high viscosity also caused problems with transferring the samples into the NMR tubes. This caused a suspicion that the depolymerisation does not mainly cut the back bone chain of the xanthan, but the side chains. In order to validate the depolymerisation method, the content of α-D-mannose in two samples with known amounts of α-D-mannose was determined by ^{1}H-NMR, and a series of depolymerised xanthan samples was prepared for determination of the molecular weights during the depolymerisation.

Determination of α-D-Mannose Content After Depolymerisation

Two xanthan samples with known contents of aldobiuronic acid (ABA), thus α-D-mannose, was depolymerised and analysed by ^{1}H-NMR, in order to determine whether the peak

of the proton on C-1 of the α-D-mannose (H-1 α-Man) in the ^{1}H-NMR spectra could be applied for calculations of the degrees of substitution of acetyl and pyruvyl groups, and the grafting densities of the modified samples. The samples were originally prepared in conjunction with an article by Christensen et al. (1993). The known and calculated values for the content of α-mannose, f_{ABA} are presented in Table 3.1.6. Calculations are shown in Appendix H, section H.3.

Table 3.1.6: Calculated contents of α-D-mannose.

Sample	**Given f_{ABA}**	**Calculated f_{ABA}**
xan-3-94-2	0.95	1.24
xan-3-94-14	0.67	0.80

From the table it is seen that the calculated content of α-D-mannose is overestimated. Hence, if the H-1 α-Man peak is used for calculations of the degrees of substitution and grafting densities, these will be underestimated. To overcome this problem, a known amount of an external reference, such as TSP used in this project, may be applied. Another solution is to develop a depolymerisation method that only breaks the β-1,4 linkages between the back bone glucose units, and which do not remove any of the side groups, for example enzymatic degradation. This was not attempted in this project, due to time limitation.

Depolymerisation Series

A second experiment in order to validate the depolymerisation method, was performed by preparing a series of depolymerised xanthan samples with different depolymerisation times and determining the molecular weight, by SEC-MALLS, at given times during the depolymerisation reaction. First a series of non-purified, non-sonicated xanthan from Kelzan XCD was prepared. Due to low mass recoveries when running SEC-MALLS, the results were regarded as not sufficiently reliable, see Table F.2.1 in Appendix F. Hence, a series of depolymerised xanS was prepared, which gave higher mass recoveries during SEC-MALLS, thus more reliable results. The mass recovery provides information of how large fraction of the injected solution that is eluted from the columns.

The molecular weight distributions for depolymerised xanS at different times are shown in Figure 3.1.10.

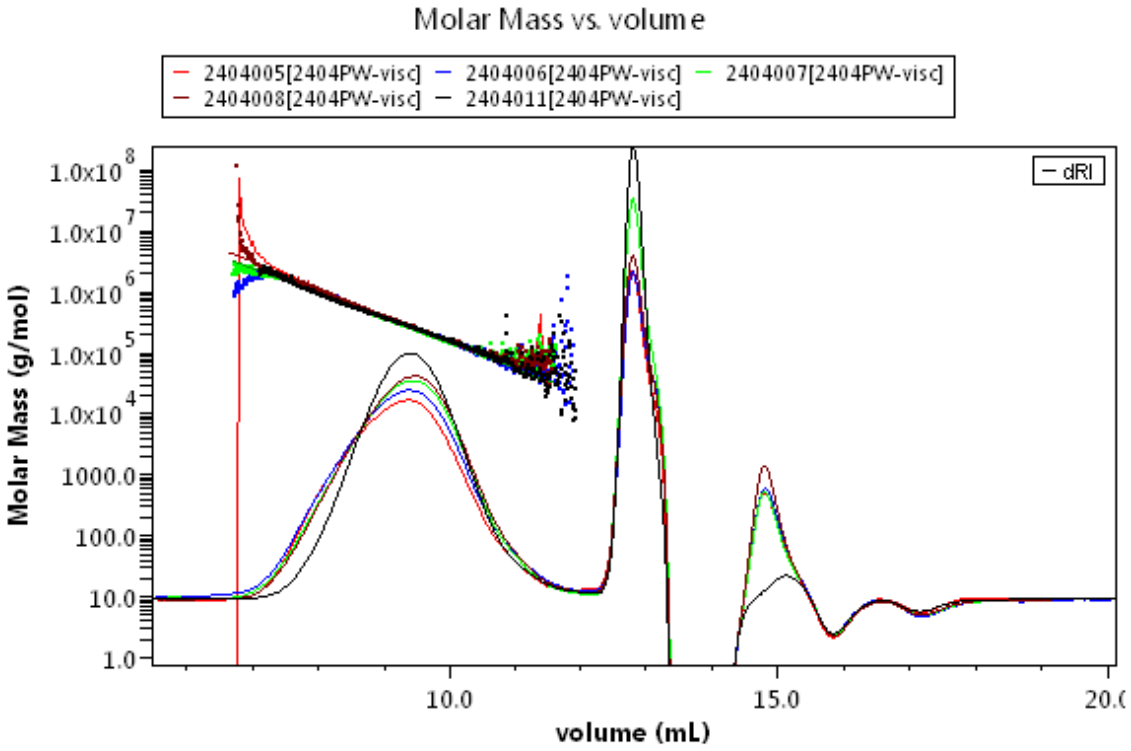

Figure 3.1.10: Molecular weight distributions of depolymerised xanS at different depolymerisation reaction times. The depolymerisation times were 0 (black line), 10 (red line), 20 (blue line), 40 (green line), and 60 minutes (purple line). The molecular weights are plotted against eluted volume. The plot was obtained by processing of SEC-MALLS results in ASTRA. SEC-MALLS buffer was 0.15 M $NaNO_3$, 0.01 M EDTA, and columns TSK G-6000-5000PWXL.

The black, red, blue, green, and purple lines represent the depolymerisation times 0, 10, 20, 40, and 60 minutes, respectively. From the figure it is seen that the concentration profiles of the samples are not shifted along the x-axis, thus most of the samples are eluted from the columns at the same time, i.e. they have similar molecular weights. One reason for this could be that aggregates are formed in the analysed solution due to the $NaNO_3$ in the SEC-MALLS buffer. To avoid this problem a buffer without salt or any other molecules that may form aggregates with xanthan could be used. A peak next to the salt peak around 14 mL is also observed, which may represent small molecules that probably occurs because parts of the xanthan molecules are released during the depolymerisation. These released units are most likely side chains or parts of the side chains of the xanthan. The results are in accordance to previously performed experiments with depolymerisation by H_2O_2 and Fe^{2+}, where it was shown changes in the composition of the xanthan side groups (Christensen et al., 1996). These results also confirm that the depolymerisation method with H_2O_2 and NaOH is not optimal for obtaining low molecular weight xanthan molecules for ^{1}H-NMR analysis.

3.1.6 Degree of Substitution of Acetyl and Pyruvyl Groups from ^{1}H-NMR

^{1}H-NMR analyses were performed for the non-modified samples of xan30, xanS, and xan30pa at 400 MHz and 80 °C. All ^{1}H-NMR spectra can be found in Appendix G. All ^{1}H-NMR analyses were performed by Wenche I. Strand at the Department of Biotechnology.

A typical example of a ^{1}H-NMR spectrum for the non-modified xanthan samples, here for xan30, is presented in Figure 3.1.11.

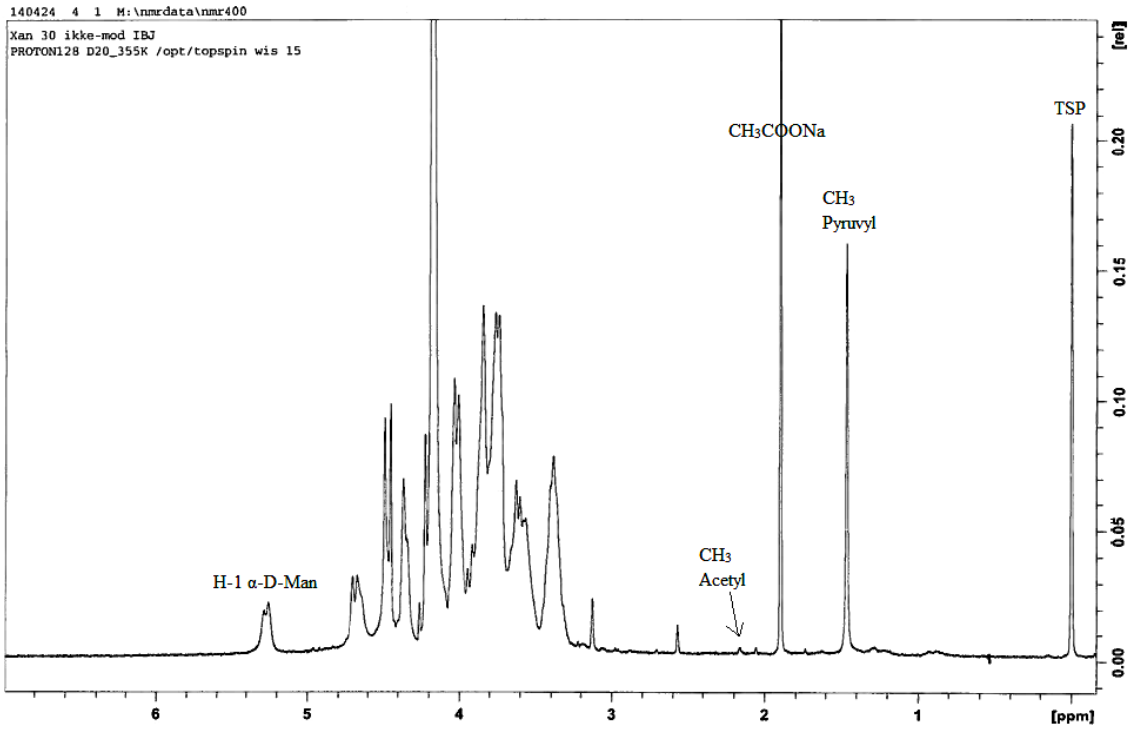

Figure 3.1.11: ^{1}H-NMR spectrum of non-modified xan30, analysed with Bruker Avance DPX 400 MHz at 80 °C.

From the figure it is seen that the peaks for the methyl groups of the bound pyruvyl and acetyl groups are found at 1.5 ppm and 2.1 ppm, respectively, while the peak for free sodium acetate is at 1.9 ppm, and the H-1 α-Man peak is found at 5.2 ppm. These results are in good accordance with previous ^{1}H-NMR analyses of xanthan (Rinaudo et al., 1983, Roy et al., 2014). A high peak is observed for the free sodium acetate, even though there was not added any before the analyses. Thus, this sodium acetate must have been released from the xanthan during depolymerisation with H_2O_2 and NaOH prior to the NMR analysis, which explains the almost not existing peak for acetyl bound to the xanthan at 2.1 ppm.

From the ^{1}H-NMR spectra of the samples xan30, xan30pa and xanS, the degree of substitution of acetyl and pyruvyl groups could be determined, by comparing the integrals

of their respective peaks with the TSP peak. The results are presented in Table 3.1.7. The raw data and calculations are presented in Table H.1.2 in Appendix H.

Table 3.1.7: Degree of substitution of acetyl and pyruvate groups, DS_{Ac} and DS_{Pyr}, respectively, for the non-modified purified sonidated samples xan30, xanS, and xan30pa. The degrees of substitution were calculated from ^{1}H-NMR-results. ^{1}H-NMR was performed with a Bruker Avance DPX 400 MHz at 80 °C.

Sample	DS_{Ac} [%]	DS_{Pyr} [%]
xan30	23.8	18.6
xanS	19.9	26.1
xan30pa	0.7	4.9

From Table 3.1.7 it can be seen that the xanS sample, prepared from the xanthan provided by Statoil, has a lower acetyl content and a higher pyruvyl content than xan30, which was prepared from Kelzan XCD. It is also seen that nearly all of the acetyl groups was removed in the acetyl and pyruvyl free sample, xan30pa, but not all of the pyruvyl groups. In order to improve the removal of pyruvyl stronger acid or longer reaction time may be applied.

3.2 Characterisation of Modified Xanthan

Two sets of test modifications were performed, with grafting of octylamine at 4 °C and roomtemperature, in order to determine the effect of temperature on grafting density. The purified sonicated samples that were hydrophobically modified were the xan30 and xan30pa, prepared from Kelzan XCD, and xanS prepared from the xanthan provided by Statoil. The non-modified and modified samples were analysed by ^{1}H-NMR in order to determine the grafting densities of octylamine. The molecular weights and the intrinsic viscosities before and after modification were determined by SEC-MALLS and analyses by single capillary viscometer, respectively. For the xan30 sample two different viscometers were used; the single capillary viscometer, and a four-bulb shear dilution viscometer, the latter is studied in section 3.3.2.

3.2.1 Grafting Densities of Modified Xanthan from ^{1}H-NMR

The grafting densities of the modified samples were determined by ^{1}H-NMR, at 80 °C. The test samples were analysed at 300 MHz, while the sonicated purified samples were analysed at 400 MHz.

A typical example of a ^{1}H-NMR spectrum for the modified xanthan samples, here for modified xan30, is presented in Figure 3.2.1.

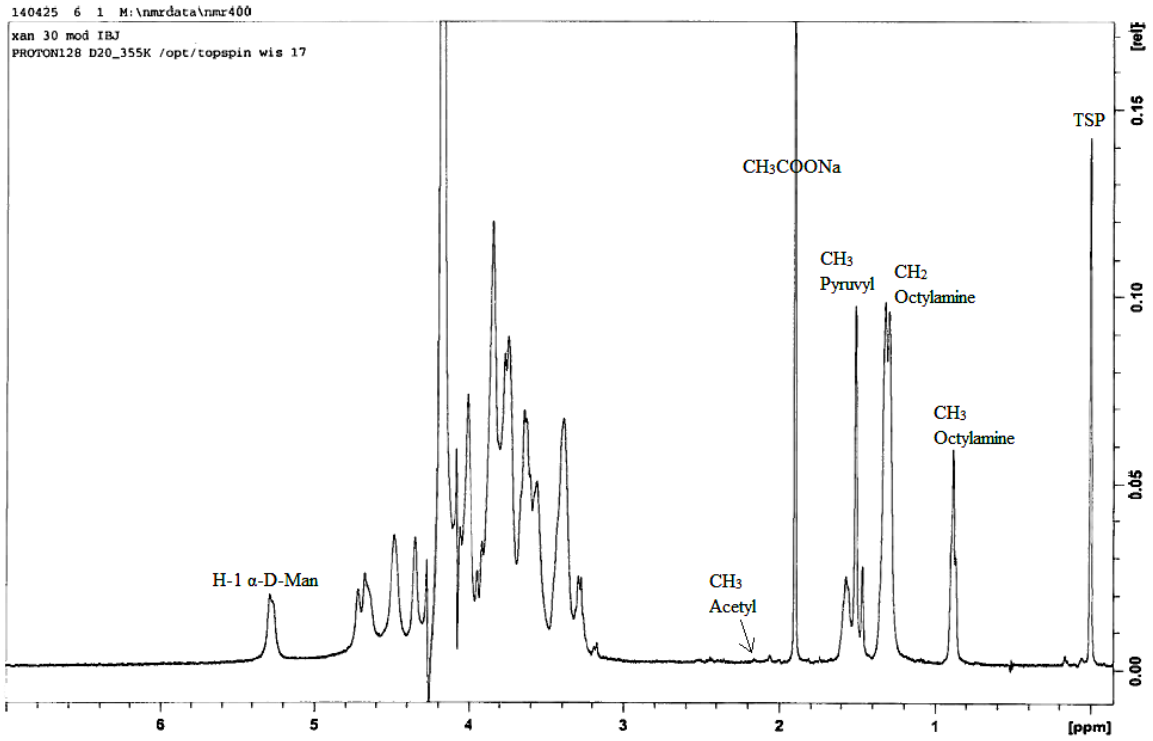

Figure 3.2.1: ^{1}H-NMR spectrum of modified xan30, analysed with Bruker Avance DPX 400 MHz at 80 °C.

As seen from the figure additional peaks to the ones shown in Figure 3.1.11 can be observed for the methyl and methylene groups of the octylamine, at 0.9 ppm and 1.25 ppm, respectively. This is in good accordance to recently found results (Roy et al., 2014).

Grafting Densities of Modified Non-Sonicated Kelzan Test Samples

Two test modification of non-sonicated Kelzan XCD were performed, and in each test modification, the octylamine was grafted onto the xanthan at both 4 °C and at room temperature, in the second step of the modification process. The calculated grafting densities from the first test modification were not reliable, due to difficulties transferring the samples into the NMR tubes, thus very insecure results. The resulting grafting densities, $\%octyl$, in addition to the degrees of substitution of acetyl and pyruvyl, DS_{Ac} and DS_{Pyr}, from the second test modification, with the grafting reaction performed at 4 °C and room temperature, test2mod1 and test2mod, respectively, are presented in Table 3.2.1. The degrees of substitution for the test samples were determined for the modified samples due to difficulties transferring the non-modified sample to the NMR-tube. All ^{1}H-NMR spectra can be found in Appendix G, and the raw data and calculations are presented in Table H.1.1 in Appendix H.

Table 3.2.1: Degrees of substitution of acetyl and pyruvyl, DS_{Ac} and DS_{Pyr}, respectively, and grafting densities, $\%octyl$, for non-sonicated, non-purified, modified xanthan test samples, calculated from ^{1}H-NMR spectra. ^{1}H-NMR was performed at 80 °C with a Bruker Avance DPX 300 MHz.

Sample	**Grafting temperature**	$\boldsymbol{DS_{Ac}}$ [%]	$\boldsymbol{DS_{Pyr}}$[%]	$\%\boldsymbol{octyl}$
test2mod1	4 °C	18.3	11.0	12.4
test2mod2	Room temperature	16.7	10.7	11.9

As seen from the table, there is not a notable difference in grafting density based on the temperature the grafting reaction is performed at. Thus, the most secure choice was considered to be performing the grafting reaction at 4 °C, in order to prevent conformational changes of the rigid double chain of xanthan during the modification.

Grafting Densities of Modified Purified Sonicated Xanthan

The calculated grafting densities for the modified purified sonicated samples, $\%octyl$, are presented in Table 3.2.2. The grafting densities were calculated from the ^{1}H-NMR spectra of the respective samples, shown in Appendix G. The raw data and calculations are presented in Table H.1.3 in Appendix H.

Table 3.2.2: Grafting densities, $\%octyl$, for the modified purified sonicated xanthan samples xan30, xanS, and xan30pa. Values are calculated from ^{1}H-NMR spectra. ^{1}H-NMR was performed at 80 °C with a Bruker Avance PDX 400 MHz.

Sample	$\boldsymbol{\%octyl}$
xan30	18.3
xanS	19.6
xan30pa	6.3

The results show that the grafting density of xanthan is highly dependent on the pyruvyl content of the xanthan. This shows that the octylamine binds both to the carboxylic acid group on the glucuronic acid and on the pyruvyl group of the outer β-D-mannose. The grafting density for xan30pa is less than half of the one for xan30. If equal fractions of the octylamine were grafted onto the carboxylic groups of the glucuronic acids and the pyruvyl groups, the grafting density would decrease with 50 % if all of the pyruvyl were removed. Since not all the pyruvyl groups were removed (see Table 3.1.7), and the grafting density of xan30pa is less than half of that for xan30, the results indicate that more than half of the octylamine is grafted onto the pyruvyl groups. This may be explained by better accessibility of the carboxylic acid group of the pyruvyl on the outer β-D-mannose than of the carboxylic acid of the glucuronic acid. Thus, octylamine may bind easier to the carboxylic acid group of the pyruvyl on the β-D-mannose.

The grafting densities found in this thesis were lower than grafting densities recently found (Roy et al., 2014), by addition of approximately the same amount of reagents. The reason may be a lower pyruvyl content of the xanthan samples applied in this project, and as shown here the grafting density is dependent on the pyruvyl content.

3.2.2 SEC-MALLS

The modified samples xan30, xan30pa, and xanS, were analysed by SEC-MALLS, with columns TSK G-6000-5000PWXL, in order to determine their molecular weight and conformation.

The buffer used when analysing the samples xan30 and xanS were initially the same as for the non-modified samples; 0.15 M $NaNO_3$ and 0.01 M EDTA. The results obtained when using this buffer showed very low mass recoveries, see Table F.2.1 in Appendix F. A reason for the low mass recoveries may be interactions between the SEC column material and the hydrophobic xanthan molecules. For hydrophobic molecules it is previously shown that acetonitrile may decrease the retention volume, i.e. increase the mass recoveries (David et al., 2001, Hodgkinson and Lowry, 1981). Thus, a buffer with 0.15 M $NaNO_3$, 0.01 M EDTA, and 20 % acetonitrile was attempted in order to achieve higher mass recoveries, for all the modified xanthan samples, xan30, xanS, and xan30pa.

Molecular Weight

The molecular weight distribution and concentration profile (dRI) for the modified xanthan samples is shown in Figure 3.2.2.

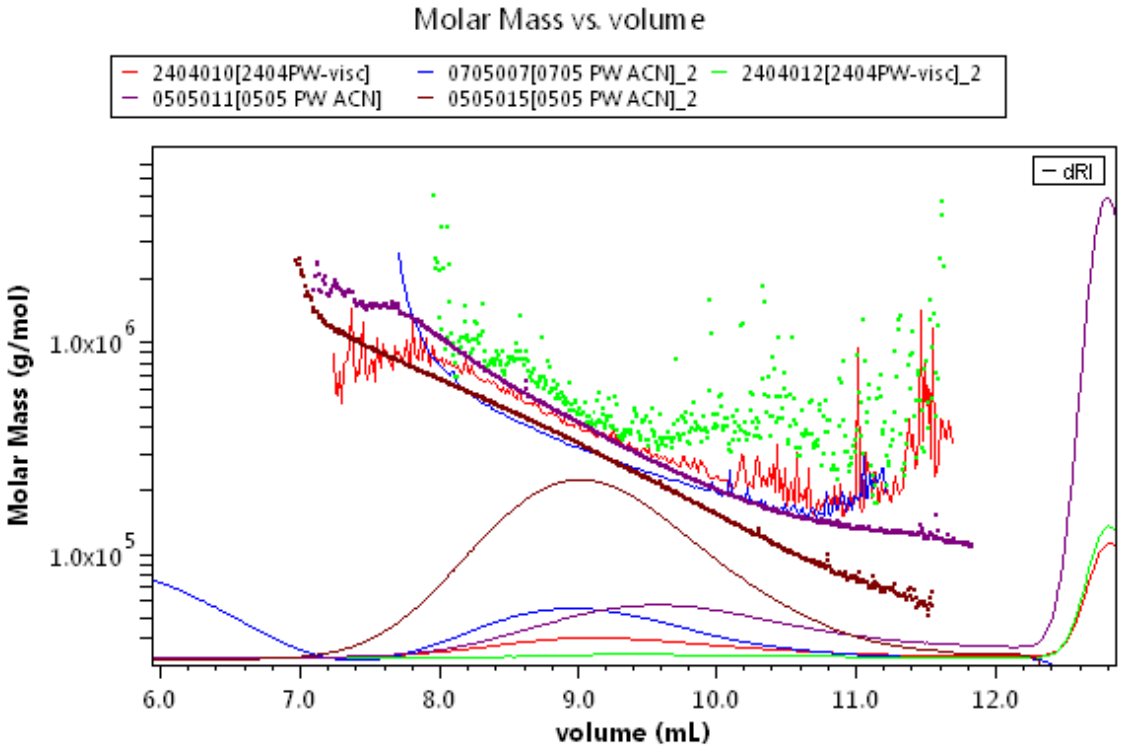

Figure 3.2.2: Concentration profiles (curved lines) and molecular weight distributions (crossing lines) of modified xanthan samples obtained from SEC-MALLS analyses with columns TSK G-6000-5000PWXL. The red and the green lines represent the modified xan30 and xanS, respectively, analysed with buffer 0.15 M $NaNO_3$ + 0.01 M EDTA. The blue, purple, and the brown lines represent the modified samples xan30, xanS, and xan30pa, respectively, analysed with buffer 0.15 M $NaNO_3$ + 0.01 M EDTA + 20 % acetonitrile.

The red and the green lines represent xan30 and xanS, respectively, analysed with buffer without acetonitrile. The blue, purple, and brown lines represent xan30, xanS, and xan30pa, respectively, analysed with buffer containing 20 % acetonitrile. It is seen for xan30 and xanS analysed with buffer without acetonitrile that the peaks of the concentration profiles are very low, thus indicating low concentrations of the eluted solutions. For the xan30 and xanS analysed with buffer containing acetonitrile, it is observed slightly higher peaks, indicating a little improvement of the eluted amount of the samples. The sample with highest mass recovery was xan30pa. This was not unexpected, due to the low grafting density, thus it was not as hydrophobic as xan30 and xanS, and would not bind to the column material to the same extent.

However, the results for the fractions of the xanthan solutions that made it through the column seemed to provide appropriate results. The remaining results from SEC-MALLS in this section are based on use of buffer with 0.15 M $NaNO_3$, 0.01 M EDTA and 20 % acetonitrile.

The molecular weights of the modified xanthan samples, M_w, are presented in Table

3.2.3. The molecular weight for each sample was calculated as the average of the molecular weights determined by SEC-MALLS, and shown, together with the uncertainties, in Table F.2.1 in Appendix F.

Table 3.2.3: The molecular weights after modification, M_w. The values were found by processing data from SEC-MALLS analyses with ASTRA. The SEC-MALLS buffer was 0.15 M $NaNO_3$ and 0.01 M EDTA with 20 % acetonitrile, and the columns were TSK G-6000-5000PWXL.

Sample	M_w **[mL/g]**
xan30	453
xanS	296
xan30pa	331

RMS Conformation Plot

The RMS conformation plots for the modified samples of xan30, xanS, and xan30pa, obtained by plotting RMS radius against molecular weight is presented in Figure 3.2.3. The RMS radius and molecular weights for each sample are determined by processing SEC-MALLS results in ASTRA. SEC-MALLS buffer was a solution of 0.15 M $NaNO_3$, 0.01 M EDTA and 20 % acetonitrile.

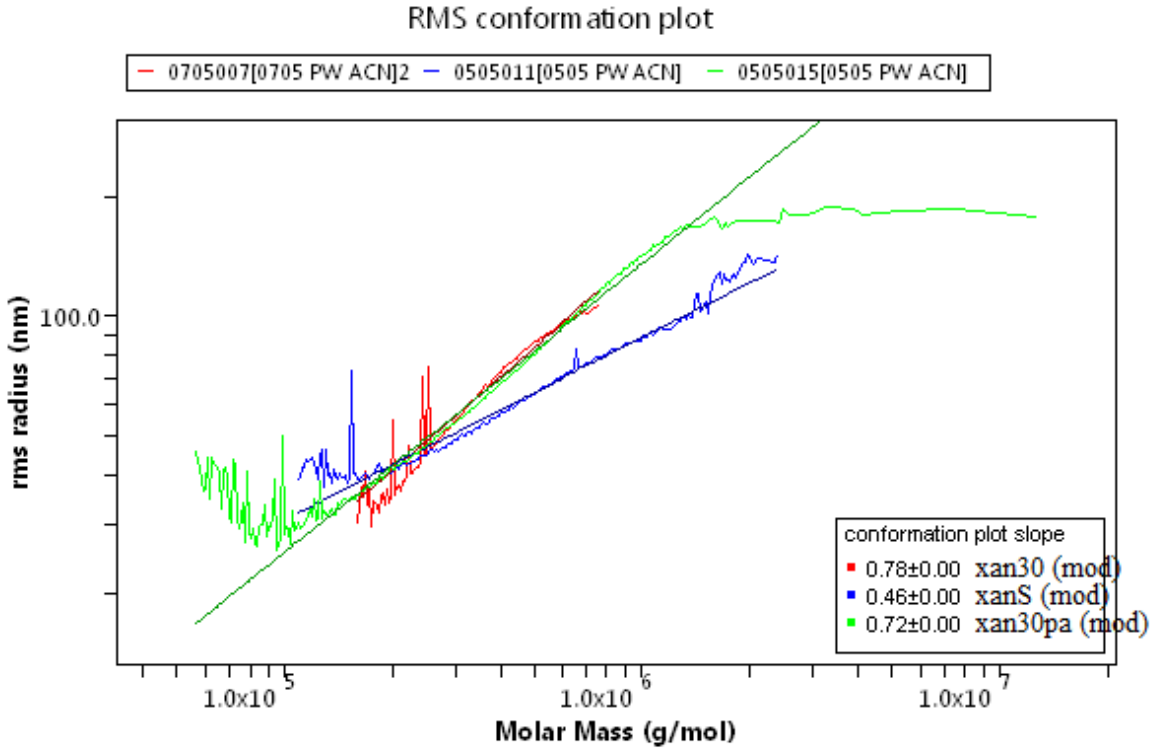

Figure 3.2.3: RMS conformation plots for the modified samples xan30 (red line), xanS (blue line) and xan30pa (green line), obtained from ASTRA. RMS radius is plotted against molecular weight, both are determined by SEC-MALLS. Buffer used for SEC-MALLS was 0.15 M $NaNO_3$, 0.01 M EDTA, and 20 % acetonitrile, and columns applied were TSK G-6000-5000PWXL.

The slopes of the linear regression lines for each sample, obtained from the RMS conformation plot in Figure 3.2.3, are presented in Table 3.2.4.

Table 3.2.4: Slopes obtained from RMS conformation plot in Figure 3.2.3 for the purified sonicated samples xan10, xan30, xan120 and xanS.

Sample	**Slope**
xan10	0.78 ± 0.00
xanS	0.46 ± 0.00
xan30pa	0.72 ± 0.00

The slopes from this RMS conformation plot show the same trend of conformations as the slopes for the non-modified samples of xan30, xanS, and xan30pa, see Table 3.1.2 and section 3.1.4. The modified xan30 sample is most rigid, followed by the acetyl and pyruvyl free xan30pa, and xanS. Again, it is seen that xanS has the most flexible conformation. The slope for xan30pa indicates that this sample has not changed its conformation, which is in accordance to the low grafting density.

Mark-Houwink-Sakurada Plot

As for the non-modified samples, Mark-Houwink-Sakurada plots were obtained for the modified samples of xan30, xanS, and xan30pa. The MHS plots were obtained by processing SEC-MALLS data with ASTRA. Both the intrinsic viscosities and the molecular weights were determined from SEC-MALLS. The plots are presented in Figure 3.2.4.

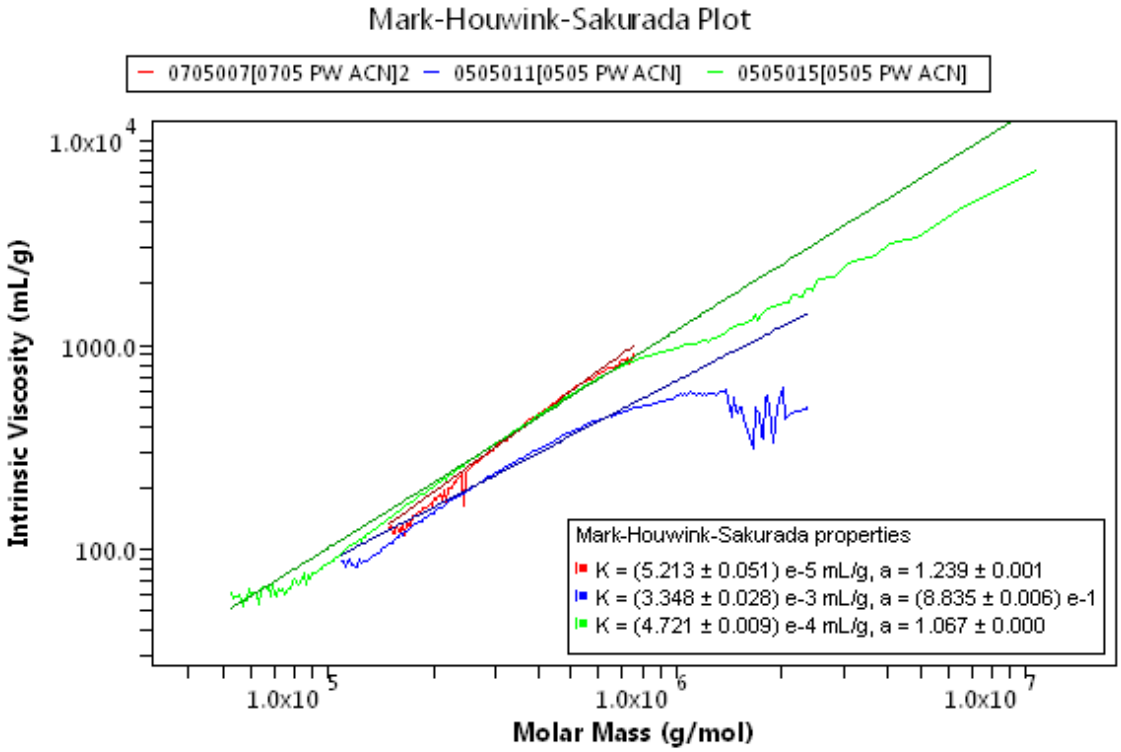

Figure 3.2.4: Mark-Houwink-Sakurada plots for modified samples of xan30 (red line), xanS (blue line), and xan30pa (green line). Buffer used for SEC-MALLS was 0.15 M $NaNO_3$, 0.01 M EDTA, and 20 % acetonitrile, and columns were TSK G-6000-5000PWXL.

The Mark-Houwink-Sakurada parameters, K and a, with standard deviations, for the modified xanthan samples xan30, xanS, and xan30pa samples are presented in Table 3.2.5.

Table 3.2.5: Mark-Houwink-Sakurada parameters, K and a, for the sonicated samples xan30, xanS and xan30pa, determined from processing SEC-MALLS data with ASTRA. SEC-MALLS was performed with columns TSK G-6000-5000PWXL, and buffer 0.15 M $NaNO_3$, 0.01 M EDTA and 20 % acetonitrile.

Sample	$\boldsymbol{K}$ **[mL/g]**	$\boldsymbol{a}$
xan30	$(5.213 \pm 0.051) \cdot 10^{-5}$	1.239 ± 0.001
xanS	$(3.348 \pm 0.028) \cdot 10^{-3}$	0.884 ± 0.001
xan30pa	$(4.721 \pm 0.009) \cdot 10^{-4}$	1.067 ± 0.000

The MHS exponent, a, implies that the modified xan30 and xan30pa are stiff coils, or nearly a rigid rods (Smidsrød and Moe, 2008). The MHS exponent of the modified xanS indicates that this sample is nearly a flexible coil (Smidsrød and Moe, 2008). As seen from the RMS conformation plot for the modified samples, xan30 is the most rigid, followed by xanS and xan30pa. The lower MHS exponent of acetyl and pyruvyl free xan30pa may be reasoned by the loss of acetyl and pyruvyl groups, which could have caused a slight change in the conformation, providing a more flexible xanthan chain.

3.2.3 Intrinsic Viscosity of Modified Purified Sonicated Xanthan Samples Determined by Single Capillary Viscometer

The intrinsic viscosities with standard deviations of the modified samples, $[\eta]$ are presented in Table 3.2.6. The intrinsic viscosities were determined by viscosity measurements with single capillary viscometer with wall shear rate 2500 s^{-1} at 20.0 °C with solvent 0.1 M NaCl, and calculated as an average of the intrinsic viscosity determined by the Huggins, Fuoss-Mead, Billmeyer, and the Hermann equations. Raw data, calculations, and standard deviations can be found in Appendix D, section D.3.

Table 3.2.6: Intrinsic viscosity of modified xanthan samples, $[\eta]$. The intrinsic viscosities were found by measurements with single capillary viscometer with wall shear rate 2500 s^{-1}, at temperature 20.0 °C, and 0.1 M NaCl as solvent.

Sample	$[\eta]$ **[mL/g]**
xan30	515
xanS	329
xan30pa	428

As for the non-modified xanthan samples, xan30 has the highest intrinsic viscosity, and xanS has the lowest. This may be explained by the apparent rigid conformation of xan30 and the more flexible conformation of xanS. A rigid conformation provides higher intrinsic viscosity than a flexible conformation, due to more interactions between the chains. The acetyl and pyruvyl free xan30pa has lower intrinsic viscosity than the xan30, which was also seen for the non-modified samples, and may have been caused by the removal of the acetyl and pyruvyl groups.

3.3 Comparison of Non-Modified and Modified Xanthan Samples

The molecular weight results and Mark-Houwink-Sakurada plots from SEC-MALLS, and intrinsic viscosities studied throughout the chapter are in this section presented as a comparison of non-modified and modified samples of xan30, xanS, and xan30pa.

3.3.1 SEC-MALLS

For all the results presented in this section, columns TSK G-6000-5000PWXL were applied. The buffer used for non-modified samples was 0.15 M $NaNO_3$ and 0.01 M EDTA, while for the modified samples the buffer in addition contained 20 % acetonitrile.

Molecular Weight

An overview of the molecular weights obtained by SEC-MALLS analyses of the non-modified and modified samples, $M_{w,i}$ and $M_{w,m}$, respectively, for xan30, xanS, and xan30pa, is presented in Table 3.3.1. Note that the molecular weights of xan30 and xanS are not determined at the same date as the molecular weights presented in Table 3.1.1. The difference in the molecular weight are most likely caused by use of different columns. The molecular weights are calculated as the average of the molecular weights determined by SEC-MALLS. An overview of the SEC-MALLS results with uncertainties is given in Table F.2.1 in Appendix F.

Table 3.3.1: The molecular weights before and after modification, $M_{w,i}$ and $M_{w,m}$, respectively, for xanthan samples xan30, xanS, and xan30pa. Buffer used for non-modified samples was 0.15 M $NaNO_3$ and 0.01 M EDTA, while for the modified samples the buffer in addition contained 20 % acetonitrile. Columns were TSK G-6000-5000PWXL.

Sample	$\boldsymbol{M_{w,i}}$ **[mL/g]**	$\boldsymbol{M_{w,m}}$ **[mL/g]**
xan30	390*	453
xanS	319*	296
xan30pa	337	331

*Note that these molecular weights were determined at a different date and with different column than the ones presented in Table 3.1.1.

From the table it is seen that for the sample xan30 there is an increase in the molecular weight due to modification, while for xanS and xan30pa the molecular weights seem to decrease. A small increase in the molecular weight would be expected, since octylamine is grafted onto the xanthan molecules, thus providing a higher molecular weight. For xan30pa, the acetyl and pyruvyl free sample, the molecular weight would be expected to be near unchanged, due to the low grafting density. This may be in accordance to the results in Table 3.3.1; the molecular weight only decreases from 337 to 331 kDa, thus it may be concluded that there is no prominent change in the molecular weight of this sample. For xanS the molecular weight also seems to decrease due to modification. The grafting density of the modified xanS was in the same range as that of the modified xan30, thus the molecular weight would be expected to increase. The reason for the apparent decrease in molecular weight may be due to uncertain results caused by interactions between the SEC column material and the hydrophobic xanthan sample.

Mark-Houwink-Sakurada Plots

Comparisons of Mark-Houwink-Sakurada (MHS) plots for the non-modified and modified samples of xan30, xanS, and xan30pa are presented in Figures 3.3.1, 3.3.2, and 3.3.3,

respectively. Both the intrinsic viscosities and molecular weights applied in these plots were obtained from SEC-MALLS analysis.

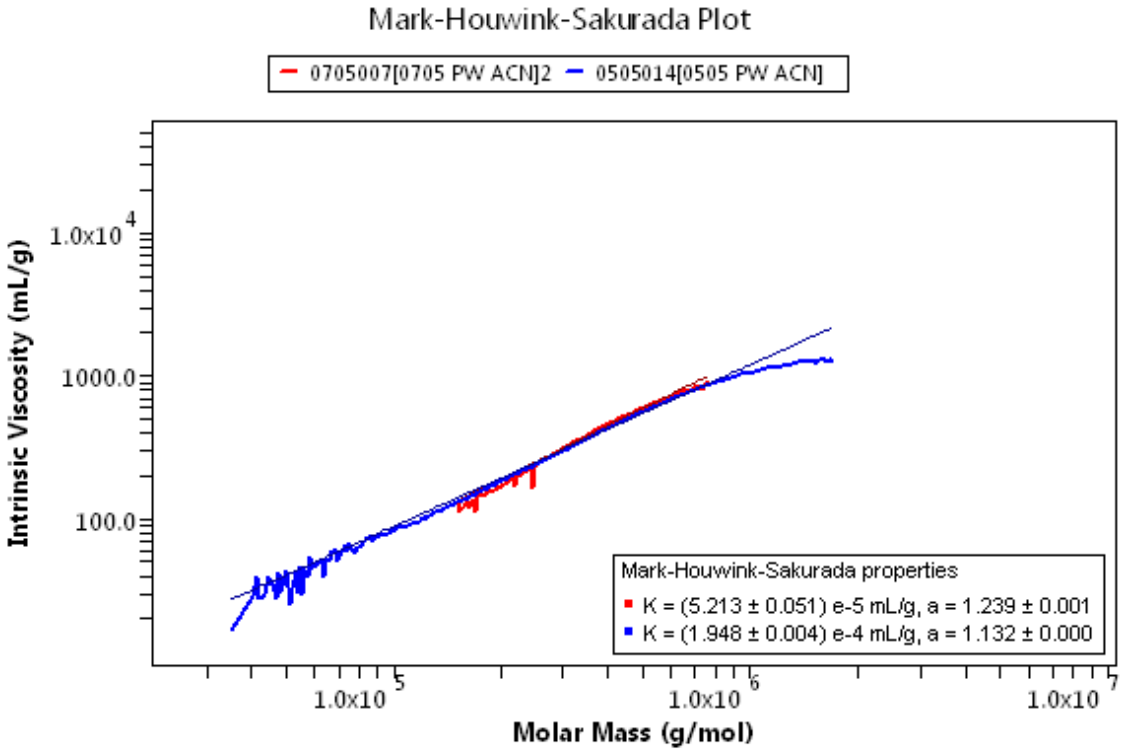

Figure 3.3.1: Mark-Houwink-Sakurada plot for non-modified and modified xan30, blue and red line, respectively. The plot was obtained from processing SEC-MALLS results with ASTRA. Buffer used for SEC-MALLS was 0.15 M $NaNO_3$ and 0.01 M EDTA for the non-modified sample, and 0.15 M $NaNO_3$, 0.01 M EDTA and 20 % acetonitrile for the modified sample. Applied columns were TSK G-6000-5000PWXL.

It is seen from Figure 3.3.1 that for xan30 there is a small increase in the MHS exponent, a, from 1.132 to 1.239 as a consequence of modification, thus there might have been a small change in the conformation of the xanthan chains, giving a more rigid structure of the modified sample. Based on previously discussed variations in the results of the modified samples due to low mass recoveries in SEC-MALLS, and the difference being quite small, it may be concluded that the sample seems to maintain its conformation during modification, although it may also have become slightly more rigid. The values of the exponent indicates that both the non-modified and the modified xan30 are stiff coils, or nearly rigid rods (Smidsrød and Moe, 2008).

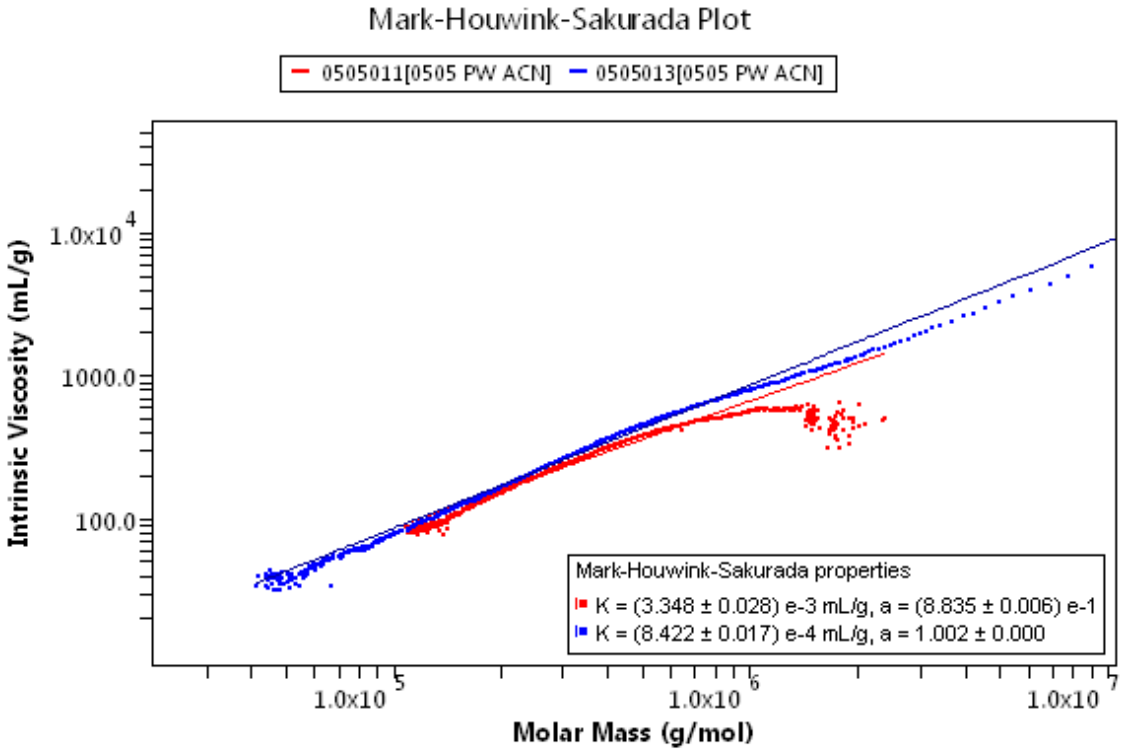

Figure 3.3.2: Mark-Houwink-Sakurada plot for non-modified and modified xanS blue and red line, respectively. The plot was obtained from processing SEC-MALLS results with ASTRA. Buffer used for SEC-MALLS was 0.15 M $NaNO_3$ and 0.01 M EDTA for the non-modified sample, and 0.15 M $NaNO_3$, 0.01 M EDTA and 20 % acetonitrile for the modified sample. Applied columns were TSK G-6000-5000PWXL.

From Figure 3.3.1 it is observed that there is a small decrease in the MHS exponent, a, from 1.002 to 0.884. As for the xan30 sample, it applies that the results for the modified samples are variable, thus a definite conclusion can not be made. Although, if the results are assumed to be correct, the xanthan chains of the sample xanS may have obtained a more flexible conformation after modification. A reason for this could be that the non-modified xanS appeared to be more flexible, thus grafting of octylamine may have caused further flexibility of the conformation.

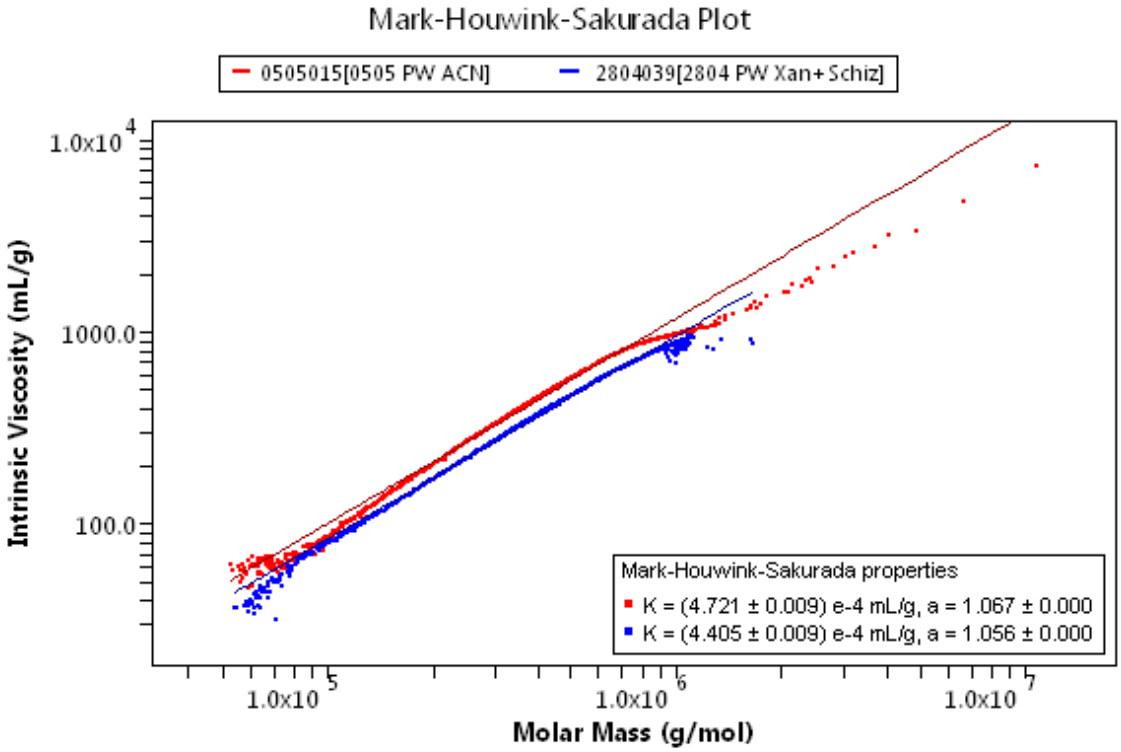

Figure 3.3.3: Mark-Houwink-Sakurada plot for non-modified and modified xan30pa blue and red line, respectively. The plot was obtained from processing SEC-MALLS results with ASTRA. Buffer used for SEC-MALLS was 0.15 M $NaNO_3$ and 0.01 M EDTA for the non-modified sample, and 0.15 M $NaNO_3$, 0.01 M EDTA and 20 % acetonitrile for the modified sample. Applied columns were TSK G-6000-5000PWXL.

From Figure 3.3.1 it is seen that for the acetyl and pyruvyl free sample xan30pa the MHS exponent, a, is nearly identical for the non-modified and modified samples, it only varies from 1.056 to 1.067. Thus, it is reasonable to believe that this sample does not change its conformation during modification, which can be reasoned by the low grafting density; less amount of octylamine bound to the xanthan causes less change of the xanthan chain conformation.

3.3.2 Intrinsic Viscosity

An overview of the intrinsic viscosities for the non-modified and modified xanthan samples are presented in Table 3.3.2. The intrinsic viscosities were determined as an average of the intrinsic viscosities calculated by Huggins, Fuoss-Mead, Billmeyer, and Hermann equations. Raw data, calculated values and standard deviations are given in Appendix D, sections D.2 and D.3.

Table 3.3.2: Intrinsic viscosity before and after modification, $[\eta]_i$ and $[\eta]_m$, respectively. The intrinsic viscosities were determined by measurements with single capillary viscometer with wall shear rate 2500 s^{-1} at 20.0 °C with buffer 0.1 M NaCl.

Sample	$[\eta]_i$ [mL/g]	$[\eta]_m$ [mL/g]
xan30	385	515
xanS	257	329
xan30pa	382	428

In order to compare the differences in viscosity behaviour for each of the non-modified and modified xanthan samples, Huggins' plots were obtained by plotting the specific viscosities over concentration, η_{sp}/c, against the concentration, for both the non-modified and the modified xanthan sample. The Huggins' plots for xan30, xan30pa, and xanS are presented in Figure 3.3.4, 3.3.5, and 3.3.6, respectively. In each plot, the blue line represents the non-modified sample, while the red line represents the modified sample.

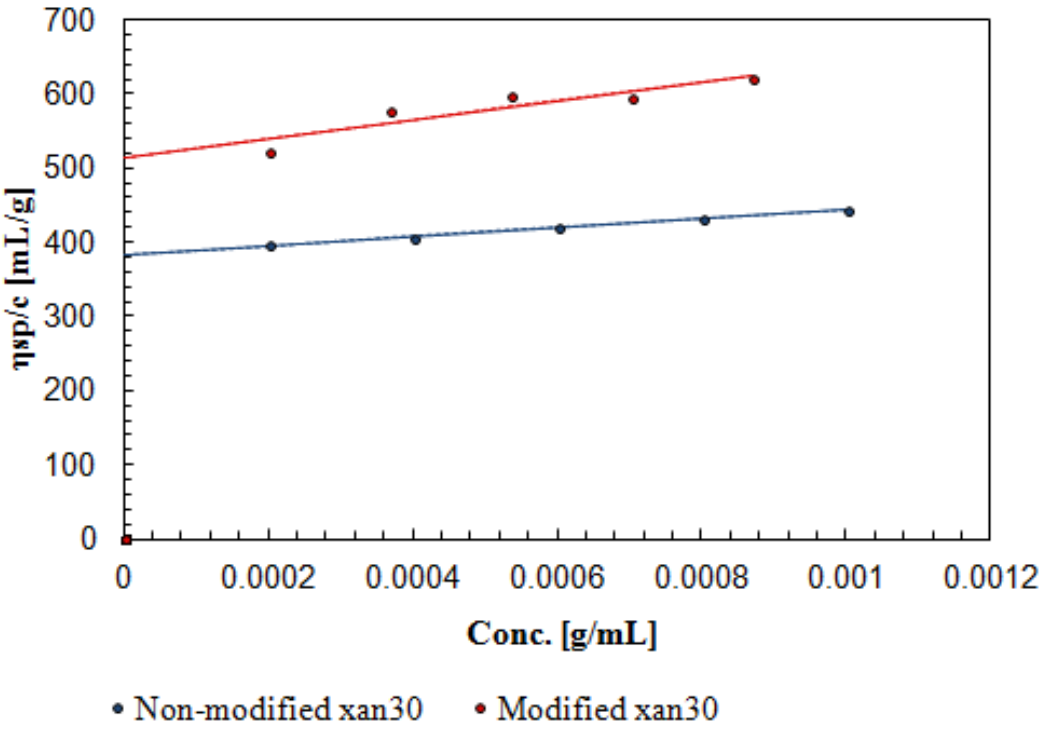

Figure 3.3.4: Huggins plot for non-modified and modified xan30, blue and red line, respectively. The specific viscosities are determined by viscosity measurements with single capillary viscometer. The shear rate at the wall was 2500 s^{-1}, the measurement temperature was 20.0 °C, and the solvent was 0.1 M NaCl.

From the figure it is seen that there is a clear difference in the specific viscosities, and thus the intrinsic viscosity, for the non-modified and the modified samples of xan30. There

is also a tendency of increasing difference as the concentration of the xanthan solution increases, the regression line for the modified sample has a steeper slope than for the non-modified. This may be explained by increasing interactions between hydrophobic groups as the concentration increases, i.e. association of the hydrophobic groups, which provides an increase in the hydrodynamic radius, hence increased solution viscosity.

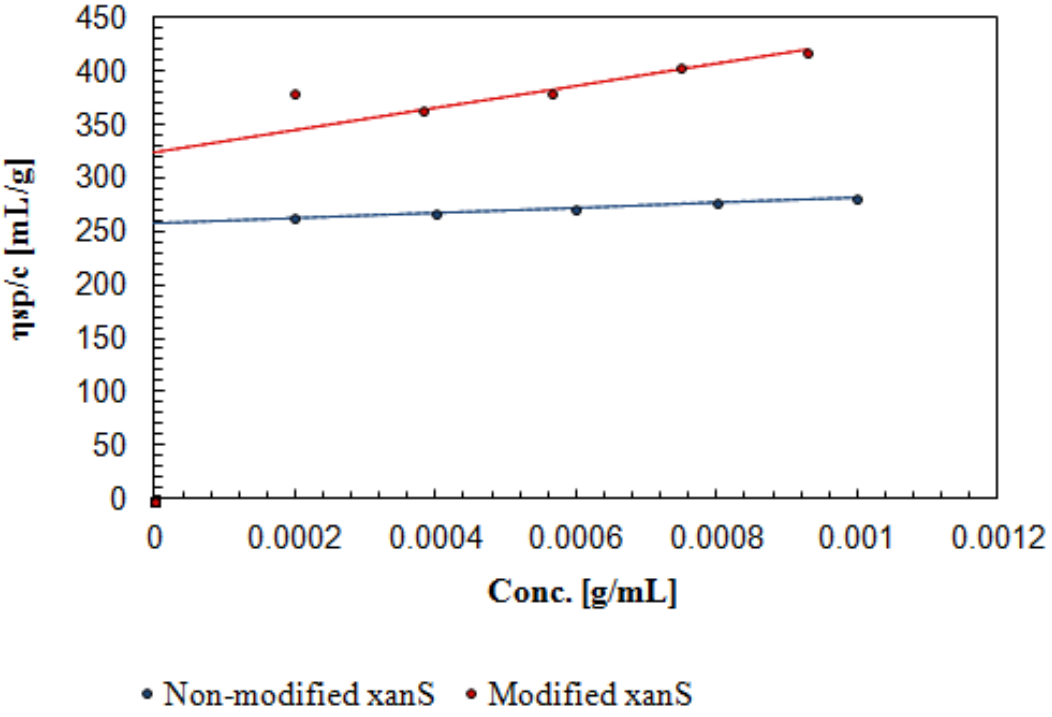

Figure 3.3.5: Huggins plot for non-modified and modified xanS, blue and red line, respectively. The specific viscosities are determined by viscosity measurements with single capillary viscometer. The shear rate at the wall was 2500 s^{-1}, the measurement temperature was 20.0 °C, and the solvent was 0.1 M NaCl. The results for the lowest concentration of modified xan30pa is not included in the regression.

Similar to the xan30 samples, it is seen from Figure 3.3.5 that there is a clear difference in η_{sp}/c, and thus the intrinsic viscosity, for the non-modified and the modified xanS samples. Here the tendency of increasing difference in specific viscosity as the concentration of the xanthan solution increases is more evident than for xan30. A reason for this could be that the xanS sample has through all the analyses in this project appeared to be more flexible than the xanthan samples prepared from Kelzan XCD, thus the hydrophobic groups have higher capability to interact with each other, providing association of the these groups, and thereby cause higher viscosity of the solution, and higher intrinsic viscosity of the xanthan molecules.

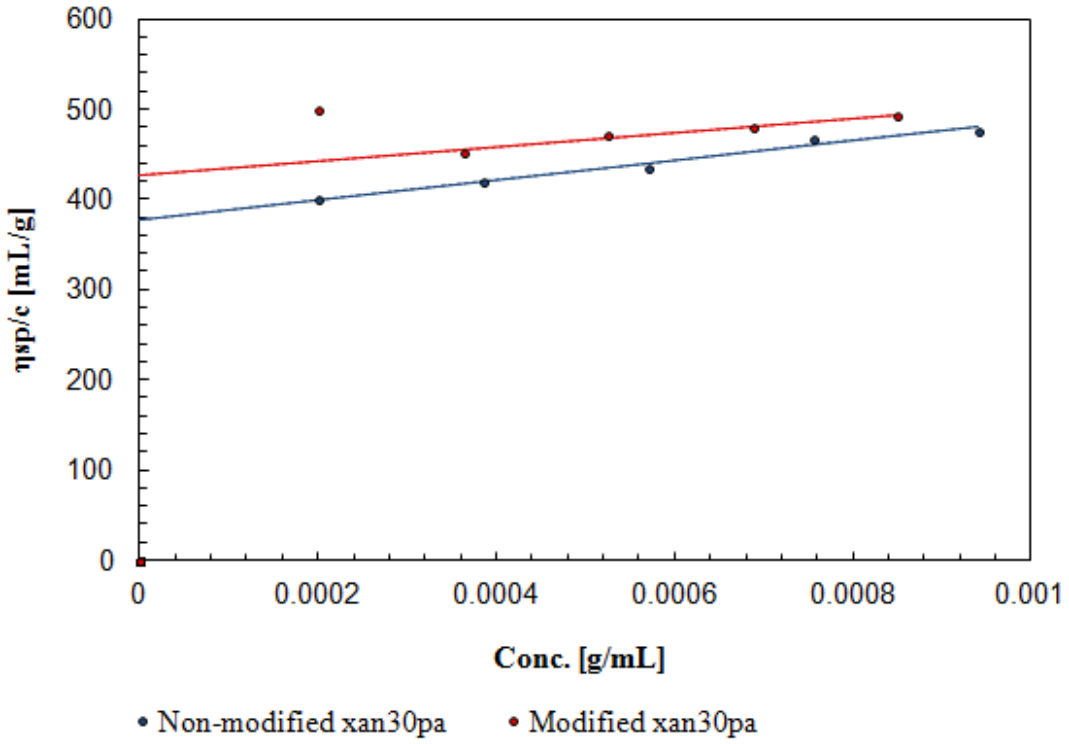

Figure 3.3.6: Huggins plot for non-modified and modified acetyl and pyruvate free sample xan30pa, blue and red line, respectively. The specific viscosities are determined by viscosity measurements with single capillary viscometer. The shear rate at the wall was 2500 s^{-1}, the measurement temperature was 20.0 °C, and the solvent was 0.1 M NaCl. The measurements for the lowest concentration of modified xan30pa is not included in the regression.

The difference in specific viscosities, and the intrinsic viscosity, for the non-modified and modified acetyl and pyruvyl free xan30pa samples is not as large as for the xan30 samples. This may be explained by the low grafting density of xan30pa. Due to less grafting of octylamine, the modified xan30pa do not have as many hydrophobic groups that can interact with each other, and the xanthan molecules do not change their conformation to the same extent, as the xan30 and xanS samples, with acetyl and pyruvyl groups intact. Thus the intrinsic viscosity will maintained at the same level as for the non-modified xan30pa. The same tendency was seen in the MHS plot in Figure 3.3.3.

As seen from Table 3.3.2 and Figure 3.3.4 to 3.3.6, the intrinsic viscosity increases as a consequence of modification for all the modified samples xan30, xanS, and xan30pa. According to the theory (Peiffer et al., 1986) the viscosity typically would decrease for hydrophobically modified polysaccharides. An increase in viscosity may indicate that the polymers have changed their conformation, or that there were interactions of cross-linking between the xanthan chains if the concentrations of the analysed samples were over the critical overlap concentration (Wang et al., 1988). The increased viscosity may indicate

that there were association of the hydrophobic groups of the modified xanthan samples, thus providing a higher hydrodynamic radius and a higher intrinsic viscosity.

Shear Rate Dependency of Intrinsic Viscosity

In order to study the dependence of intrinsic viscosity of the xanthan samples, there was performed an experiment with a four-bulb shear dilution viscometer for the non-modified and the modified samples of xan30. The intrinsic viscosities were calculated both by the Huggins and the Fuoss-Mead method at each shear rate, shown in Tables 3.3.3 and 3.3.4, and Figures 3.3.7 and 3.3.8. The raw data for non-modified and modified xan30 are presented in sections E.1 and E.2, respectively, in Appendix E. The viscosities at zero shear rate were determined for the non-modified and the modified sample xan30, by extrapolation to zero shear.

Table 3.3.3: Intrinsic viscosity for non-modified xan30, determined by use of four-bulb shear dilution viscometer. Both the intrinsic viscosity calculated by the Huggins and the Fuoss-Mead method are given. The viscosity at shear rate 2500 s^{-1} is determined from measurements with the single capillary viscometer. All shear rates are at the wall. The measurement temperature for all viscosity measurements was 20.0 °C.

Shear rate [s^{-1}]	**[η] [mL/g] Huggins**	**[η] [mL/g] Fuoss-Mead**
713	630	631
427	683	676
273	758	738
158	858	814
2500	384	385

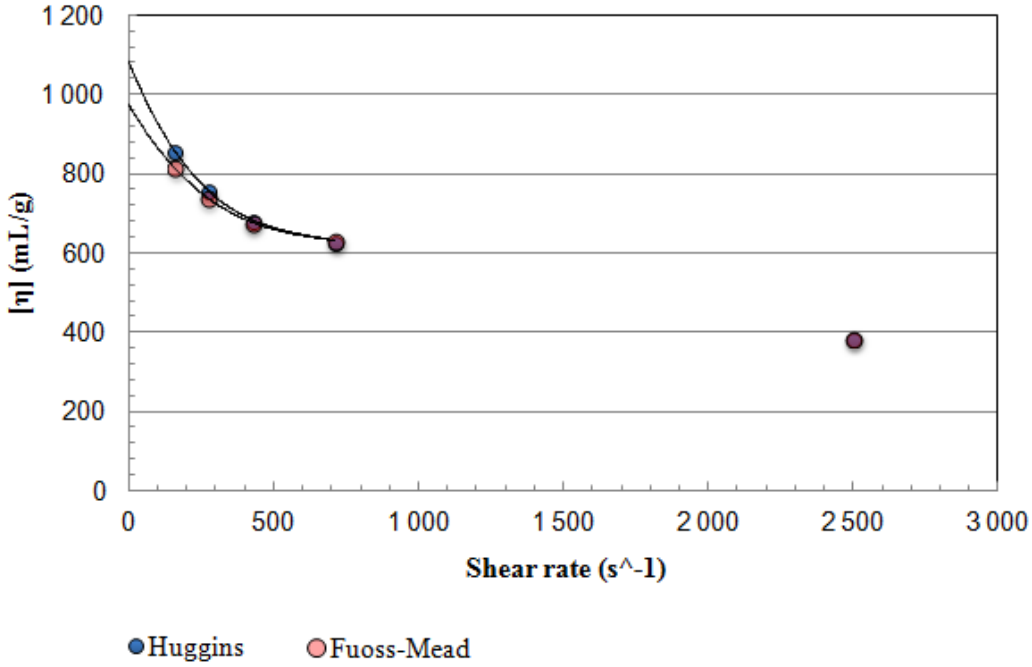

Figure 3.3.7: Intrinsic viscosity plotted against wall shear rate. The results are obtained from measurements of the non-modified xan30 sample with four-bulb shear dilution viscometer. The point at 2500 s^{-1} represents the intrinsic viscosity determined by the single capillary viscometer. The measurement temperature for all viscosity measurements was 20.0 °C, and the solvent was 0.1 M NaCl.

From Figure 3.3.7 it can be seen that the intrinsic viscosity of xan30 is dependent on shear rate, and that the sample is shear thinning, as the intrinsic viscosity decreases with increasing shear rate. The intrinsic viscosity at zero shear determined by Huggins is 900 mL/g, and by Fuoss-Mead 1100 mL/g. Both of these values are significantly higher than the intrinsic viscosity of non-modified xan30 determined by the single capillary viscometer. It is also observed that the intrinsic viscosity determined by the single capillary viscometer does not fit with the curve obtained from the intrinsic viscosities determined from the four-bulb shear dilution viscometer. A reason for this could be incorrect calibration of one of the viscometers. It is also observed that the curve show a tendency to flatten out at the highest shear rate of the four-bulb viscometer, which could be caused by incorrect calibration of the bulb with the highest shear rate. Also, the difference in intrinsic viscosity calculated by Huggins equation and Fuoss-Mead tend to increase at lower shear rates, which may be caused by pollutions in the xanthan solution.

Table 3.3.4: Intrinsic viscosity for modified xan30, determined by use of four-bulb shear dilution viscometer. Both the intrinsic viscosity calculated by the Huggins and the Fuoss-Mead method are given. The viscosity at shear rate 2500 s^{-1} is determined from measurements with the single capillary viscometer. All shear rates are at the wall. The measurement temperature for all viscosity measurements was 20.0 °C, and the solvent was 0.1 M NaCl.

Shear rate [s^{-1}]	**[η] [mL/g] Huggins**	**[η] [mL/g] Fuoss-Mead**
713	475	477
427	492	495
273	539	537
158	557	557
2500	514	515

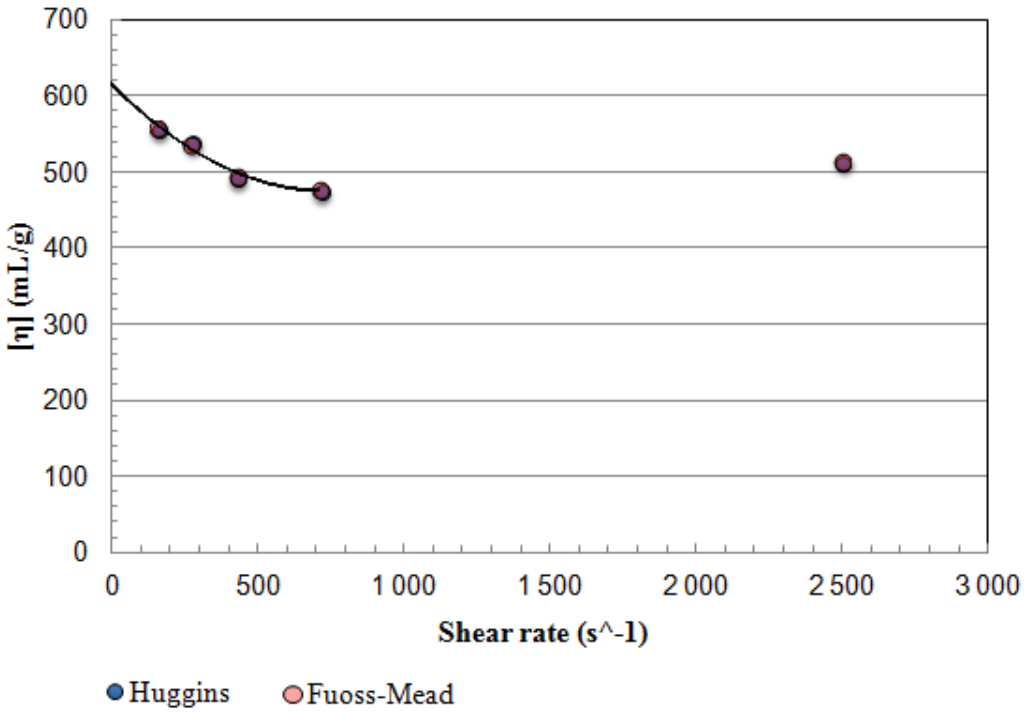

Figure 3.3.8: Intrinsic viscosity plotted against wall shear rate. The results are obtained from measurements of the modified xan30 sample with four-bulb shear dilution viscometer. The point at 2500 s^{-1} represents the intrinsic viscosity determined by the single capillary viscometer. The measurement temperature for all viscosity measurements was 20.0 °C.

From Figure 3.3.8 it can be seen that the intrinsic viscosities for the modified xan30 also is dependent on the shear rate, and that the sample is shear thinning. The intrinsic viscosities determined by the Huggins and Fuoss-Mead methods are in accordance with each other, and the intrinsic viscosity at zero shear is 620 mL/g, which is significantly higher than the intrinsic viscosity for modified xan30 determined by measurements with the single capillary viscometer. It is also seen that the intrinsic viscosity determined from

measurements with the single capillary viscometer with shear rate 2500 s^{-1} does not fit with the intrinsic viscosities determined by the four-bulb viscometer. The reason for this may be incorrect calibration of the viscometer.

The results from the four-bulb viscometer actually shows the opposite tendency of intrinsic viscosity of the non-modified and modified xan30 compared to the results from the single capillary viscometer, see Table 3.3.2. The reason for this is not known, and all of the non-modified and modified should be analysed with the four-bulb shear dilution viscometer, in order to obtain reliable results.

Chapter 4

General discussion

4.1 Depolymerisation of Xanthan by Sonication

Sonication was shown to be a good method for depolymerising of xanthan chains. The sonication of xanthan had most decreasing effect on the molecular weight and the intrinsic viscosity in the beginning, then the decrease tend to flatten out as the sonication time increases. The reason for this may be that the xanthan chains are longest in the beginning, thereby easier to break. As the chains are cut into smaller parts, they will be harder and harder to depolymerise, thus longer sonication time is necessary in order to depolymerise shorter chains. This trend was seen both by the decrease in molecular weight and intrinsic viscosity. The dependency of intrinsic viscosity of molecular weight was in good accordance to previous results (Sato et al., 1984).

4.2 Conformation of Non-Modified Purified Sonicated Xanthan

Both the RMS conformation plots and the Mark-Houwink-Sakurada plots obtained from SEC-MALLS showed that the purified, sonicated, non-modified xanthan samples behave like rigid rods, or stiff coils. It is previously shown that short xanthan molecules are more rigid than longer xanthan molecules (Sato et al., 1984), but here the sample xan120 with the longest sonication time, thus lowest molecular weight, seemed to be less rigid than xan10 and xan30 with sonication times 10 and 30 minutes, respectively. This may be explained by the high mechanical and chemical forces the samples are exposed to during the sonication. If samples with even longer sonication times had been prepared, it may be that after a particular time, when size of the xanthan molecules are sufficiently reduced, the increase of flexibility of the xanthan chains will stop, and they will become more and

more rigid.

Throughout the results the xanS sample, which was prepared from the Statoil xanthan, has appeared to be more flexible than the samples xan10, xan30, and xan120, prepared from Kelzan XCD. A reason for this may be that this sample was prepared from another start xanthan, or that the conformation was changed during sonication due to high temperature, which may have caused a conformational change from rigid to more flexible.

The acetyl and pyruvyl free sample xan30pa, prepared from xan30, was showed to have less rigid conformation than xan30. The reason for this may be the removal of the acetyl and pyruvyl groups, which could have caused a change in the xanthan chain conformation.

4.3 Depolymerisation by H_2O_2 and NaOH of Xanthan for ^{1}H-NMR

The depolymerisation reaction by H_2O_2 and NaOH prior to the ^{1}H-NMR analysis causes removal of both mannose and glucuronic acid which can be explained by an attack of the inner α-D-mannose, hence a removal of the whole side chain (Christensen et al., 1996). This was shown by analysing samples with known contents of α-D-mannose, and by determination of the molecular weights of xanS at different times during the depolymerisation. The calculated contents of α-D-mannose were higher than the given values, thus the peak of the H-1 on the α-D-mannose cannot be used as an internal reference for calculations of the degree of substitutions of acetyl and pyruvyl, neither the grafting density of octylamine of the modified xanthan samples. By SEC-MALLS analyses it was seen that the molecular weight was nearly unchanged during the depolymerisation, thus the xanthan backbone were probably not degraded. In order to perform calculations an external reference, TSP, had to be used. As a consequence, the calculated degrees of substitution and grafting densities may be inaccurate, due to uncertainties in the amounts of both TSP and xanthan solution transferred into the NMR tubes. A solution to this problem could be enzymatic depolymerisation of the molecules, with enzymes that cleaves the β-1,4 linkages between the glucose units of the xanthan backbone. This may be obtained by applying enzymes such as cellulases (Rinaudo and Milas, 1980). If a method for breaking only the β-1,4 linkages in the backbone of the xanthan is achieved, the H-1 α-D-mannose peak of the ^{1}H-NMR spectra may be used as an internal reference, thus all calculations based on ^{1}H-NMR results will be considerably easier and more accurate.

4.4 Grafting Density of Modified Xanthan

The grafting densities of the modfied xanthan samples were determined by ^{1}H-NMR spectroscopy.

By determining the grafting densities for two test modifications, with the grafting reaction of octylamine (the second step in the modification reaction) performed at 4 °C and room temperature, respectively, it was seen that the grafting density was not dependent on the temperature during grafting of octylamine onto the xanthan. Hence, in order to prevent a conformational transition of the xanthan during the modification process, to a disordered state, the grafting of octylamine was performed at 4 °C for the purified sonicated samples xan30, xanS, and xan30pa. Reliable results were only obtained for the second test modification, due to difficulties transferring the xanthan solutions into NMR tubes.

The grafting densities for modified xan30 and xanS were in the same range. It was for the first time showed that the modified acetyl and pyruvyl free sample xan30pa had a significantly lower grafting density, less than half of the grafting density for xan30, indicating that at more than half of the octylamine is grafted onto the carboxylic acid group at the pyruvyl group of the outer β-D-mannose. The reason for this may be that the carboxylic acid on the pyruvyl group is more accessible for the octylamine than the acid group of the glucuronic acid is, since it is located at the very end of the side chain.

4.5 Conformation of Modified Purified Sonicated Xanthan

For the modified purified sonicated xanthan samples of xan30, xanS, and xan30pa, the trend of conformation was the same as for the non-modified samples. The modified xan30 was the most rigid sample, followed by the modified xan30pa and xanS. Again, xanS had the most flexible conformation, as shown for the non-modified xanS sample. The modified xan30pa was less rigid than the modified xan30, which also was seen for the non-modified samples, and may be explained by the removal of acetyl and pyruvyl groups.

By comparing the Mark-Houwink-Sakurada plots of the non-modified and modified samples xan30, xanS, and xan30pa, it was seen that xan30 seemed to obtain a more rigid conformation as a consequence of modification by octylamine. The conformation of xanS was found to become more flexible after the modification. The reason for this may be that this sample was not as rigid as xan30 before modification, thus grafting of octylamine could have increased the flexibility further. The xan30pa was shown to not change its

conformation, which can be explained by its low grafting density, thus few hydrophobic groups available for interactions.

4.6 SEC-MALLS Analysis of Modified Xanthan

The modified xanthan samples gave very low mass recoveries during SEC-MALLS analyses when using a buffer of 0.15 M $NaNO_3$ and 0.01 M EDTA. The reason is probably that the hydrophobic samples interacts with the column materials. As an attempt to improve the mass recoveries acetonitrile was added to the buffer, to give a concentration of 20 %. There was observed some increase of the mass recoveries, but the values were still not satisfactory. The modified sample that obtained the highest mass recovery was, not unexpected, the acetyl and pyruvyl sample xan30pa. This is most likely due to the low grafting density of octylamine; this sample was less hydrophobic than xan30 and xanS, hence it did not bind to the column material to the same extent.

4.7 Intrinsic Viscosity of Non-Modified and Modified Sonicated Purified Xanthan

From measurements with single capillary viscometer it was seen that the intrinsic viscosities for the modified purified sonicated xanthan samples were higher than that of the non-modified purified sonicated samples. Theoretically, the intrinsic viscosity would decrease for the modified samples (Peiffer et al., 1986), due to intramolecular interactions of the hydrophobic groups, forming aggregates; that is if the conformation is not changed. But as shown in this project, the conformation of the xanthan samples changed during modification, thus this may be a reason for the increased intrinsic viscosities. Another reason may be that the concentrations of the analysed xanthan samples were over the critical overlap concentration. For such cases it has previously been shown that the intrinsic viscosity of modified polymers can exceed that of the non-modified (Wang et al., 1988), due to interactions of cross-linking between the chains. This may indicate that the xanthan samples were associative.

The increase in intrinsic viscosity was largest for xan30. From the RMS conformation plots of non-modified and modified xan30 it could be seen that the conformation appeared to be more flexible after modification. This may explain the increased intrinsic viscosity, due to interactions between the hydrophobic groups. However, from the MHS plots, it was seen that the conformation appeared to be more rigid. The reason for these varying results for the modified sample may be caused by the low mass recoveries seen from

the SEC-MALLS analyses of the modified xanthan samples. The intrinsic viscosity of xanS was not changed to the same extent as for xan30, but this sample also showed a prominent increase in intrinsic viscosity after modification. Also, for xanS, the increase in η_{sp}/c with increasing concentration was larger than for xan30, which may be explained by increased interactions between xanthan chains as the xanthan concentration of the solution increases. The increase of intrinsic viscosity of the acetyl and pyruvyl free sample xan30pa was considerably lower than for xan30 and xanS, which may be explained by the low acetyl and pyruvyl content.

For xan30 it was seen that the intrinsic viscosity was dependent on shear rate, by measurements with a four-bulb shear dilution viscometer. Both the non-modified and the modified sample appeared to be shear thinning. From intrinsic viscosity measurements by the four-bulb shear dilution viscometer at different shear rates, the intrinsic viscosities at zero shear were found to be higher both for the non-modified and the modified xan30, than for measurements with the single capillary viscometer. Hence, the relationship between the intrinsic viscosities and the molecular weight after sonication may not fit as nicely with the literature (Sato et al., 1984), as first thought, and shown in Figure 3.1.7. Also, the intrinsic viscosity at zero shear of the modified xan30 appeared to be lower than that for the non-modified xan30.

In order to validate the results, viscosity measurements with both the single capillary viscometer and the four-bulb shear dilution viscometer should be performed several times. In addition, the viscosity at different shear rates should be determined for all of the sonicated non-modified and modified samples. In that manner, it would be possible to see if the viscosity is lower for all of the modified samples when performing the measurements with the four-bulb shear dilution viscometer.

4.8 Further Work

The intrinsic viscosity measurements with single capillary viscometer should be repeated, in order to validate the results. In addition the intrinsic viscosity at different shear rates, by measurements with the four-bulb shear dilution viscometer, should be repeated, and also performed for all the non-modified and modified xanthan samples in order to determine if there was an error with the xan30 sample studied in this project.

There should be developed an improved method for depolymerisation of samples to be analysed by ^{1}H-NMR, that do not influence the side chains of the xanthan. The depolymerisation should only provide breakage of the β-1,4 bonds between the glucose units in the backbone. Enzymes are shown to have this desired effect, and initially cellulase could be introduced.

Regarding analysis of hydrophobic xanthan samples with SEC-MALLS, there should be developed a buffer that prevents the molecules from interacting with the column material. Except acetonitrile, methods for achieving this were not studied, due to time limitation. A buffer containing cyclodextrin could be attempted.

Chapter 5

Conclusions

Sonication of xanthan samples was shown to have a good effect on decreasing the molecular weight and the intrinsic viscosity of the xanthan molecules, providing molecules of sizes suitable for analyses by SEC-MALLS, intrinsic viscosity measurements, and ^{1}H-NMR.

RMS conformation plots of the purified sonicated xanthan samples prepared from Kelzan XCD indicated that the conformation was not changed during shorter sonication times, but longer sonication time caused a slightly more flexible xanthan, due to mechanical and chemical forces, or too high temperature during sonication. The xanthan sample prepared from xanthan provided by Statoil had a more flexible conformation throughout all of the analyses, which may have been caused by too high temperature during sonication, or the fact that it was prepared from a different xanthan.

It was shown that during depolymerisation of xanthan by H_2O_2 and NaOH prior to ^{1}H-NMR analysis the side chains were cut off, rather than breaking the β-1,4 linkages between the glucose units in the xanthan backbone.

The chemical modification of xanthan by grafting of octylamine gave grafting densities that were in accordance to recently found results. By comparing the grafting densities determined from ^{1}H-NMR of a xanthan sample without acetyl and pyruvyl groups and samples with these groups intact, it was for the first time shown that more than half of the octylamine binds to the β-D-mannose of the pyruvyl group.

From Mark-Houwink-Sakurada plots of the non-modified and the modified xanthan samples it was seen that for xan30 hydrophobical modification provided a more rigid conformation, while from RMS conformation plots it was seen that modification caused a more flexible structure. These varying results may be due to interactions between the hydrophobic xanthan and the SEC-MALLS columns material. The modified xanS appeared to be more flexible than the non-modified xanS, seen both by RMS conformation plots and MHS plots. From MHS plots and RMS conformation plots of non-modified and

modified xan30pa it was not seen a change of conformation, which is in accordance to its low grafting density.

By measurements of non-modified and modified sonicated xanthan samples with a capillary viscometer it was seen that the intrinsic viscosity increased as a consequence of modification with octylamine. The increase was less for the acetyl and pyruvyl free sample, which may be explained by its low grafting density.

However, by determination of intrinsic viscosity at different shear rates by a four-bulb shear dilution viscometer, of the non-modified and modified xan30, it was seen that the xanthan was shear thinning, and had a higher intrinsic viscosity at zero shear than determined with the single capillary viscometer. It was also observed that the viscosity at zero shear decreased during modification, which is the opposite of the trend found by measurements with the single capillary viscometer. A good explanation to this was not found, but one reason may be pollution of one of the solution, or change in conformation. In order to obtain more reliable results for intrinsic viscosity, measurements with both the single capillary viscometer and the four-bulb shear dilution viscometer should be performed for all the non-modified and the modified xanthan samples.

References

Bejenariu, A., Popa, M., Dulong, V., Picton, L., and Le Cerf, D. (2009). Trisodium trimetaphosphate crosslinked xanthan networks: synthesis, swelling, loading and releasing behaviour. *Polymer Bulletin*, 62(4):525–538.

Benoiton, N. L. and Chen, F. M. F. (1981). 2-alkoxy-5(4h)-oxazolones from n-alkoxycarbonylamino acids and their implication in carbodiimide-mediated reactions in peptide synthesis. *Canadian Journal of Chemistry*, 59(2):384–389.

Bergey, D. and Holt, J. (1994). *Bergey's Manual of Determinative Bacteriology*. Williams & Wilkins.

Billmeyer, F. W. (1949). Methods for estimating intrinsic viscosity. *Journal of Polymer Science*, 4(1):83–86.

Biswas, S., Vaze, O. S., Movassaghian, S., and Torchilin, V. P. (2013). *Polymeric Micelles for the Delivery of Poorly Soluble Drugs*, pages 411–476. John Wiley & Sons Ltd.

Bradshaw, I., Nisbet, B., Kerr, M., and Sutherland, I. (1983). Modified xanthan—its preparation and viscosity. *Carbohydrate Polymers*, 3(1):23–38.

Cains, P. W., Martin, P. D., and Price, C. J. (1998). The use of ultrasound in industrial chemical synthesis and crystallization. 1. applications to synthetic chemistry. *Organic Process Research & Development*, 2(1):34–48.

Carey, F. (2008). *Organic Chemistry*. McGraw-Hill Higher Education.

Chang, H. L. (1978). Polymer flooding technology yesterday, today, and tomorrow. *Journal of Petroleum Technology*, 30(08):1113–1128.

Christensen, B. E. (1996). Conformation-stability relationships in xanthan gum.

Christensen, B. E. (2013). *Compendium TBT4135 Biopolymers*. NTNU-trykk, Trondheim, Norway.

Christensen, B. E., Myhr, M. H., and Smidsrød, O. (1996). Degradation of double-

stranded xanthan by hydrogen peroxide in the presence of ferrous ions: comparison to acid hydrolysis. *Carbohydrate research*, 280(1):85–99.

Christensen, B. E. and Smidsrød, O. (1991). Hydrolysis of xanthan in dilute acid: Effects on chemical composition, conformation, and intrinsic viscosity. *Carbohydrate Research*, 214(1):55 – 69.

Christensen, B. E., Smidsrød, O., Elgsæter, A., and Stokke, B. T. (1993). Depolymerization of double-stranded xanthan by acid hydrolysis: characterization of partially degraded double strands and single-stranded oligomers released from the ordered structures. *Macromolecules*, 26(22):6111–6120.

Colinet, I., Dulong, V., Hamaide, T., Cerf, D. L., and Picton, L. (2009). Unusual rheological properties of a new associative polysaccharide in salt media. *Carbohydrate Polymers*, 77(4):743 – 749.

David, C., Millot, M. C., and Sébille, B. (2001). High-performance liquid chromatographic study of the interactions between immobilized β-cyclodextrin polymers and hydrophobically end-capped polyethylene glycols. *Journal of Chromatography B: Biomedical Sciences and Applications*, 753(1):93 – 99. 7th International Symposium of the European Society for Biochromatography (ESBC 2000).

Driveklepp, M. . (2013). Intrinsic viscosity determination of polyacrylamide for application in enhanced oil recovery.

Dulong, V., Cerf, D. L., Picton, L., and Muller, G. (2006). Carboxymethylpullulan hydrogels with a ionic and/or amphiphilic behavior: Swelling properties and entrapment of cationic and/or hydrophobic molecules. *Colloids and Surfaces A: Physicochemical and Engineering Aspects*, 274(1–3):163 – 169.

Dulong, V., Mocanu, G., Picton, L., and Cerf, D. L. (2012). Amphiphilic and thermosensitive copolymers based on pullulan and jeffamine®: Synthesis, characterization and physicochemical properties. *Carbohydrate Polymers*, 87(2):1522 – 1531.

El-Faham, A. and Albericio, F. (2011). Peptide coupling reagents, more than a letter soup. *Chemical reviews*, 111(11):6557–6602.

Esquenet, C. and Buhler, E. (2001). Phase behavior of associating polyelectrolyte polysaccharides. 1. aggregation process in dilute solution. *Macromolecules*, 34(15):5287–5294.

Finley, J. W., Schmidt, S. J., and Serianni, A. S. (1990). *NMR applications in biopolymers*. Plenum Press, New York.

Garcıa-Ochoa, F., Santos, V., Casas, J., and Gomez, E. (2000). Xanthan gum: production, recovery, and properties. *Biotechnology advances*, 18(7):549–579.

Günther, H. (2013). *NMR spectroscopy: basic principles, concepts and applications in chemistry*. Wiley-VCH, Weinheim an der Bergstrasse, Germany.

Hamcerencu, M., Desbrieres, J., Popa, M., and Riess, G. (2009). Stimuli-sensitive xanthan derivatives/n-isopropylacrylamide hydrogels: Influence of cross-linking agent on interpenetrating polymer network properties. *Biomacromolecules*, 10(7):1911–1922.

Han, S.-Y. and Kim, Y.-A. (2004). Recent development of peptide coupling reagents in organic synthesis. *Tetrahedron*, 60(11):2447 – 2467.

Harnoy, G., Gatt, S., and Barenholtz, Y. (1989). Enhanced oil recovery. US Patent 4,811,791.

Hodgkinson, S. C. and Lowry, P. J. (1981). Hydrophobic-interaction chromatography and anion-exchange chromatography in the presence of acetonitrile. a two-step purification method for human prolactin. *Biochem. J.*, 199(3):619–627.

Huggins, M. L. (1942). The viscosity of dilute solutions of long-chain molecules. iv. dependence on concentration. *Journal of the American Chemical Society*, 64(11):2716–2718.

Izdebski, J., Pachulska, M., and Orlowska, A. (1994). *N*-cyclohexyl-*N'*-isopropylcarbodiimide: a hybrid that combines the structural features of dcc and dic. *International Journal of Peptide and Protein Research*, 44(5):414–419.

Jansson, P.-e., Kenne, L., and Lindberg, B. (1975). Structure of the extracellular polysaccharide from xanthomonas campestris. *Carbohydrate Research*, 45(1):275–282.

Kang, K. S. and Pettit, D. J. (1993). *Industrial Gums: Polysaccharides and Their Derivatives, Whistler, E. R. and BeMiller, J. N. (Ed.)*, chapter Xanthan, gellan, wellan, and rhamsan, pages 341–398. Academic Press.

Katzbauer, B. (1998). Properties and applications of xanthan gum. *Polymer Degradation and Stability*, 59(1):81–84.

Kelco Oil Field Group (2001). Kelzan xcd polymer, a dispersable biopolymer for rheology control. Available from http://www.kofg.com/PRODUCTS/A. [Online, accessed 08.06.14].

Kumar, A., Singh, K., and Ahuja, M. (2009). Xanthan-g-poly(acrylamide): Microwave-assisted synthesis, characterization and in vitro release behavior. *Carbohydrate Polymers*, 76(2):261 – 267.

Madigan, M., Clark, D., Stahl, D., and Martinko, J. (2010). *Brock Biology of Microorganisms 13th Edition*. Benjamin Cummings, 13th edition.

Mead, D. J. and Fuoss, R. M. (1942). Viscosities of solutions of polyvinyl chloride. *Journal of the American Chemical Society*, 64(2):277–282.

Melton, L. D., Mindt, L., and Rees, D. A. (1976). Covalent structure of the extracellular polysaccharide from *Xanthomonas campestris*: evidence from partial hydrolysis studies. *Carbohydrate research*, 46(2):245–257.

Mendes, A. C., Baran, E. T., Nunes, C., Coimbra, M. A., Azevedo, H. S., and Reis, R. L. (2011). Palmitoylation of xanthan polysaccharide for self-assembly microcapsule formation and encapsulation of cells in physiological conditions. *Soft Matter*, 7:9647–9658.

Milas, M. and Rinaudo, M. (1979). Conformational investigation on the bacterial polysaccharide xanthan. *Carbohydrate Research*, 76(1):189 – 196.

Milas, M. and Rinaudo, M. (1986). Properties of xanthan gum in aqueous solutions: Role of the conformational transition. *Carbohydrate Research*, 158(0):191 – 204.

Milas, M., Rinaudo, M., and Tinland, B. (1985). The viscosity dependence on concentration, molecular weight and shear rate of xanthan solutions. *Polymer Bulletin*, 14(2):157–164.

Mori, S. and Barth, H. (1999). *Size Exclusion Chromatography*. Laboratory Series. Springer.

Nasr-El-Din, H. A., Hawkins, B. F., and Green, K. A. (1991). Viscosity behavior of alkaline, surfactant, polyacrylamide solutions used for enhanced oil recovery. In *Society of Petroleum Engineers*.

Nasr-El-Din, H. A. and Noy, J. L. (1992). Flow behaviour of alkali, surfactant, and xanthan solutions used for enhanced oil recovery. *Oil & Gas Science and Technology - Rev. IFP*, 47(6):771–791.

Needham, R. B. and Doe, P. H. (1987). Polymer flooding review. *Journal of Petroleum Technology*, 39(12):1503–1507.

Paoletti, S., Cesàro, A., and Delben, F. (1983). Thermally induced conformational transition of xanthan polyelectrolyte. *Carbohydrate Research*, 123(1):173 – 178.

Papagianni, M., Psomas, S., Batsilas, L., Paras, S., Kyriakidis, D., and Liakopoulou-Kyriakides, M. (2001). Xanthan production by *Xanthomonas campestris* in batch cultures. *Process Biochemistry*, 37(1):73–80.

Peiffer, D., Lundberg, R., and Duvdevani, I. (1986). Synthesis and rheological properties of low charge density polyampholytes in nonaqueous solvents. *Polymer*, 27(9):1453 – 1462.

PetroTel (2010). Polymer eor. http://www.petrotel.com/?page=EOR_Polymer&lang=en. [Online, accessed 25.05.14].

Podzimek, S. (2011). *Light scattering, size exclusion chromatography, and asymmetric flow field flow fractionation: powerful tools for the characterization of polymers, proteins, and nanoparticles*. Wiley, Hoboken, NJ.

Rebek, J. and Feitler, D. (1974). Mechanism of the carbodiimide reaction. ii. peptide synthesis on the solid phase. *Journal of the American Chemical Society*, 96(5):1606–1607.

Rehm, B. (2009). *Microbial Production of Biopolymers and Polymer Precursors: Applications and Perspectives*. Caister Academic.

Rinaudo, M. and Milas, M. (1980). Enzymic hydrolysis of the bacterial polysaccharide xanthan by cellulase. *International Journal of Biological Macromolecules*, 2(1):45 – 48.

Rinaudo, M., Milas, M., Lambert, F., and Vincendon, M. (1983). Proton and carbon-13 nmr investigation of xanthan gum. *Macromolecules*, 16(5):816–819.

Roy, A. (2014). (Personal communication, spring 2014).

Roy, A., Comesse, S., Grisel, M., Hucher, N., Souguir, Z., and Renou, F. (2014). Hydrophobically modified xanthan: An amphiphilic but not associative polymer. *Biomacromolecules*, 15(4):1160–1170.

Sabhapondit, A., Borthakur, A., and Haque, I. (2003). Water soluble acrylamidomethyl propane sulfonate (amps) copolymer as an enhanced oil recovery chemical. *Energy & Fuels*, 17(3):683–688.

Sato, T., Norisuye, T., and Fujita, H. (1984). Double-stranded helix of xanthan: Dimensional and hydrodynamic properties in 0.1 m aqueous sodium chloride. *Macromolecules*, 17(12):2696–2700.

Sheehan, J. C. and Hess, G. P. (1955). A new method of forming peptide bonds. *Journal of the American Chemical Society*, 77(4):1067–1068.

Sheng, J. (2010). *Modern Chemical Enhanced Oil Recovery: Theory and Practice*. Elsevier Science.

Shirai, S., Yoshimura, S., and Einaga, Y. (2006). Intrinsic viscosity of polyoxyethylene alkyl ether ciej micelles. *Polym. J*, 38(1):37–43.

Smidsrød, O. and Moe, S. T. (2008). *Biopolymer chemistry*. Tapir Academic Press, Trondheim.

Smith, I. H. and Pace, G. W. (1982). Recovery of microbial polysaccharides. *Journal of Chemical Technology and Biotechnology*, 32(1):119–129.

Song, H., Zhang, S.-F., Ma, X.-C., Wang, D.-Z., and Yang, J.-Z. (2007). Synthesis and application of starch-graft-poly(am-co-amps) by using a complex initiation system of cs-aps. *Carbohydrate Polymers*, 69(1):189 – 195.

Souguir, Z., Roudesli, S., About-Jaudet, E., Cerf, D. L., and Picton, L. (2007). Synthesis and physicochemical characterization of a novel ampholytic pullulan derivative with amphiphilic behavior in alkaline media. *Journal of Colloid and Interface Science*, 313(1):108 – 116.

Stokke, B. T., Elgsaeter, A., and Smidsrod, O. (1986). Electron microscopic study of single-and double-stranded xanthan. *International Journal of Biological Macromolecules*, 8(4):217 – 225.

Tako, M. and Nakamura, S. (1984). Rheological properties of deacetylated xanthan in aqueous media. *Agricultural and Biological Chemistry*, 48(12):2987–2993.

Taylor, K. and Nasr-El-Din, H. (1998). Water-soluble hydrophobically associating polymers for improved oil recovery: A literature review. *Journal of Petroleum Science and Engineering*, 19(3–4):265 – 280.

Tiwari, B., Muthukumarappan, K., O'Donnell, C., and Cullen, P. (2010). Rheological properties of sonicated guar, xanthan and pectin dispersions. *International Journal of Food Properties*, 13(2):223–233.

Uhl, J. T., Ching, T. Y., and Bae, J. H. (1995). A laboratory study of new, surfactant-containing polymers for high-salinity reservoirs. society of petroleum engineers. *Society of Petroleum Engineers*, 3(01):113–119.

Vega, I., Sánchez, L., and D'Accorso, N. (2008). Synthesis and characterization of copolymers with 1,3-oxazolic pendant groups. *Reactive and Functional Polymers*, 68(1):233 – 241.

Wang, K., Iliopoulos, I., and Audebert, R. (1988). Viscometric behaviour of hydrophobically modified poly(sodium acrylate). *Polymer Bulletin*, 20(6):577–582.

Wever, D., Picchioni, F., and Broekhuis, A. (2011). Polymers for enhanced oil recovery: A paradigm for structure–property relationship in aqueous solution. *Progress in Polymer Science*, 36(11):1558 – 1628. Special Topic: Energy Related Materials.

Wyatt, P. J. (1993). Light scattering and the absolute characterization of macromolecules. *Analytica Chimica Acta*, 272(1):1 – 40.

Wyatt Technology Corporation (2014). Molecular conformation. Available from

http://www.wyatt.com/products/software/molecular-conformation.html. [Online, accessed 01.06.14].

Yang, L., Zhang, B., Wen, L., Liang, Q., and Zhang, L.-M. (2007). Amphiphilic cholesteryl grafted sodium alginate derivative: Synthesis and self-assembly in aqueous solution. *Carbohydrate Polymers*, 68(2):218 – 225.

Zhang, L.-M. (2001). Cellulosic associative thickeners. *Carbohydrate Polymers*, 45(1):1 – 10.

Zimm, B. H. (1948). The scattering of light and the radial distribution function of high polymer solutions. *The Journal of Chemical Physics*, 16(12):1093–1099.

Appendices

Appendix A

Concentrations of Xanthan Solutions

A.1 Concentrations of Stock Solution and Diluted Solution of Kelzan Test Sample

The concentrations of stock solution and diluted solution of the Kelzan test sample for sonication are shown in Table A.1.1.

Table A.1.1: Overview of amounts of Kelzan XCD and MQ water used for stock solution and diluted solution of Kelzan test sample for sonication.

Amount xanthan [g]	0.9998
Amount xanthan corrected for water content [g]	0.9167
Amount water [g]	99.25
Total amount [g]	100.166723
Xanthan concentration [mg xanthan/g total]	9.1520
Dilution:	
Total volume [mL]	1000
Xanthan concentration [mg xanthan/mL total]	0.9167

A.2 Concentration of Stock Solution and Diluted Solution For Preparation of xan10, xan30 and xan120

The concentrations of stock solution and diluted solution of the Kelzan XCD sample for preparation of the samples xan10, xan30, and xan120 are shown in Table A.2.1.

Table A.2.1: Overview of concentration of stock solution prepared from Kelzan XCD, and dilution, used for preparation of the samples xan10, xan30 and xan120.

Amount xanthan [g]	4.9974
Amount xanthan, corrected for water content [g]	4.5821
Amount water [g]	499.97
Total amount [g]	504.55
Xanthan concentration [mg xanthan/g total]	9.0816
Dilution:	
Amount xanthan solution [g]	99.65
Total amount [g]	1000
Xanthan concentration [mg/g]	0.9050

The concentrations of stock solution and diluted solution of the Statoil xanthan for preparation of the sample xanS are shown in Table A.2.2.

Table A.2.2: Overview of concentration of stock solution, and diluted solution, used for preparation of the samples xanS.

Amount xanthan [g]	0.2029
Amount xanthan, corrected for water content [g]	0.1860
Amount water [g]	40.0016
Total amount [g]	40.1880
Xanthan concentration [mg xanthan/g total]	4.6293
Dilution:	
Amount water added [g]	159.80
Total amount [g]	199.99
Xanthan concentration [mg/g]	0.9303

The amounts of NaCl used for preparation of xanthan solutions from Kelzan XCD and the Statoil xanthan are shown in Table A.2.3.

Table A.2.3: Overview of amounts NaCl added to each stocksolution in order to obtain a NaCl concntration of 0.1 M.

Xanthan solution	**Volume of xanthan solution [mL]**	**Amount NaCl [g]**
Kelzan	1000	5.8440
Statoil	200	1.1688

A.3 Determination of Water Content

The weights of xanthan before and after drying, for determination of water content, are shown in Table A.3.1.

Table A.3.1: Weight of glass used for weighing out xanthan sample, m_{glass}, total weight, m_{total}, and amount of xanthan, $m_{xanthan}$.

	$\boldsymbol{m_{glass}}$ [g]	$\boldsymbol{m_{total}}$ [g]	$\boldsymbol{m_{xanthan}}$ [g]
Before drying	9.1679	9.411	0.2431
After drying	9.1679	9.3908	0.2229

$$\%solid = \frac{m_{xanthan} \text{ before drying}}{m_{xanthan} \text{ after drying}} \tag{A.3.1}$$

Equation (A.3.1) gave a dry weight of $\%solid = 92\%$, thus, the water content is 8 %. The water content for the xanthan provided from Statoil was assumed to be equal to the water content calculated for the Kelzan.

Appendix B

Phenol-Sulfuric Acid Analysis

B.1 Purified Sonicated Xanthan Samples xan10, xan30, and xan120

The concentrations and measured absorbances (at 485 nm) of analysed solutions with known concentrations for making the standard curve for phenol-sulfuric acid analysis, and xan10, xan30, xan120 with unknown concentrations, are shown in Table B.1.1, and the standard curve obtained is presented in Figure B.1.1.

Table B.1.1: Concentrations and measured absorbance (at 485 nm) of analysed solutions with known concentrations for making the standard curve for phenol-sulfuric acid analysis, and xan10, xan30, xan120 with unknown concentrations.

		Absorbance, replicate				
Sample	**Conc.** [µL/mL]	**1**	**2**	**3**	**4**	**Average**
1	0	0	0	0	0	0
2	10	0.061	0.056	0.050	0.056	0.056
3	20	0.117	0.112	0.119	0.102	0.113
4	40	0.191	0.195	0.222	0.206	0.204
5	50	0.251	0.254	0.254	0.245	0.251
6	60	0.304	0.350	0.338	0.300	0.323
7	80	0.397	0.461	0.389	0.394	0.410
8	100	0.486	0.621	0.555	0.562	0.556
xan10	Unknown	0.280	0.205	0.215	0.232	0.233
xan30	Unknown	0.134	0.139	0.158	0.182	0.153
xan120	Unknown	0.209	0.224	0.208	0.218	0.215

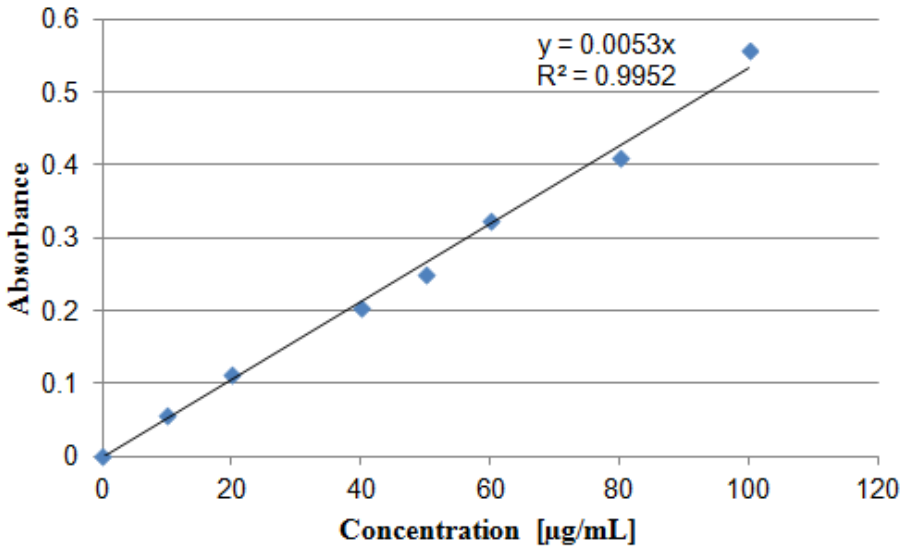

Figure B.1.1: Standard curve for phenol-sulfuric acid analysis of xanthan, for determination of concentration of xan10, xan30, and xan120 after sonication and purification.

The absorbance is given by $y = 0.0053x$ where x is the concentration, thus the concentrations of the unknown solution may be calculated, see Table B.1.2.

Table B.1.2: Concentration of purified sonicated xanS, determined by phenol-sulfuric acid analysis.

Sample	**Conc. for analysis** [µL/mL]	**Conc. xanthan solution** [µL/mL]	**Conc. xanthan solution [mg/mL]**
xan10	43.96	4396.23	4.40
xan30	28.92	2891.51	2.89
xan120	40.40	4039.81	4.04

B.2 Purified Sonicated Xanthan Sample xanS

The concentrations and measured absorbances (at 485 nm) of analysed solutions with known concentrations for making the standard curve for phenol-sulfuric acid analysis, and xanS with unknown concentration, are shown in Table B.2.1, and the standard curve obtained is presented in Figure B.2.1.

Table B.2.1: Concentrations and measured absorbance (at 485 nm) of analysed solutions with known concentrations for making the standard curve for phenol-sulfuric acid analysis, and xanS with unknown concentration.

		Absorbance, replicate				
Ample	**Conc.** [µL/mL]	**1**	**2**	**3**	**4**	**Avergae**
1	0	0	0	0	0	0
3	20	0.158	0.162	0.164	0.162	0.162
4	40	0.334	0.322	0.323	0.319	0.325
6	60	0.487	0.513	0.498	0.492	0.498
7	80	0.647	0.643	0.635	0.623	0.637
8	100	0.844	0.779	0.779	0.781	0.796
xanS	Unknown	0.478	0.455	0.470	0.466	0.467

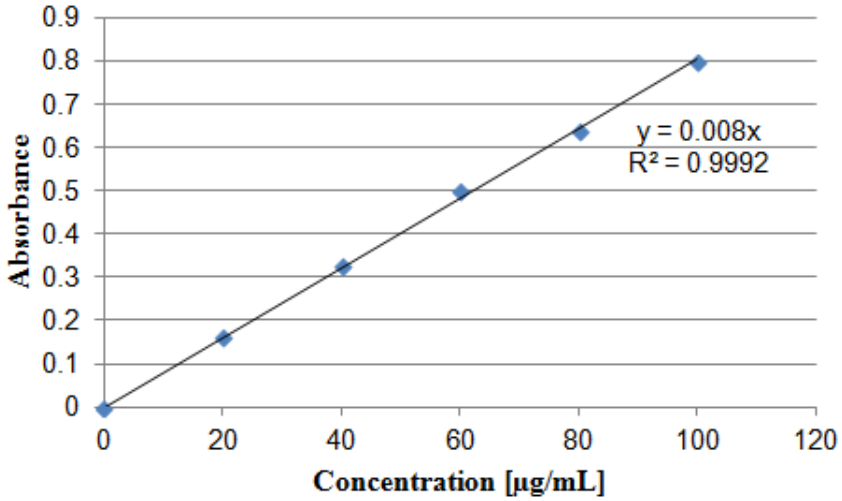

Figure B.2.1: Standard curve for phenol-sulfuric acid analysis of xanthan, for determination of concentration of xanS after sonication and purification.

The absorbance is given by $y = 0.008x$ where x is the concentration, thus the concentration of the unknown xanS solution may be calculated, see Table B.2.2.

Table B.2.2: Concentration of purified sonicated xanS, determined by phenol-sulfuric acid analysis.

Sample	**Conc. for analysis** [µL/mL]	**Conc. xanthan solution** [µL/mL]	**Conc. xanthan solution [mg/mL]**
xanS	58.41	5840.63	5.84

Appendix C

Amounts and Calculation for NHS, EDAC and Octylamine Applied for Modification

C.1 Amounts of Xanthan, EDAC, NHS, and Octylamine Applied During Modification

The amounts of xanthan, EDAC, NHS, and octylamine, $m_{xanthan}$, m_{EDAC}, m_{NHS}, and m_{C_8}, respectively, applied during modification are given in Table C.1.1.

Table C.1.1: Amounts of xanthan, EDAC, NHS and C_8, $m_{xanthan}$, m_{EDAC}, m_{NHS}, and m_{C_8}, respectively, used for modification.

Sample	$\boldsymbol{m_{xanthan}}$ **[mg]**	$\boldsymbol{m_{EDAC}}$**[mg]**	$\boldsymbol{m_{NHS}}$ **[mg]**	$\boldsymbol{m_{C_8}}$ [µL]
test1	30	35	22	31
test2	100	118	72	102
xan30	30	35	22	31
xanS	30	35	22	31
xan30pa	15	18	11	16

C.2 Calculations

It was assumed that there was 2 carboxylic acid groups (-COOH) per repeating unit of xanthan, since this is the maximum amount. There was added 3 -COOH equivalents of EDAC, NHS, and octylamine, hence all reagents were in excess.

The number of moles of one repeating unit of xanthan was calculated from equation

(C.2.1).

$$n_0 = \frac{m_{xanthan}}{M_{w,0}} \tag{C.2.1}$$

Here $m_{xanthan}$ is the amount of xanthan, see Table C.1.1, and $M_{w,0}$ is the molecular weight of one repeating unit of xanthan, assumed to be 977 g/mol.

The number of moles of 3 equivalents of NHS, EDAC and octylamine, with respect to -COOH groups when there is 2 -COOH per repeating unit, was calculated by equation (C.2.2).

$$n = 2 \cdot 3 \cdot n_0 \tag{C.2.2}$$

Since all the reagent are added in equal amounts of moles, $n = n_{NHS} = n_{EDAC} = n_{C_8}$.

The amount of NHS added is calculated by equation (C.2.3).

$$m_{NHS} = n \cdot M_{w,NHS} \tag{C.2.3}$$

Here $M_{w,NHS}$ is the molecular weight of NHS, 115.09 g/mol.

The purity of EDAC was 98 %, thus the amount of EDAC added is calculated by equation (C.2.4).

$$m_{EDAC} = n \cdot M_{w,EDAC} \cdot \frac{1}{0.98} \tag{C.2.4}$$

Here $M_{w,EDAC}$ is the molecular weight of EDAC, 191.70 g/mol.

The purity of octylamine was 99 %, and the density, d, was 0.782 g/mL, thus the volume of aqueous solution of octylamine added, V_{C_8} is calculated by equation (C.2.5).

$$V_{C_8} = \frac{m_{C_8}}{d} = \frac{n \cdot M_{w,C_8}}{d} \cdot \frac{1}{0.99} \tag{C.2.5}$$

Appendix D

Raw Data For Intrinsic Viscosity From Single Capillary Viscometer

All raw data and calculated values from the intrinsic viscosity measurements with the single capillary viscometer may be found on the attached CD.

The standard deviations shown in this Appendix were calculated by:

$SD = \sqrt{\frac{1}{N-1}\sum(X_1 - \bar{X})^2} = \sqrt{\frac{1}{N-1}\sum d_i^2}$

All the presented results are obtained from measurements with single capillary viscometer, with wall shear rate 2500 s^{-1}. In all the tables throughout this appendix, η_r is the relative viscosity of the xanthan solutions, calculated by t/t_0, where t is the flow-through time of the xanthan solution and t_0 is the flow-through time of the solvent, which here is 0.1 M NaCl. The specific viscosity is calculated as $\eta_{sp} = \eta_r - 1$.

D.1 Sonicated Non-Purified Kelzan Test Sample

The solvent time, t_0, of 0.1 M NaCl used for intrinsic viscosity calculations for the Kelzan test sample is shown in Table D.1.1.

Table D.1.1: Hagenbach correction of solvent time used in intrinsic viscosity calculations for Kelzan test sample

Hagenbach factor	30800
Solvent time [s]	207.4
Solvent time (Hagenbach-corrected) [s]	206.7

Table D.1.2: Calculated values from viscosity measurements with single capillary viscometer with wall shear rate 2500 s^{-1} for Kelzan test sample.

Conc (g/mL)	Hagenb. corr. time (s)	η_r	η_{sp}	Huggins η_{sp}/c (mL/g)	Herman log η_{sp}/c (mL/g)	Fouss-Mead $(\ln \eta_r)/c$ (mL/g)	Billmeyer $[2(\eta_{sp} - \ln \eta_r)]^{1/2}/c$ (mL/g)
8.20E-04	231.31	1.12	0.12	145.21	2.16	137.19	140
6.65E-04	226.41	1.10	0.10	143.41	2.16	136.98	139
5.10E-04	221.53	1.07	0.07	140.70	2.15	135.88	137
3.55E-04	219.85	1.06	0.06	179.24	2.25	173.76	176
2.00E-04	214.26	1.04	0.04	182.92	2.26	179.66	181

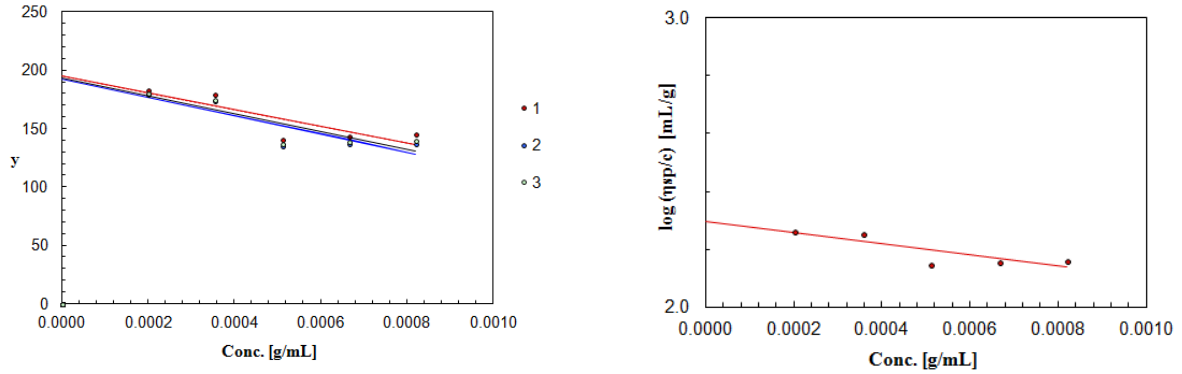

(a) Huggins (1), Fuoss-Mead (2), and Billmeyer (3)

(b) Hermann plot (Huggins semilog)

Figure D.1.1: Plots of viscosity data for Kelzan test sample. (a) The denomination of the y-axis, y, equals η_{sp}, $\ln \eta_r/c$, or $[2(\eta_{sp} - \ln \eta_r)]^{1/2}/c$ for Huggins (red), Fuoss-Mead (blue), and Billmeyer (green), respectively. (b) Hermann plot.

Table D.1.3: Intrinsic viscosity of Kelzan test sample calculated by Huggins, Fuoss-Mead, Billmeyer, and Hermann methods, and the average intrinsic viscosity with standard deviation SD, and Huggins constant, k'.

		$[\eta]$ (ml/g)	k'	di^2
1 (Huggins)	η_{sp}/c vs. c	194.90	-1.89	0.1482
2 (Fuoss-Mead)	$(\ln \eta_r)/c$ vs. c	192.74	-1.61	3.1507
3 (Billmeyer)	$[2(\eta_{sp} - \ln \eta_r)]1/2/c$ vs. c	193.47	-1.71	1.0963
4 (Herman)	$\log \eta_{sp}/c$ vs. c	196.95		5.9394
Average		195		
SD		2		

D.2 Non-Modified Purified Sonicated Xanthan Samples

The solvent time, t_0, of 0.1 M NaCl used for intrinsic viscosity calculations for the purified sonicated samples xan10, xan30, and xan120 is shown in Table D.2.1, and for xan30pa

and xanS in Table D.2.2.

Table D.2.1: Hagenbach correction of solvent time used in intrinsic viscosity calculations for non-modified xan10, xan30, and xan120.

Hagenbach factor	30800
Solvent time [s]	206.6
Solvent time (Hagenbach-corrected) [s]	205.9

Table D.2.2: Hagenbach correction of solvent time used in intrinsic viscosity calculations for non-modified xan30pa and xanS.

Hagenbach factor	30800
Solvent time [s]	206.7
Solvent time (Hagenbach-corrected) [s]	206.0

D.2.1 Non-Modified xan10

Table D.2.3: Calculated values from viscosity measurements with single capillary viscometer with wall shear rate 2500 s^{-1} for non-modified xan10.

Conc (g/mL)	**Hagenb. corr. time (s)**	η_r	η_{sp}	**Huggins η_{sp}/c (mL/g)**	**Herman log η_{sp}/c (mL/g)**	**Fouss-Mead (ln η_r)/c (mL/g)**	**Billmeyer $[2(\eta_{sp} - \ln \eta_r)]^{1/2}/c$ (mL/g)**
1.00E-03	319.44	1.55	0.55	551.37	2.74	439.14	474
8.00E-04	294.59	1.43	0.43	538.35	2.73	447.69	476
6.00E-04	270.57	1.31	0.31	523.38	2.72	455.16	477
4.00E-04	248.75	1.21	0.21	520.15	2.72	472.54	488
2.00E-04	225.31	1.09	0.09	471.12	2.67	450.22	457

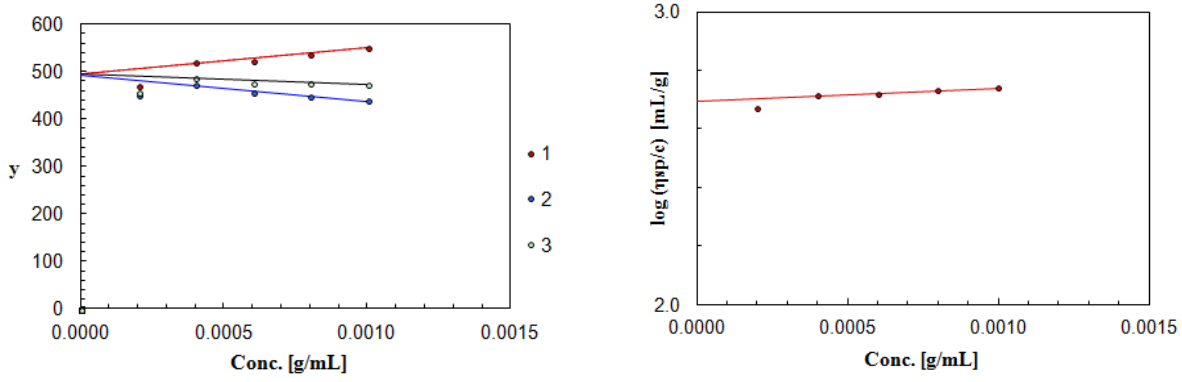

(a) Huggins (1), Fuoss-Mead (2), and Billmeyer (3)

(b) Herman plot (Huggins semilog)

Figure D.2.1: Plots of viscosity data for non-modified xan10. Note that the lowest concentration is not included in the linear regressions. (a) The denomination of the y-axis, y, equals η_{sp}, $\ln \eta_r/c$, or $[2(\eta_{sp} - \ln \eta_r)]^{1/2}/c$ for Huggins (red), Fuoss-Mead (blue), and Billmeyer (green), respectively. (b) Herman plot.

Table D.2.4: Intrinsic viscosity of xan10 calculated by Huggins, Fuoss-Mead, Billmeyer, and Hermann methods, and the average intrinsic viscosity with standard deviation SD, and Huggins constant, k'.

		$[\eta]$ (ml/g)	k'	di^2
1 (Huggins)	η_{sp}/c vs. c	495.30	0.22	1.1057
2 (Fuoss-Mead)	$(\ln \eta_r)/c$ vs. c	491.32	0.28	8.5404
3 (Billmeyer)	$[2(\eta_{sp} - \ln \eta_r)]1/2/c$ vs. c	493.77	0.24	0.2273
4 (Herman)	$\log \eta_{sp}/c$ vs. c	496.59		5.5112
Average		494		
SD		2		

D.2.2 Non-Modified xan30

Table D.2.5: Calculated values from viscosity measurements with single capillary viscometer with wall shear rate 2500 s^{-1} for non-modified xan30.

Conc (g/mL)	**Hagenb. corr. time (s)**	η_r	η_{sp}	**Huggins η_{sp}/c (mL/g)**	**Herman log η_{sp}/c (mL/g)**	**Fouss-Mead $(\ln \eta_r)/c$ (mL/g)**	**Billmeyer $[2(\eta_{sp} - \ln \eta_r)]^{1/2}/c$ (mL/g)**
1.00E-03	297.23	1.44	0.44	443.50	2.65	367.07	391
8.00E-04	277.24	1.35	0.35	433.03	2.64	371.81	391
6.00E-04	257.87	1.25	0.25	420.59	2.62	375.04	390
4.00E-04	239.44	1.16	0.16	407.11	2.61	377.18	387
2.00E-04	222.22	1.08	0.08	396.08	2.60	381.18	386

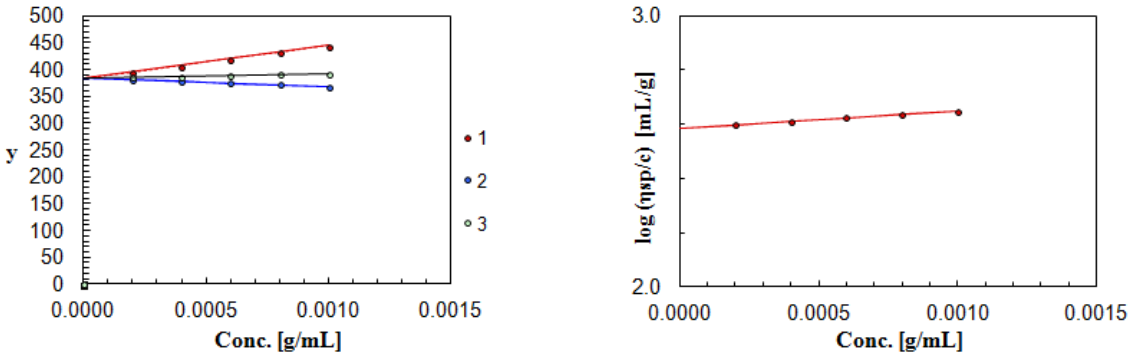

(a) Huggins (1), Fuoss-Mead (2), and Billmeyer (3)

(b) Herman plot (Huggins semilog)

Figure D.2.2: Plots of viscosity data for non-modified xan30. (a) The denomination of the y-axis, y, equals η_{sp}, $\ln \eta_r/c$, or $[2(\eta_{sp} - \ln \eta_r)]^{1/2}/c$ for Huggins (red), Fuoss-Mead (blue), and Billmeyer (green), respectively. (b) Herman plot.

Table D.2.6: Intrinsic viscosity of xan30 calculated by Huggins, Fuoss-Mead, Billmeyer, and Hermann methods, and the average intrinsic viscosity with standard deviation SD, and Huggins constant, k'.

		$[\eta]$ (ml/g)	k'	di^2
1 (Huggins)	η_{sp}/c vs. c	383.84	0.41	0.4702
2 (Fuoss-Mead)	$(\ln \eta_r)/c$ vs. c	384.53	0.39	0.0000
3 (Billmeyer)	$[2(\eta_{sp} - \ln \eta_r)]1/2/c$ vs. c	384.74	0.38	0.0464
4 (Herman)	$\log \eta_{sp}/c$ vs. c	384.99		0.2173
Average		385		
SD		0		

D.2.3 Non-Modified xan120

Table D.2.7: Calculated values from viscosity measurements with single capillary viscometer with wall shear rate 2500 s^{-1} for non-modified xan120.

Conc (g/mL)	Hagenb. corr. time (s)	η_r	η_{sp}	Huggins η_{sp}/c (mL/g)	Herman log η_{sp}/c (mL/g)	Fouss-Mead $(\ln \eta_r)/c$ (mL/g)	Billmeyer $[2(\eta_{sp} - \ln \eta_r)]^{1/2}/c$ (mL/g)
1.00E-03	238.44	1.16	0.16	157.99	2.20	146.69	150
8.00E-04	231.42	1.12	0.12	154.87	2.19	146.00	149
6.00E-04	224.58	1.09	0.09	151.13	2.18	144.67	147
4.00E-04	218.02	1.06	0.06	147.05	2.17	142.89	144
2.00E-04	212.13	1.03	0.03	151.07	2.18	148.83	150

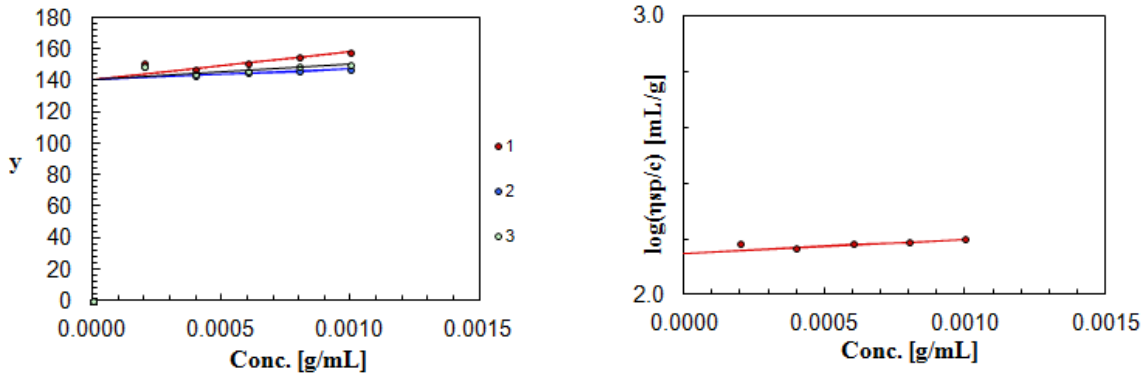

(a) Huggins (1), Fuoss-Mead (2), and Billmeyer (3)

(b) Herman plot (Huggins semilog)

Figure D.2.3: Plots of viscosity data for non-modified xan120. Note that the results for the lowest concentration were not included in the linear regressions. (a) The denomination of the y-axis, y, equals η_{sp}, $\ln \eta_r/c$, or $[2(\eta_{sp} - \ln \eta_r)]^{1/2}/c$ for Huggins (red), Fuoss-Mead (blue), and Billmeyer (green), respectively. (b) Herman plot.

Table D.2.8: Intrinsic viscosity of xan120 calculated by Huggins, Fuoss-Mead, Billmeyer, and Hermann methods, and the average intrinsic viscosity with standard deviation SD, and Huggins constant, k'.

		$[\eta]$ (ml/g)	k'	di^2
1 (Huggins)	η_{sp}/c vs. c	139.96	0.93	0.1528
2 (Fuoss-Mead)	$(\ln \eta_r)/c$ vs. c	140.60	0.82	0.0625
3 (Billmeyer)	$[2(\eta_{sp} - \ln \eta_r)]1/2/c$ vs. c	140.43	0.85	0.0064
4 (Herman)	$\log \eta_{sp}/c$ vs. c	140.41		0.0037
Average		140		
SD		0		

D.2.4 Non-Modified xan30pa

Table D.2.9: Calculated values from viscosity measurements with single capillary viscometer with wall shear rate 2500 s^{-1} for non-modified xan30pa.

Conc (g/mL)	**Hagenb. corr. time (s)**	η_r	η_{sp}	**Huggins η_{sp}/c (mL/g)**	**Herman log η_{sp}/c (mL/g)**	**Fouss-Mead $(\ln \eta_r)/c$ (mL/g)**	**Billmeyer $[2(\eta_{sp} - \ln \eta_r)]^{1/2}/c$ (mL/g)**
9.40E-04	298.25	1.45	0.45	476.21	2.68	393.55	419
7.55E-04	278.92	1.35	0.35	468.63	2.67	401.23	423
5.70E-04	257.23	1.25	0.25	436.03	2.64	389.42	404
3.85E-04	239.31	1.16	0.16	419.63	2.62	388.99	399
2.00E-04	222.50	1.08	0.08	399.82	2.60	384.64	390

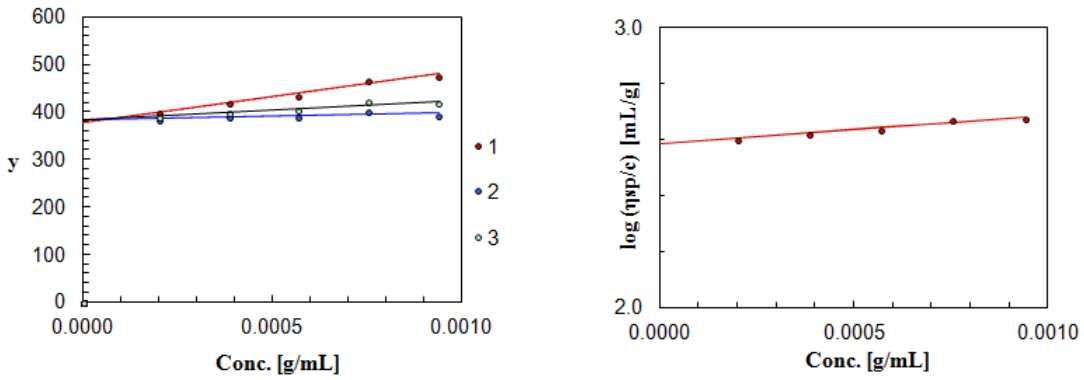

(a) Huggins (1), Fuoss-Mead (2), and Billmeyer (3)

(b) Herman plot (Huggins semilog)

Figure D.2.4: Plots of viscosity data for non-modified xan30pa. (a) The denomination of the y-axis, y, equals η_{sp}, $\ln \eta_r/c$, or $[2(\eta_{sp} - \ln \eta_r)]^{1/2}/c$ for Huggins (red), Fuoss-Mead (blue), and Billmeyer (green), respectively. (b) Herman plot.

Table D.2.10: Intrinsic viscosity of xan30pa calculated by Huggins, Fuoss-Mead, Billmeyer, and Hermann methods, and the average intrinsic viscosity with standard deviation SD, and Huggins constant, k'.

		$[\eta]$ (ml/g)	k'	di^2
1 (Huggins)	η_{sp}/c vs. c	377.66	0.77	16.9070
2 (Fuoss-Mead)	$(\ln \eta_r)/c$ vs. c	384.17	0.59	5.7731
3 (Billmeyer)	$[2(\eta_{sp} - \ln \eta_r)]1/2/c$ vs. c	382.85	0.63	1.1662
4 (Herman)	$\log \eta_{sp}/c$ vs. c	382.40		0.3959
Average		382		
SD		3		

D.2.5 Non-Modified xanS

Table D.2.11: Calculated values from viscosity measurements with single capillary viscometer with wall shear rate 2500 s^{-1} for non-modified xanS.

Conc (g/mL)	Hagenb. corr. time (s)	η_r	η_{sp}	Huggins η_{sp}/c (mL/g)	Herman log η_{sp}/c (mL/g)	Fouss-Mead $(\ln \eta_r)/c$ (mL/g)	Billmeyer $[2(\eta_{sp} - \ln \eta_r)]^{1/2}/c$ (mL/g)
1.00E-03	264.03	1.28	0.28	281.64	2.45	248.14	259
8.00E-04	251.70	1.22	0.22	277.24	2.44	250.40	259
6.00E-04	239.65	1.16	0.16	272.16	2.43	252.10	259
4.00E-04	227.99	1.11	0.11	266.74	2.43	253.45	258
2.00E-04	216.89	1.05	0.05	264.08	2.42	257.34	260

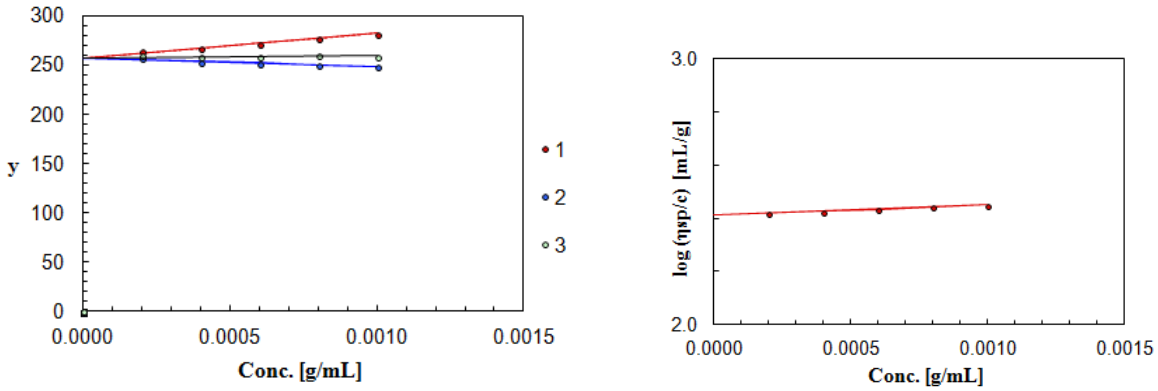

(a) Huggins (1), Fuoss-Mead (2), and Billmeyer (3)

(b) Herman plot (Huggins semilog)

Figure D.2.5: Plots of viscosity data for non-modified xanS. (a) The denomination of the y-axis, y, equals η_{sp}, $\ln \eta_r/c$, or $[2(\eta_{sp} - \ln \eta_r)]^{1/2}/c$ for Huggins (red), Fuoss-Mead (blue), and Billmeyer (green), respectively. (b) Herman plot.

Table D.2.12: Intrinsic viscosity of xanS calculated by Huggins, Fuoss-Mead, Billmeyer, and Hermann methods, and the average intrinsic viscosity with standard deviation SD, and Huggins constant, k'.

		$[\eta]$ (ml/g)	k'	di^2
1 (Huggins)	η_{sp}/c vs. c	257.03	0.38	0.0563
2 (Fuoss-Mead)	$(\ln \eta_r)/c$ vs. c	257.19	0.37	0.0053
3 (Billmeyer)	$[2(\eta_{sp} - \ln \eta_r)]1/2/c$ vs. c	257.34	0.36	0.0057
4 (Herman)	$\log \eta_{sp}/c$ vs. c	257.50		0.0552
Average		257		
SD		0		

D.3 Modified Purified Sonicated Xanthan Samples

The solvent time, t_0, of 0.1 M NaCl used for intrinsic viscosity calculations for the purified sonicated samples xan10, xan30, and xan120 is shown in Table D.3.1,

Table D.3.1: Hagenbach correction of solvent time used in intrinsic viscosity calculations for modified xan30, xan30pa, and xanS.

Hagenbach factor	30800
Solvent time [s]	206.7
Solvent time (Hagenbach-corrected) [s]	206.0

D.3.1 Modified xan30

Table D.3.2: Calculated values from viscosity measurements with single capillary viscometer with wall shear rate 2500 s^{-1} for modified xan30.

Conc (g/mL)	**Hagenb. corr. time (s)**	η_r	η_{sp}	**Huggins** η_{sp}/c **(mL/g)**	**Herman** $\log \eta_{sp}/c$ **(mL/g)**	**Fouss-Mead** $(\ln \eta_r)/c$ **(mL/g)**	**Billmeyer** $[2(\eta_{sp} - \ln \eta_r)]^{1/2}/c$ **(mL/g)**
8.70E-04	317.31	1.54	0.54	620.86	2.79	496.41	535
7.02E-04	292.15	1.42	0.42	595.48	2.77	497.53	528
5.35E-04	271.98	1.32	0.32	598.37	2.78	519.12	544
3.67E-04	249.56	1.21	0.21	575.77	2.76	522.34	540
2.00E-04	227.56	1.10	0.10	522.62	2.72	497.07	505

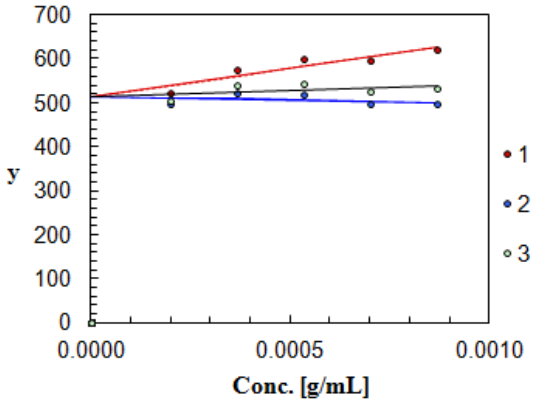

(a) Huggins (1), Fuoss-Mead (2), and Billmeyer (3)

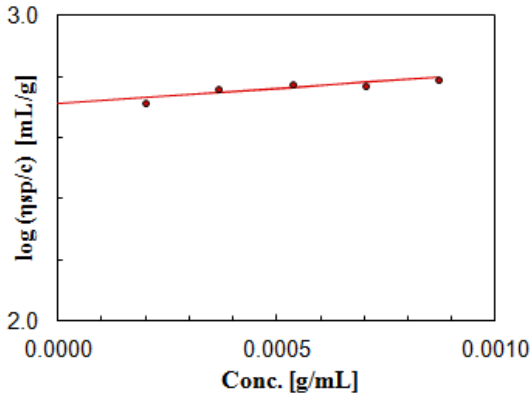

(b) Herman plot (Huggins semilog)

Figure D.3.1: Plots of viscosity data for modified xan30. (a) The denomination of the y-axis, y, equals η_{sp}, $\ln \eta_r/c$, or $[2(\eta_{sp} - \ln \eta_r)]^{1/2}/c$ for Huggins (red), Fuoss-Mead (blue), and Billmeyer (green), respectively. (b) Herman plot.

Table D.3.3: Intrinsic viscosity of modified xan30 calculated by Huggins, Fuoss-Mead, Billmeyer, and Hermann methods, and the average intrinsic viscosity with standard deviation SD, and Huggins constant, k'.

		$[\eta]$ (ml/g)	k'	di^2
1 (Huggins)	η_{sp}/c vs. c	513.60	0.49	1.4785
2 (Fuoss-Mead)	$(\ln \eta_r)/c$ vs. c	514.84	0.44	0.0010
3 (Billmeyer)	$[2(\eta_{sp} - \ln \eta_r)]1/2/c$ vs. c	515.32	0.44	0.2586
4 (Herman)	$\log \eta_{sp}/c$ vs. c	515.49		0.4572
Average		515		
SD		1		

D.3.2 Modified xan30pa

Table D.3.4: Calculated values from viscosity measurements with single capillary viscometer with wall shear rate 2500 s^{-1} for modified xan30pa.

Conc (g/mL)	**Hagenb. corr. time (s)**	η_r	η_{sp}	**Huggins η_{sp}/c (mL/g)**	**Herman log η_{sp}/c (mL/g)**	**Fouss-Mead $(\ln \eta_r)/c$ (mL/g)**	**Billmeyer $[2(\eta_{sp} - \ln \eta_r)]^{1/2}/c$ (mL/g)**
8.50E-04	292.42	1.42	0.42	493.34	2.69	411.99	438
6.88E-04	274.16	1.33	0.33	480.68	2.68	415.28	436
5.25E-04	257.24	1.25	0.25	473.49	2.68	422.88	439
3.63E-04	239.86	1.16	0.16	452.41	2.66	418.89	430
2.00E-04	226.65	1.10	0.10	500.53	2.70	477.04	485

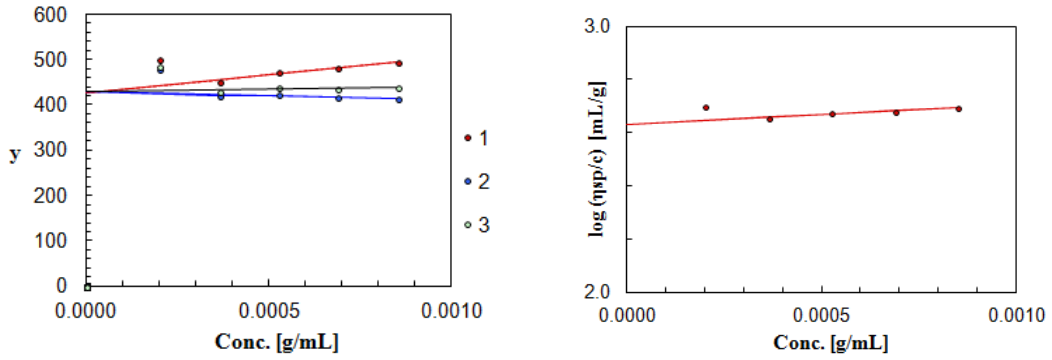

(a) Huggins (1), Fuoss-Mead (2), and Billmeyer (3)

(b) Herman plot (Huggins semilog)

Figure D.3.2: Plots of viscosity data for modified xan30pa. (a) The denomination of the y-axis, y, equals η_{sp}, $\ln \eta_r/c$, or $[2(\eta_{sp} - \ln \eta_r)]^{1/2}/c$ for Huggins (red), Fuoss-Mead (blue), and Billmeyer (green), respectively. Note that the results from the lowest concentration were not included in the linear regression. (b) Herman plot.

Table D.3.5: Intrinsic viscosity of modified xan30pa calculated by Huggins, Fuoss-Mead, Billmeyer, and Hermann methods, and the average intrinsic viscosity with standard deviation SD, and Huggins constant, k'.

		$[\eta]$ (ml/g)	k'	di^2
1 (Huggins)	η_{sp}/c vs. c	426.45	0.44	1.5787
2 (Fuoss-Mead)	$(\ln \eta_r)/c$ vs. c	427.83	0.40	0.0152
3 (Billmeyer)	$[2(\eta_{sp} - \ln \eta_r)]1/2/c$ vs. c	428.11	0.40	0.1624
4 (Herman)	$\log \eta_{sp}/c$ vs. c	428.44		0.5329
Average		428		
SD		1		

D.3.3 Modified xanS

Table D.3.6: Calculated values from viscosity measurements with single capillary viscometer with wall shear rate 2500 s^{-1} for modified xanS.

Conc (g/mL)	**Hagenb. corr. time (s)**	η_r	η_{sp}	**Huggins η_{sp}/c (mL/g)**	**Herman log η_{sp}/c (mL/g)**	**Fouss-Mead $(\ln \eta_r)/c$ (mL/g)**	**Billmeyer $[2(\eta_{sp} - \ln \eta_r)]^{1/2}/c$ (mL/g)**
9.30E-04	286.26	1.39	0.39	418.75	2.62	353.66	374
7.47E-04	268.21	1.30	0.30	404.06	2.61	353.11	369
5.65E-04	250.34	1.22	0.22	380.70	2.58	344.81	356
3.82E-04	234.68	1.14	0.14	364.09	2.56	340.90	348
2.00E-04	221.67	1.08	0.08	379.68	2.58	365.95	370

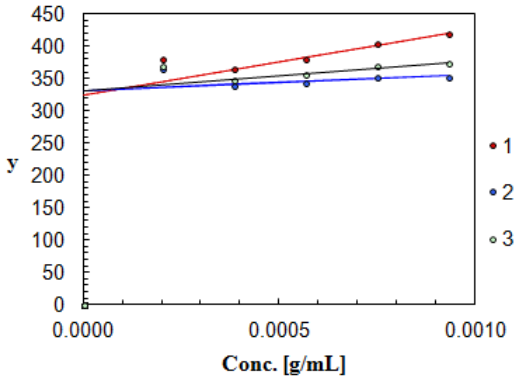

(a) Huggins (1), Fuoss-Mead (2), and Billmeyer (3)

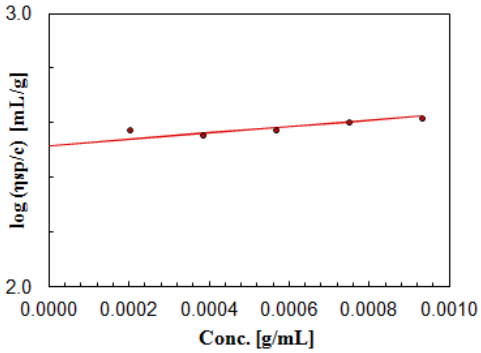

(b) Herman plot (Huggins semilog)

Figure D.3.3: Plots of viscosity data for modified xanS. Note that the results from the lowest concentration are not included in the linear regression lines. (a) The denomination of the y-axis, y, equals η_{sp}, $\ln \eta_r/c$, or $[2(\eta_{sp} - \ln \eta_r)]^{1/2}/c$ for Huggins (red), Fuoss-Mead (blue), and Billmeyer (green), respectively. (b) Herman plot.

Table D.3.7: Intrinsic viscosity of modified xanS calculated by Huggins, Fuoss-Mead, Billmeyer, and Hermann methods, and the average intrinsic viscosity with standard deviation SD, and Huggins constant, k'.

		$[\eta]$ (ml/g)	k'	di^2
1 (Huggins)	η_{sp}/c vs. c	324.60	0.97	17.6206
2 (Fuoss-Mead)	$(\ln \eta_r)/c$ vs. c	331.39	0.73	6.7476
3 (Billmeyer)	$[2(\eta_{sp} - \ln \eta_r)]1/2/c$ vs. c	329.74	0.79	0.8976
4 (Herman)	$\log \eta_{sp}/c$ vs. c	329.45		0.4260
Average		329		
SD		3		

D.4 Intrinsic Viscositites and Molecular Weights From the Literature

Table D.4.1: Molecular weight, M_w, and intrinsic viscosity, $[\eta]$, from article by Sato et al. (1984).

Sample	**Mw (kDa)**	**$[\eta]$ (mL/g)**
X4-5	7400	9000
X5-6	3940	5110
X5-8	2560	3580
X3-5	1420	1800
X9-3	994	1010
X7-3h	603	575
C6-3-7	362	320
X6-4-4	240	181
X10-4	209	152
X6-4-7	164	106
X8-3-5	112	60.8
X8-3-8	74	35

Appendix E

Raw Data From Four-Bulb Shear Dilution Viscometer

All raw data and calculated values from the intrinsic viscosity measurements with the four-bulb shear dilution viscometer may be found on the attached CD.

This appendix presents the viscosity data, and Huggins and Fuoss-Mead plots for each bulb of the four-bulb shear dilution viscometer, for the non-modified and modified xan30 samples. All the presented results are obtained from measurements with four-bulb shear dilution viscometer. All reported shear rates are at the wall. In the tables throughout this appendix, η_r is the relative viscosity of the xanthan solutions, calculated by t/t_0, where t is the flow-through time of the xanthan solution and t_0 is the flow-through time of the solvent, which here is 0.1 M NaCl. The specific viscosity is calculated as $\eta_{sp} = \eta_r - 1$.

E.1 Non-Modified xan30

Table E.1.1: Viscosity data for non-modified xan30 analysed with four-bulb shear dilution viscometer, bulb no. 1.

Shear rate (s^{-1})	**c** (g/mL)	η_r	η_{sp}	**Huggins** η_{sp}/c (mL/g)	**Fouss-Mead** ln η_r/c (mL/g)
712.61	8.56E-04	1.647648	0.647648	757	583
	7.01E-04	1.523171	0.523171	746	600
	5.45E-04	1.38641	0.38641	709	599
	3.75E-04	1.27059	0.27059	722	639
	2.00E-04	1.150142	0.150142	751	699
	0.00E+00		Intercept	630	631

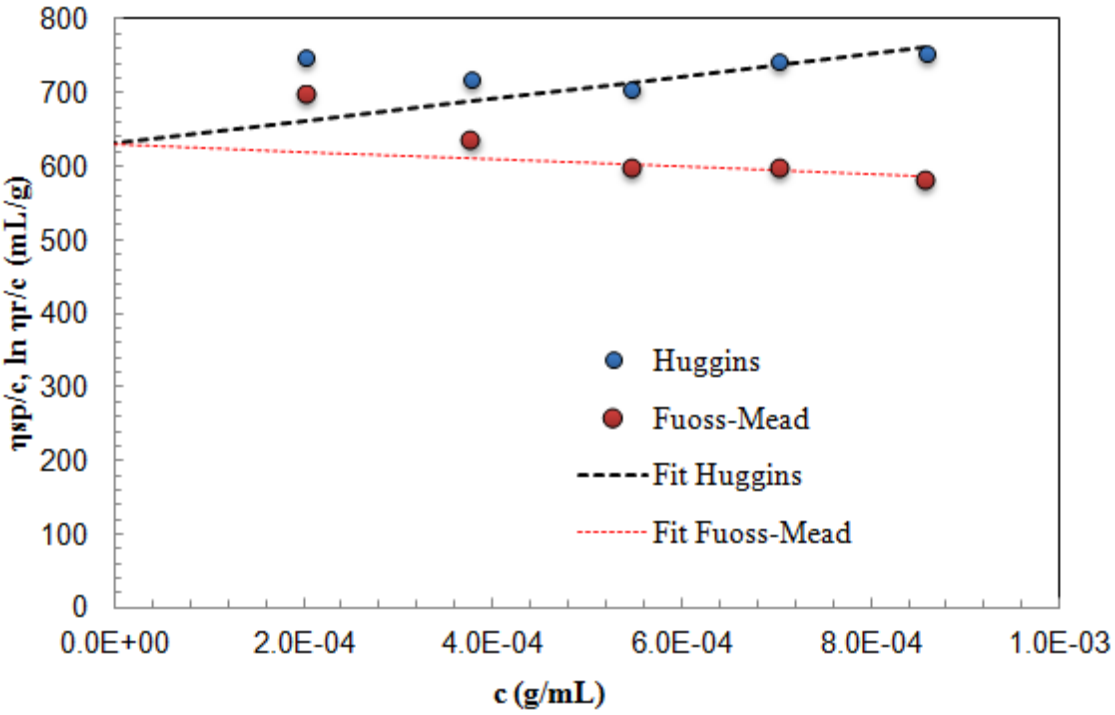

Figure E.1.1: Huggins (blue) and Fuoss-Mead (red) plot for non-modified xan30 analysed with four-bulb shear dilution viscometer, for bulb no. 1.

Table E.1.2: Viscosity data for non-modified xan30 analysed with four-bulb shear dilution viscometer, bulb no. 2.

Shear rate (s^{-1})	**c** (g/mL)	η_r	η_{sp}	**Huggins** η_{sp}/c (mL/g)	**Fouss-Mead** ln η_r/c (mL/g)
427.32	8.56E-04	1.682665	0.682665	798	608
	7.01E-04	1.552545	0.552545	788	628
	5.45E-04	1.411128	0.411128	754	632
	3.75E-04	1.286041	0.286041	763	671
	2.00E-04	1.151037	0.151037	755	703
	0.00E+00		Intercept	683	676

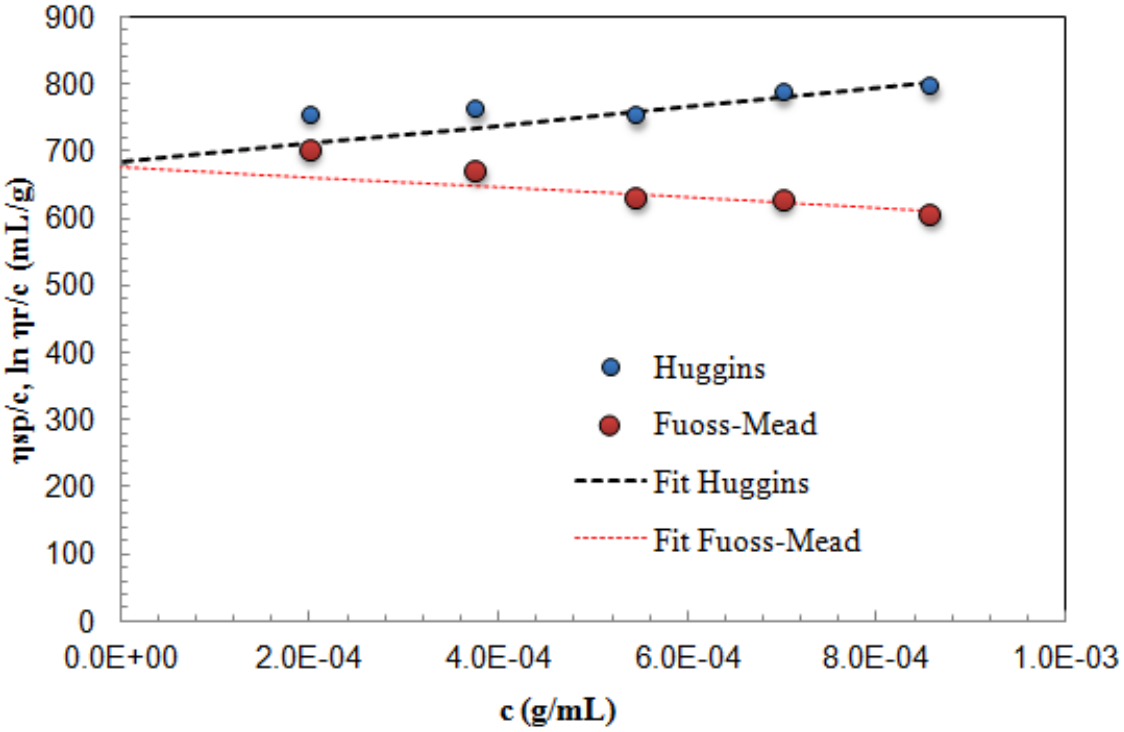

Figure E.1.2: Huggins (blue) and Fuoss-Mead (red) plot for non-modified xan30 analysed with four-bulb shear dilution viscometer, for bulb no. 2.

Table E.1.3: Viscosity data for non-modified xan30 analysed with four-bulb shear dilution viscometer, bulb no. 3.

Shear rate (s^{-1})	**c** (g/mL)	η_r	η_{sp}	**Huggins** η_{sp}/c (mL/g)	**Fouss-Mead** ln η_r/c (mL/g)
273.37	8.56E-04	1.723752	0.723752	846	636
	7.01E-04	1.587468	0.587468	838	659
	5.45E-04	1.442817	0.442817	813	673
	3.75E-04	1.316268	0.316268	843	733
	2.00E-04	1.17076	0.17076	854	788
	0.00E+00		Intercept	758	738

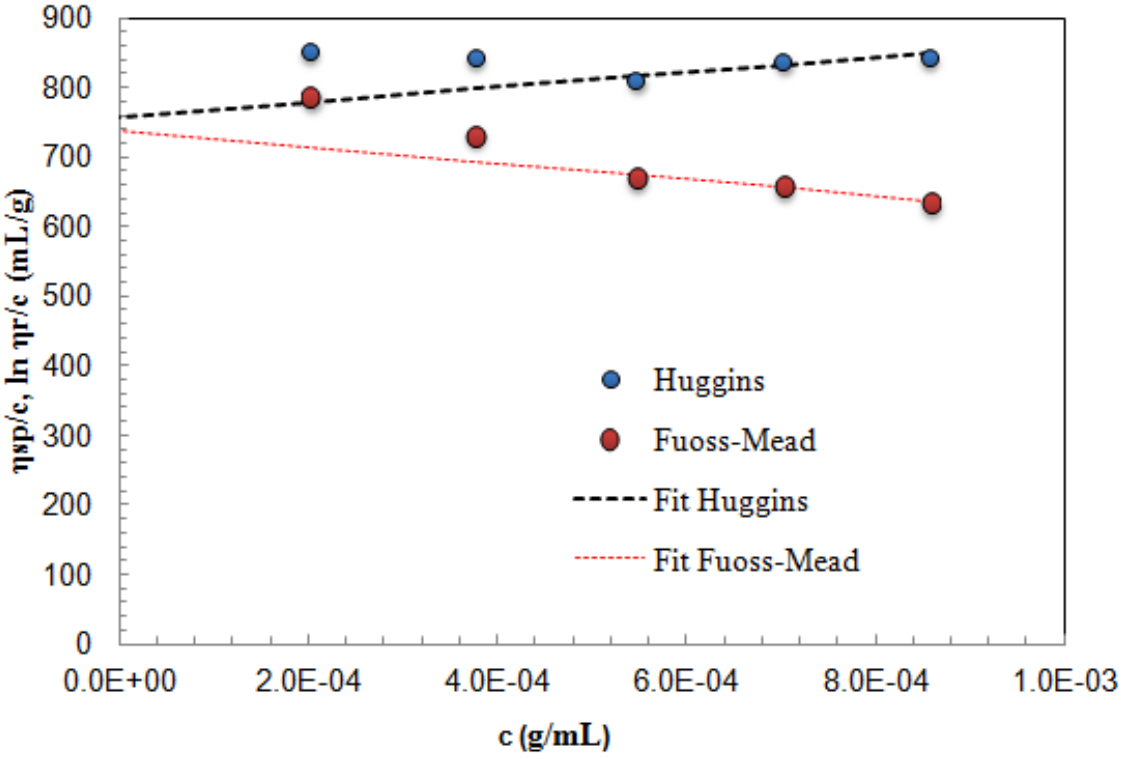

Figure E.1.3: Huggins (blue) and Fuoss-Mead (red) plot for non-modified xan30 analysed with four-bulb shear dilution viscometer, for bulb no. 3.

Table E.1.4: Viscosity data for non-modified xan30 analysed with four-bulb shear dilution viscometer, bulb no. 4.

Shear rate (s^{-1})	**c** (g/mL)	η_r	η_{sp}	**Huggins** η_{sp}/c (mL/g)	**Fouss-Mead** ln η_r/c (mL/g)
158.02	8.56E-04	1.756949	0.756949	884	658
	7.01E-04	1.620902	0.620902	886	689
	5.45E-04	1.476334	0.476334	874	715
	3.75E-04	1.324433	0.324433	865	749
	2.00E-04	1.179357	0.179357	897	825
	0.00E+00		Intercept	858	814

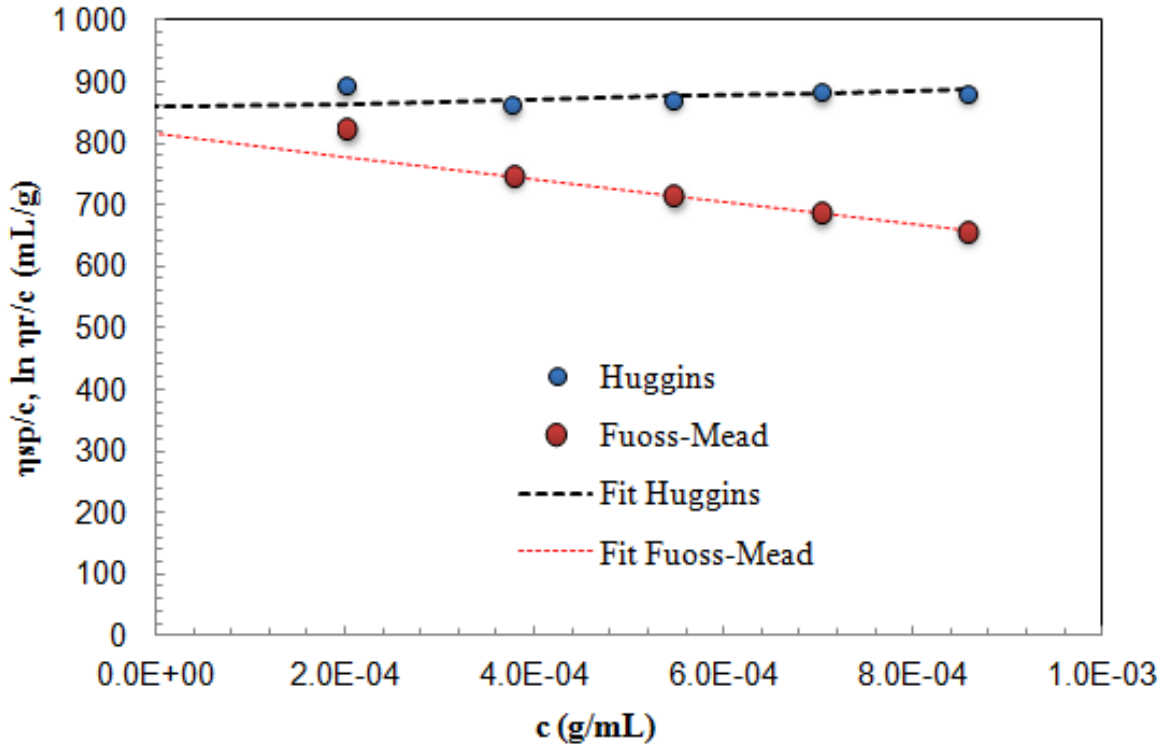

Figure E.1.4: Huggins (blue) and Fuoss-Mead (red) plot for non-modified xan30 analysed with four-bulb shear dilution viscometer, for bulb no. 4.

The raw data from viscosity measurements of modified xan30 with the 4-bulb shear dilution is presented in Table E.1.5.

Table E.1.5: Raw data from 4-bulb shear dilution viscometer analysis of xan30.

Bulb no.	Viscometer const.	Shear rate const.	c (g/ml)	t_1	t_2	t_3	t_{avg}	$\dot{\gamma}$ (s^{-1})	$\dot{\gamma}^{0.5}$	η_r	η_{sp}	η_{sp}/c (ml/g)
1	0.0041742	170944	0	239.95	239.70	240.00	239.88	712.61	26.69			
2	0.0044736	95949	0	224.27	224.38	224.96	224.54	427.32	20.67			
3	0.0045348	60657	0	221.99	220.41	223.27	221.89	273.37	16.53			
4	0.004767	34188	0	216.24	215.00	217.80	216.35	158.02	12.57			
1	0.0041742	170944	8.56E-04	394.14	395.16	396.43	395.24	432.50	20.80	1.648	0.648	757
2	0.0044736	95949	8.56E-04	377.73	378.55	377.18	377.82	253.95	15.94	1.683	0.683	798
3	0.0045348	60657	8.56E-04	381.62	382.73	383.10	382.48	158.59	12.59	1.724	0.724	846
4	0.004767	34188	8.56E-04	380.12	381.01	379.20	380.11	89.94	9.48	1.757	0.757	884
1	0.0041742	170944	7.01E-04	367.36	366.16	362.63	365.38	467.85	21.63	1.523	0.523	746
2	0.0044736	95949	7.01E-04	350.42	348.19	347.20	348.60	275.24	16.59	1.553	0.553	788
3	0.0045348	60657	7.01E-04	353.58	351.37	351.78	352.24	172.20	13.12	1.587	0.587	838
4	0.004767	34188	7.01E-04	352.03	351.85	348.15	350.68	97.49	9.87	1.621	0.621	886
1	0.0041742	170944	5.45E-04	334.37	333.04	330.32	332.58	514.00	22.67	1.386	0.386	709
2	0.0044736	95949	5.45E-04	318.06	318.09	314.40	316.85	302.82	17.40	1.411	0.411	754
3	0.0045348	60657	5.45E-04	319.60	322.27	318.57	320.15	189.47	13.76	1.443	0.443	813
4	0.004767	34188	5.45E-04	317.87	322.80	317.53	319.40	107.04	10.35	1.476	0.476	874
1	0.0041742	170944	3.75E-04	306.51	300.40	307.47	304.79	560.85	23.68	1.271	0.271	722
2	0.0044736	95949	3.75E-04	290.08	283.85	292.36	288.76	332.28	18.23	1.286	0.286	763
3	0.0045348	60657	3.75E-04	297.37	285.41	293.42	292.07	207.68	14.41	1.316	0.316	843
4	0.004767	34188	3.75E-04	289.46	280.65	289.50	286.54	119.31	10.92	1.324	0.324	865
1	0.0041742	170944	2.00E-04	277.34	274.46	272.48	275.90	619.59	24.89	1.150	0.150	751
2	0.0044736	95949	2.00E-04	257.70	259.20	257.28	258.45	371.25	19.27	1.151	0.151	755
3	0.0045348	60657	2.00E-04	259.79	259.77	258.46	259.78	233.49	15.28	1.171	0.171	854
4	0.004767	34188	2.00E-04	254.12	256.18	254.31	255.15	133.99	11.58	1.179	0.179	897

E.2 Modified xan30

Table E.2.1: Viscosity data for modified xan30 analysed with four-bulb shear dilution viscometer, bulb no. 1.

Shear rate (s^{-1})	**c** (g/mL)	η_r	η_{sp}	**Huggins** η_{sp}/c (mL/g)	**Fouss-Mead** ln η_r/c (mL/g)
712.61	8.56E-04	1.490961	0.490961	574	467
	7.01E-04	1.388717	0.388717	555	468
	5.45E-04	1.304968	0.304968	560	488
	3.75E-04	1.19176	0.19176	511	468
	2.00E-04	1.09943	0.09943	497	474
	0.00E+00		Intercept	475	477

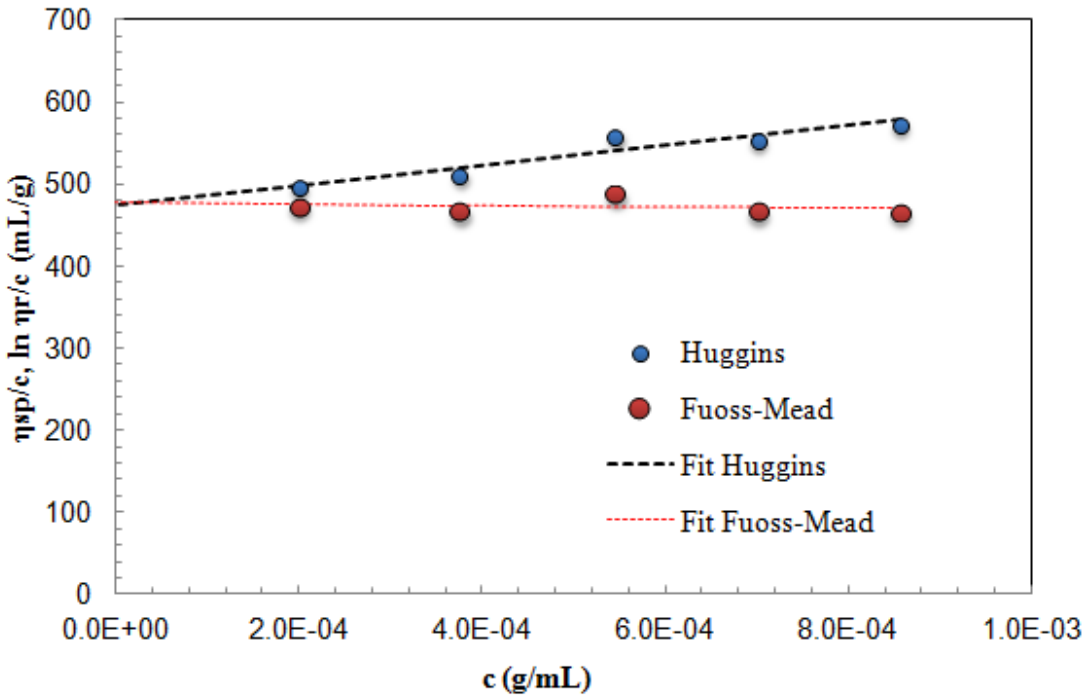

Figure E.2.1: Huggins (blue) and Fuoss-Mead (red) plot for modified xan30 analysed with four-bulb shear dilution viscometer, for bulb no. 1.

Table E.2.2: Viscosity data for modified xan30 analysed with four-bulb shear dilution viscometer, bulb no. 2.

Shear rate (s^{-1})	**c** (g/mL)	η_r	η_{sp}	**Huggins** η_{sp}/c (mL/g)	**Fouss-Mead** ln η_r/c (mL/g)
427.32	8.56E-04	1.505099	0.505099	590	478
	7.01E-04	1.404507	0.404507	577	485
	5.45E-04	1.309051	0.309051	567	494
	3.75E-04	1.197221	0.197221	526	480
	2.00E-04	1.103784	0.103784	519	494
	0.00E+00		Intercept	492	495

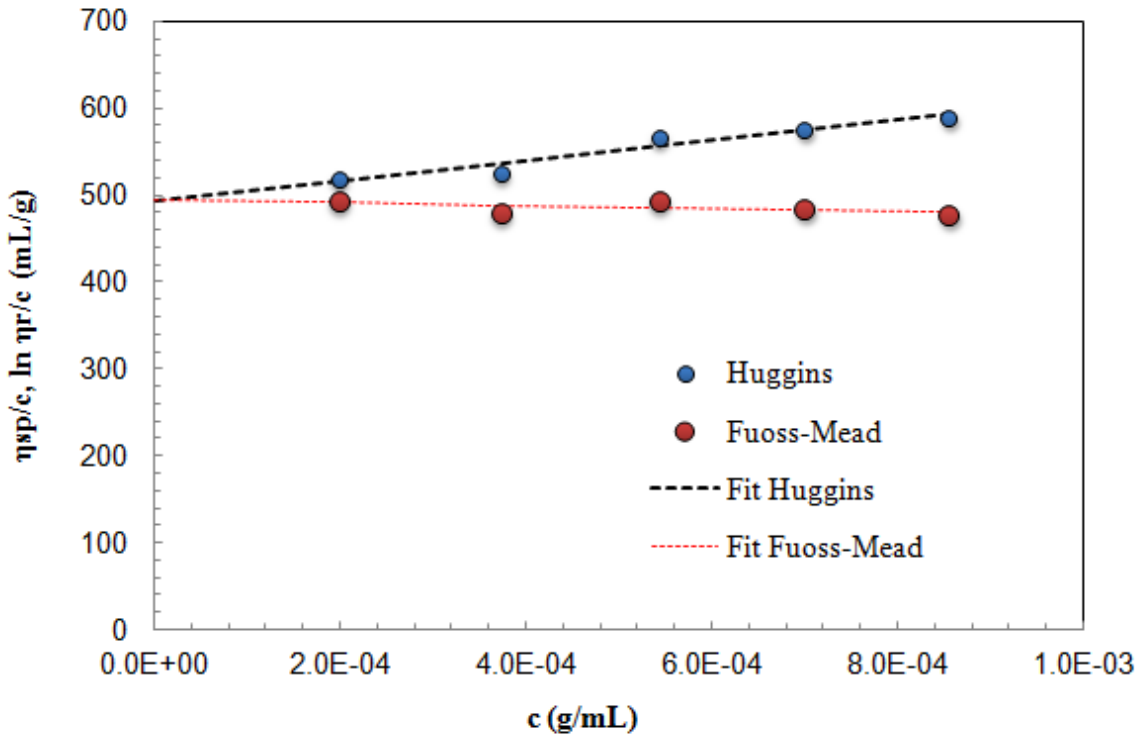

Figure E.2.2: Huggins (blue) and Fuoss-Mead (red) plot for modified xan30 analysed with four-bulb shear dilution viscometer, for bulb no. 2.

Table E.2.3: Viscosity data for modified xan30 analysed with four-bulb shear dilution viscometer, bulb no. 3.

Shear rate (s^{-1})	**c** (g/mL)	η_r	η_{sp}	**Huggins** η_{sp}/c (mL/g)	**Fouss-Mead** ln η_r/c (mL/g)
273.37	8.56E-04	1.516502	0.516502	603	486
	7.01E-04	1.420854	0.420854	600	501
	5.45E-04	1.327835	0.327835	602	520
	3.75E-04	1.206168	0.206168	550	500
	2.00E-04	1.112263	0.112263	561	532
	0.00E+00		Intercept	539	537

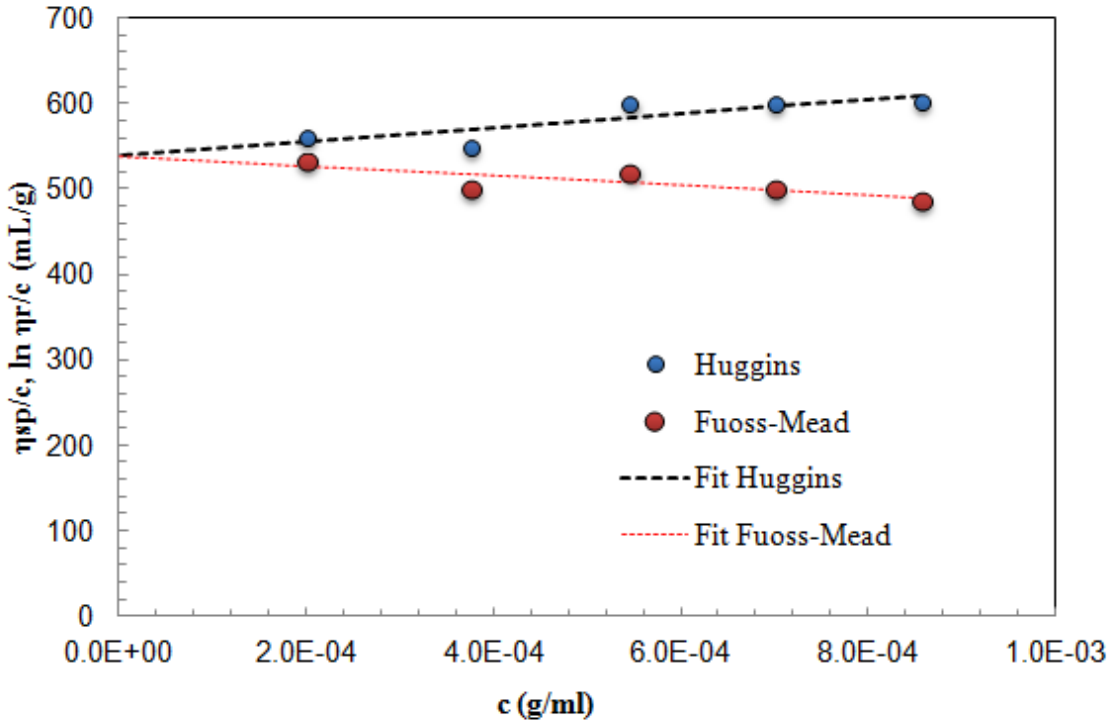

Figure E.2.3: Huggins (blue) and Fuoss-Mead (red) plot for modified xan30 analysed with four-bulb shear dilution viscometer, for bulb no. 3.

Table E.2.4: Viscosity data for modified xan30 analysed with four-bulb shear dilution viscometer, bulb no. 4.

Shear rate (s^{-1})	**c** (g/mL)	η_r	η_{sp}	**Huggins** η_{sp}/c (mL/g)	**Fouss-Mead** ln η_r/c (mL/g)
158.02	8.56E-04	1.551954	0.551954	645	513
	7.01E-04	1.451898	0.451898	645	532
	5.45E-04	1.354755	0.354755	651	557
	3.75E-04	1.213346	0.213346	569	516
	2.00E-04	1.117651	0.117651	588	556
	0.00E+00		Intercept	557	557

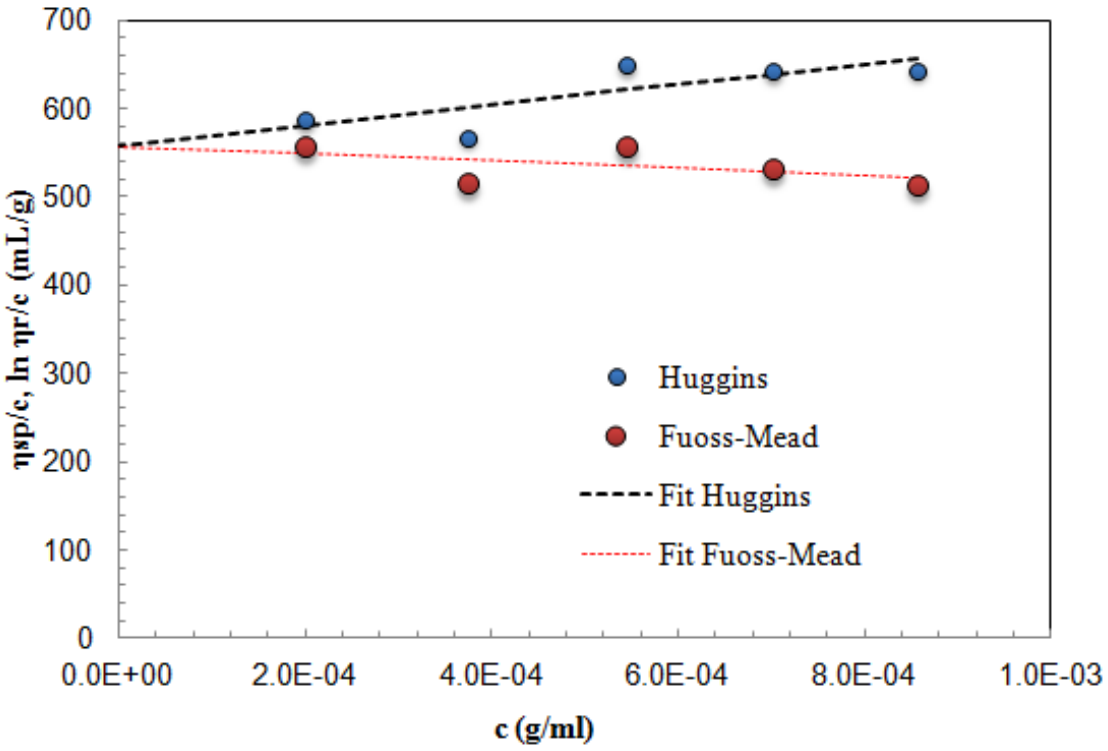

Figure E.2.4: Huggins (blue) and Fuoss-Mead (red) plot for modified xan30 analysed with four-bulb shear dilution viscometer, for bulb no. 4.

The raw data from viscosity measurements of modified xan30 with the 4-bulb shear dilution is presented in Table E.2.5.

Table E.2.5: Raw data from 4-bulb shear dilution viscometer analysis of modified xan30.

Bulb no.	Viscometer const.	Shear rate const.	c (g/ml)	t_1	t_2	t_3	t_{avg}	$\dot{\gamma}$ (s^{-1})	$\dot{\gamma}^{0.5}$	η_r	η_{sp}	η_{sp}/c (ml/g)
1	0.0041742	170944	0	239.95	239.70	240.00	239.88	712.61	26.69			
2	0.0044736	95949	0	224.27	224.38	224.96	224.54	427.32	20.67			
3	0.0045348	60657	0	221.99	220.41	223.27	221.89	273.37	16.53			
4	0.004767	34188	0	216.24	215.00	217.80	216.35	158.02	12.57			
1	0.0041742	170944	8.56E-04	358.34	357.46	357.17	357.66	477.96	21.86	1.491	0.491	574
2	0.0044736	95949	8.56E-04	339.75	336.25	337.85	337.95	283.91	16.85	1.505	0.505	590
3	0.0045348	60657	8.56E-04	339.36	334.01	336.12	336.50	180.26	13.43	1.517	0.517	603
4	0.004767	34188	8.56E-04	336.85	336.27	334.16	335.76	101.82	10.09	1.552	0.552	645
1	0.0041742	170944	7.01E-04	333.50	334.04	331.85	333.13	513.15	22.65	1.389	0.389	555
2	0.0044736	95949	7.01E-04	314.90	317.14	314.05	315.36	304.25	17.44	1.405	0.405	577
3	0.0045348	60657	7.01E-04	313.62	318.87	313.33	315.27	192.39	13.87	1.421	0.421	600
4	0.004767	34188	7.01E-04	310.06	321.60	310.68	314.11	108.84	10.43	1.452	0.452	645
1	0.0041742	170944	5.45E-04	313.40	315.01	310.71	313.04	546.08	23.37	1.305	0.305	560
2	0.0044736	95949	5.45E-04	291.07	299.59	291.13	293.93	326.43	18.07	1.309	0.309	567
3	0.0045348	60657	5.45E-04	289.29	305.13	289.48	294.63	205.87	14.35	1.328	0.328	602
4	0.004767	34188	5.45E-04	284.76	309.66	284.87	293.10	116.64	10.80	1.355	0.355	651
1	0.0041742	170944	3.75E-04	285.02	286.59	286.04	285.88	597.95	24.45	1.192	0.192	511
2	0.0044736	95949	3.75E-04	268.91	268.94	268.61	268.82	356.93	18.89	1.197	0.197	526
3	0.0045348	60657	3.75E-04	268.16	267.67	267.08	267.64	226.64	15.05	1.206	0.206	550
4	0.004767	34188	3.75E-04	262.04	262.48	262.99	262.50	130.24	11.41	1.213	0.213	569
1	0.0041742	170944	2.00E-04	263.66	263.81	264.79	263.74	648.17	25.46	1.099	0.099	497
2	0.0044736	95949	2.00E-04	247.34	248.34	249.15	247.84	387.14	19.68	1.104	0.104	519
3	0.0045348	60657	2.00E-04	246.43	247.17	248.76	246.80	245.77	15.68	1.112	0.112	561
4	0.004767	34188	2.00E-04	242.71	240.89	244.39	241.80	141.39	11.89	1.118	0.118	588

Appendix F

Raw Data From SEC-MALLS

All ASTRA files obtained from SEC-MALLS analyses may be found on the attached CD. The sample names in the tables in this appendix correspond to the file name on the CD.

F.1 SEC-MALLS Results From February and March, of Non-Modified, Purified Sonicated Samples

The results obtained by SEC-MALLS with columns TSK G-4000-3000PWXL and buffer 0.15 M $NaNO_3$ and 0.01 M EDTA are presented in Table F.1.1.

Table F.1.1: SEC-MALLS results from February and March 2014, for non-modified purified sonicated xanthan samples. Columns TSK G-4000-3000PWXL, buffer 0.15 M $NaNO_3$ + 0.01 M EDTA.

Sample name	**Sample description**	**Mw (kDa)**	**Uncert.**	**Injected mass (ug)**	**Calculated mass (ug)**	**Mass recovery (%)**	**dn/dc (mL/g)**
1902002[1802 Xan]	Xan 10 18/2	594.2	0.80 %	40	23.57	58.9	0.15
1902009[1902 Xan]	Xan 10 18/2	595.9	0.90 %	80	46.78	58.5	0.15
1902012[1902 Xan]	Xan 10 18/2	621.9	0.90 %	120	66.75	55.6	0.15
1902003[1802 Xan]	Xan 30 18/2	369.6	0.40 %	40	19.73	49.3	0.15
1902010[1902 Xan]	Xan 30 18/2	361.4	0.40 %	80	39.44	49.3	0.15
1902013[1902 Xan]	Xan 30 18/2	376.9	0.40 %	120	58.79	49	0.15
1902004[1802 Xan]	Xan 120 18/2	183.5	0.40 %	40	27.49	68.7	0.15
1902011[1902 Xan]	Xan 120 18/2	180.7	0.20 %	80	56.57	70.7	0.15
1902014[1902 Xan]	Xan 120 18/2	182.4	0.30 %	120	83.29	69.4	0.15
1903002[1903Xan]	Xan S	370	1.20 %	116	78.28	67.5	0.15
1903003[1903Xan]	Xan S	356.7	1.20 %	58	43.06	74.2	0.15
1903004[1903Xan]	Xan S	357.6	1.20 %	58	43.37	74.8	0.15

F.2 SEC-MALLS Results From April and May, of Non-Modified and Modified Purified Sonicated Xanthan Samples

The results obtained by SEC-MALLS with columns TSK G-6000-5000PWXL are presented in Table F.2.1. Buffer used for the analyses was 0.15 M $NaNO_3$ and 0.01 M EDTA, except for the samples with sample name ending with "ACN"; this indicates that the buffer in addition contained 20 % acetonitrile.

Table F.2.1: SEC-MALLS results from April and May 2014. Columns TSK G-6000-5000PWXL, and buffer 0.15 M $NaNO_3$ + 0.01 M EDTA. Sample name ending with ACN indicates that the buffer in addition contained 20 % acetonitrile.

Sample name	Sample description	Mw (kDa)	Uncert.	Injected mass (ug)	Calculated mass (ug)	Mass recovery (%)	Intrinsic viscosity (mL/g)	Uncert.	dn/dc (mL/g)
2404009[2404PW-visc]	Xan30 i	395.9	2.00 %	50	35.47	70.9	410.485	0.40 %	0.15
2804009[2804 PW Xan+Schiz]	Xan30 i	400.3	1.00 %	100	67.74	67.7	428.296	0.20 %	0.15
0505014[0505 PW ACN]	Xan30 i	373.3	0.80 %	100	62.28	62.3	397.088	0.20 %	0.148
2404010[2404PW-visc]	Xan30 m	401.2	6.50 %	50	7.72	15.4	455.286	1.40 %	0.15
0505003[0505 PW ACN]	Xan30 m	555.4	1.20 %	100	21.82	21.8	497.303	0.40 %	0.15
0505012[0505 PW ACN]	Xan30 m	500.5	0.90 %	100	25	25	437.487	0.40 %	0.148
0705007[0705 PW ACN]	Xan30 m	353.7	1.20 %	100	16.22	16.2	386.822	0.70 %	0.15
2404011[2404PW-visc]	XanS i	338.5	1.30 %	50	40.42	80.8	269.226	0.50 %	0.15
2804010[2804 PW Xan+Schiz]	XanS i	324.1	0.70 %	100	81.32	81.3	267.023	0.20 %	0.15
0505005[0505 PW ACN]	XanS i	295.5	0.80 %	100	76.68	76.7	244.265	0.20 %	0.148
0505013[0505 PW ACN]	XanS i	317.3	0.60 %	100	68.62	68.6	268.881	0.20 %	0.148
2404012[2404PW-visc]	XanS m	513.4	21.40 %	50	1.07	2.1	454.487	8.80 %	0.15
2804041[2804 PW Xan+Schiz]	XanS m	497.4	9.40 %	100	1.13	1.1	375.075	8.50 %	0.15
0505011[0505 PW ACN]	XanS m	318.2	0.80 %	100	23.17	23.2	226.176	0.90 %	0.148
0705008[0705 PW ACN]	XanS m	275.9	2.50 %	100	7.97	8	238.231	2.20 %	0.15
0905015[0705 PW ACN]	XanS m	218.8	1.30 %	50	16.78	33.6	166.767	1.40 %	0.15
1205002[1205 PWXL ACN]	XanS m	349.5	11.00 %	50	9.49	19	227.823	1.80 %	0.15
2804039[2804 PW Xan+Schiz]	Xan30pa i	337.4	0.80 %	100	76.93	76.9	304.777	0.20 %	0.15
0705004[0705 PW ACN]	Xan30pa i	576.6	1.60 %	100	4.49	4.5	613.192	1.00 %	0.15
0705009[0705 PW ACN]	Xan30pa i	508.6	1.00 %	100	14.67	14.7	542.725	0.60 %	0.15
0505008[0505 PW ACN]	Xan30pa i	319.9	0.80 %	100	76.04	76	342.556	0.20 %	0.148
0505015[0505 PW ACN]	Xan30pa m	342.9	0.80 %	100	69.46	69.5	375.937	0.20 %	0.148
0705013[0705 PW ACN]	Xan30pa m	84.4	1.00 %	100	133.76	133.8	90.789	0.30 %	0.15

Table F.2.2: SEC-MALLS results from April 2014, for non-modified non-purified Kelzan, and purified sonicated xanS samples, at different depolymerisation reaction times. Columns TSK G-6000-5000PWXL, buffer 0.15 M $NaNO_3$ + 0.01 M EDTA.

Sample name	**Sample description**	**Depolymerisation time [min]**	**Mw (kDa)**	**Uncert.**	**Injected mass (ug)**	**Calculated mass (ug)**	**Mass recovery (%)**	**dn/dc (mL/g)**
0704012[0704alg+xan]	Kelzan 5	5	2 500	0.10 %	60.00	15.65	26.1	0.15
0704013[0704alg+xan]	Kelzan 10	10	2 605	0.30 %	60.00	20.49	34.2	0.15
0704014[0704alg+xan]	Kelzan 20	20	2 844	0.20 %	60.00	23.57	39.3	0.15
0704015[0704alg+xan]	Kelzan 30	15	2 404	0.20 %	60.00	28.86	48.1	0.15
0704016[0704alg+xan]	Kelzan 45	45	2 482	0.40 %	60.00	34.79	58	0.15
0704017[0704alg+xan]	Kelzan 60	60	2 187	0.30 %	60.00	34.93	58.2	0.15
0904005[0904ss]	Kelzan 5	5	2 463	0.20 %	60.00	15.28	25.5	0.15
0904006[0904ss]	Kelzan 10	10	2 371	0.80 %	60.00	20.9	34.8	0.15
0904007[0904ss]	Kelzan 20	20	2 452	0.40 %	60.00	24.03	40.1	0.15
0904008[0904ss]	Kelzan 30	30	2 023	0.40 %	30.00	30.18	100.6	0.15
0904009[0904ss]	Kelzan 45	45	2 819	0.10 %	30.00	17.88	59.6	0.15
0904010[0904ss]	Kelzan 60	60	2 049	0.20 %	90.00	18.27	20.3	0.15
2404011[2404PW-visc]	Xan S-0	0	338.5	1.30 %	50	40.42	80.8	0.15
2404005[2404PW-visc]	Xan S-10	10	517.8	2.00 %	50	38.62	77.2	0.15
2404006[2404PW-visc]	Xan S-20	20	448.6	3.00 %	50	41.68	83.4	0.15
2404007[2404PW-visc]	Xan S-40	40	420.8	2.00 %	50	41.56	83.1	0.15
2404008[2404PW-visc]	Xan S-60	60	436.5	1.90 %	50	42.12	84.2	0.15

Appendix G

NMR spectra

G.1 Non-Modified Xanthan Samples

The ^{1}H-NMR spectra, with integrals, for the non-modified samples are presented in Figure G.1.1 - G.1.4.

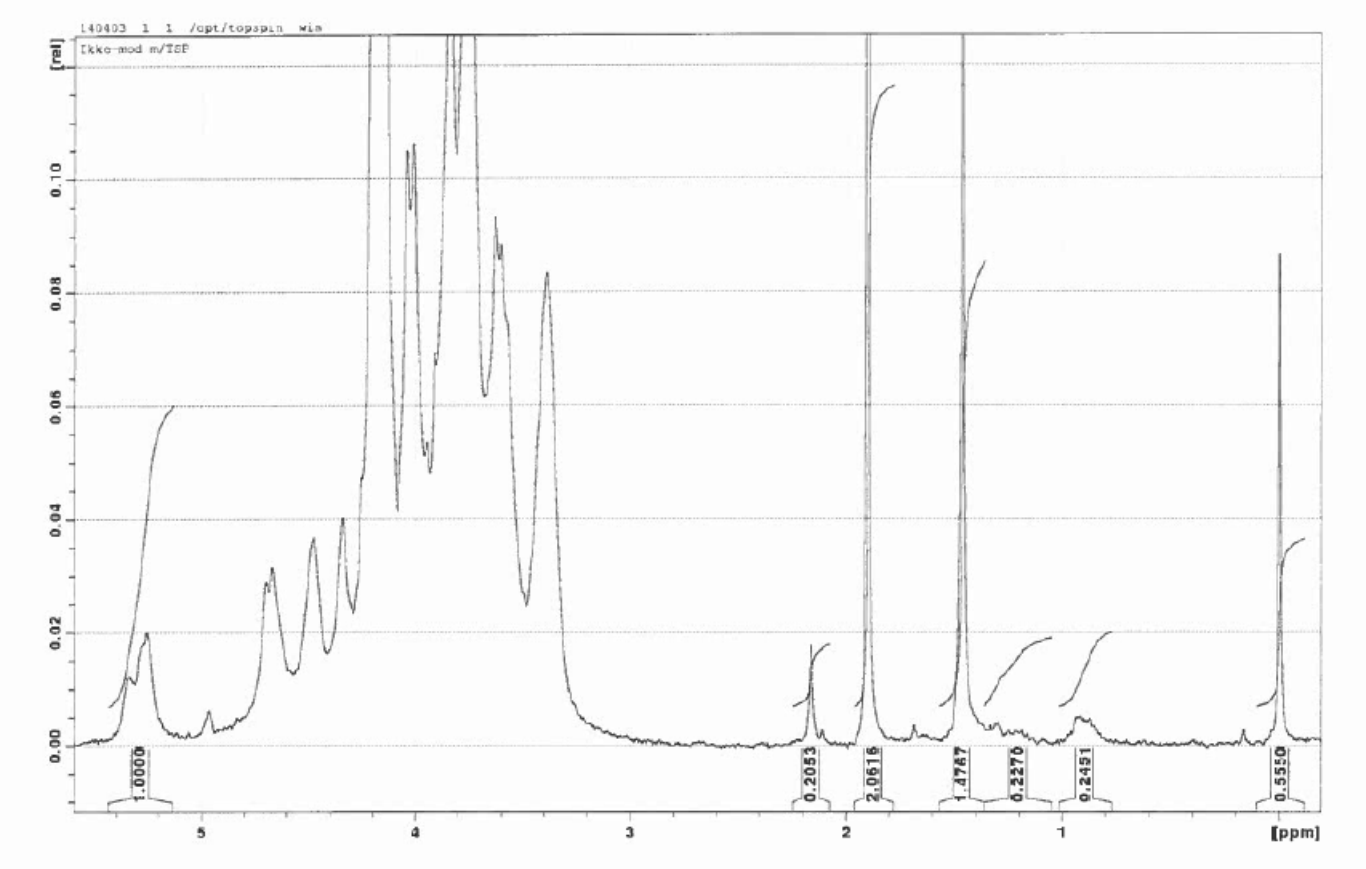

Figure G.1.1: ^{1}H-NMR spectrum of non-modified sample test1. Analysed with Bruker Avance DPX 300 MHz at 80 °C

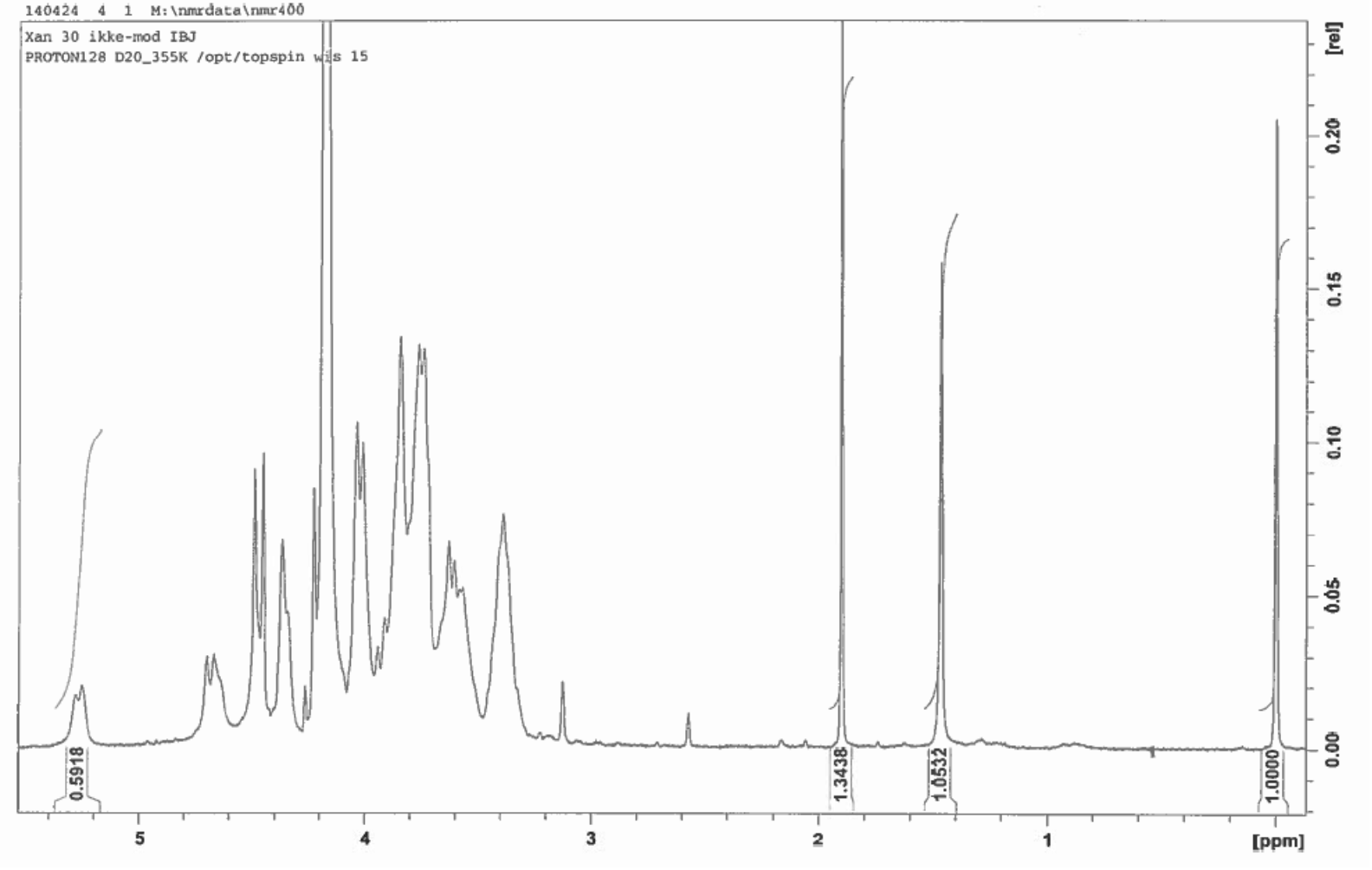

Figure G.1.2: ^{1}H-NMR spectrum of non-modified sample xan30. Analysed with Bruker Avance DPX 400 MHz at 80 °C

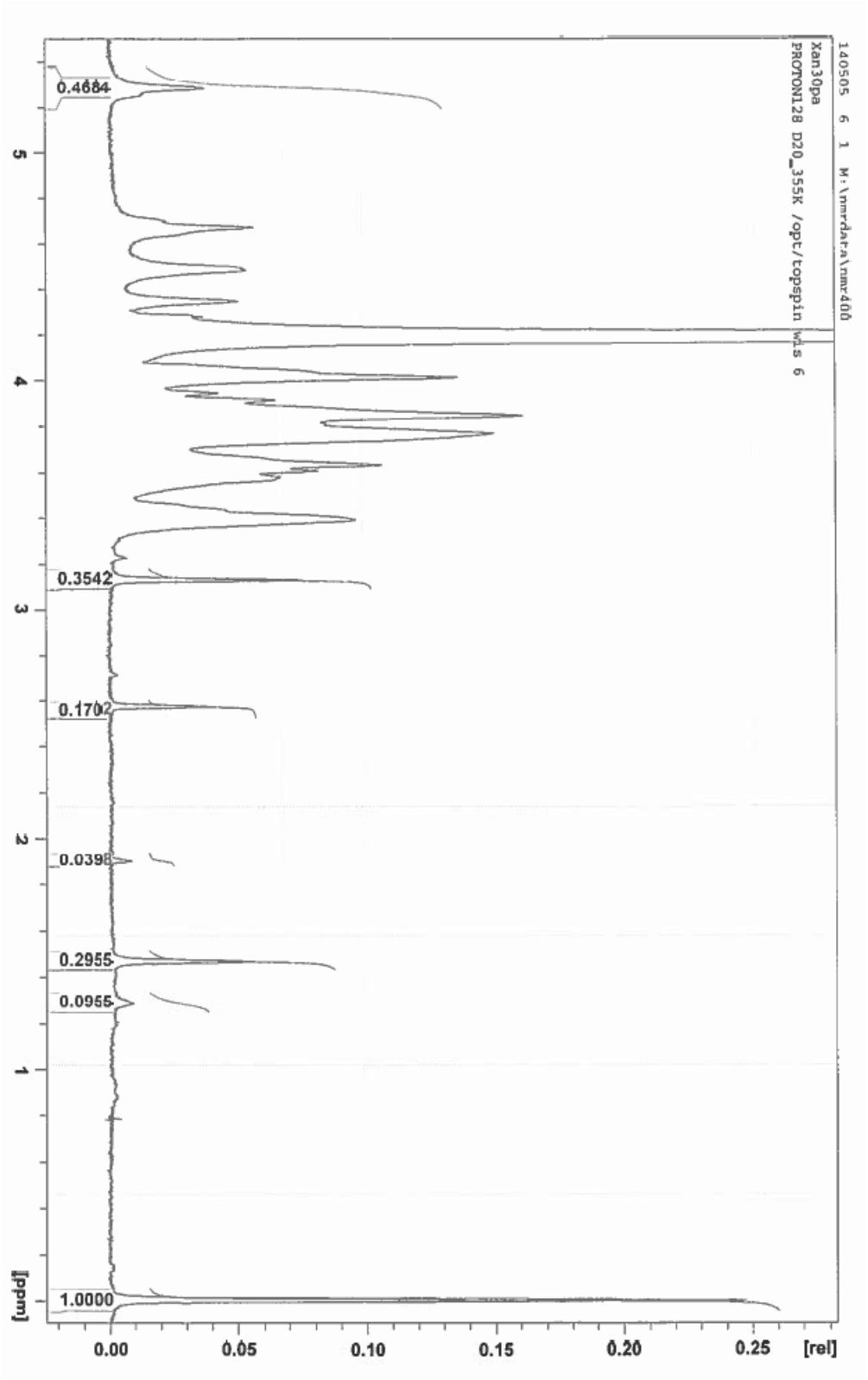

Figure G.1.3: ^{1}H-NMR spectrum of non-modified sample xan30pa. Analysed with Bruker Avance DPX 400 MHz at 80 °C

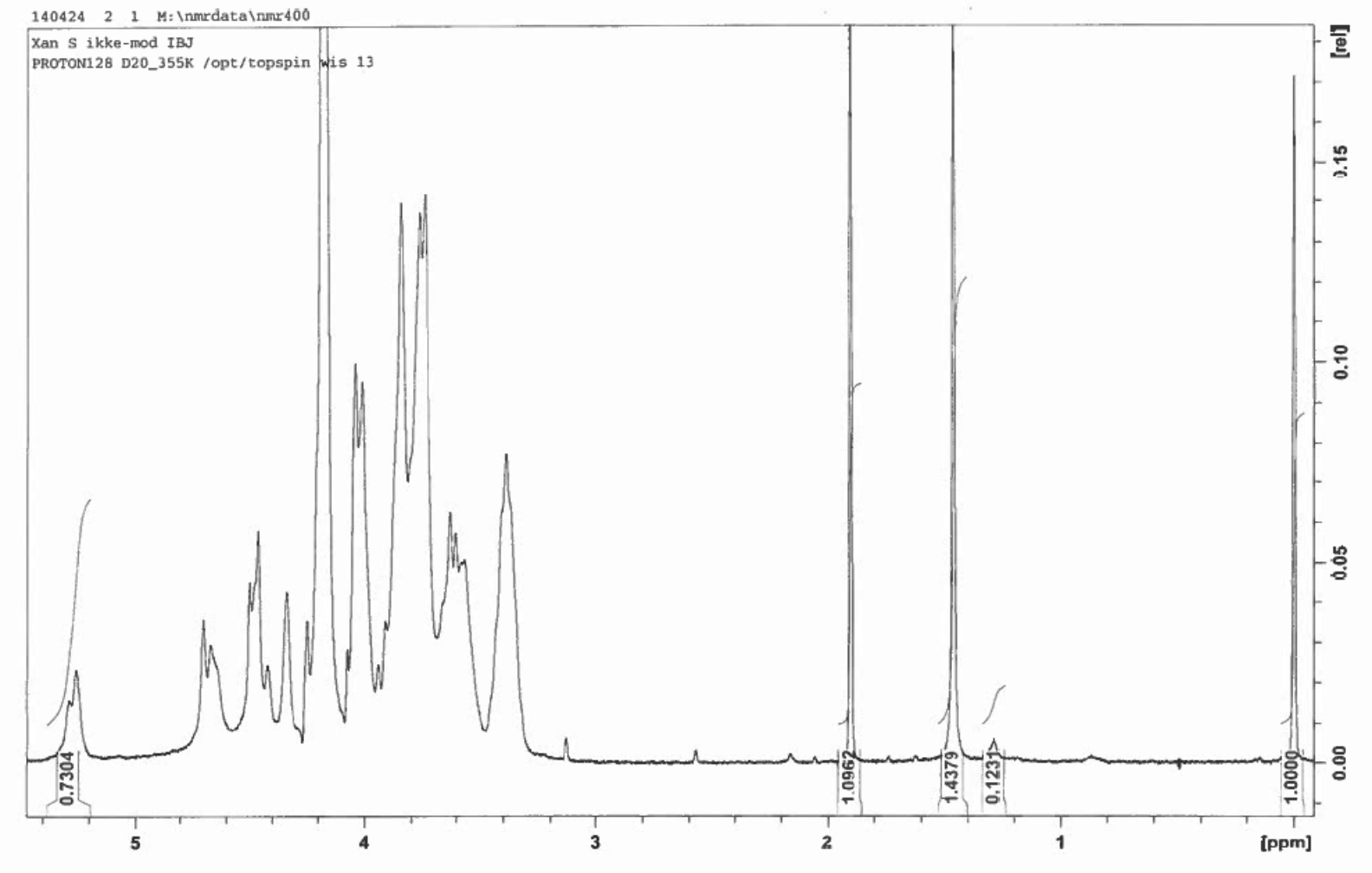

Figure G.1.4: ^{1}H-NMR spectrum of non-modified sample xanS. Analysed with Bruker Avance DPX 400 MHz at 80 °C

G.2 Modified Xanthan Samples

The ^{1}H-NMR spectra, with integrals, for the modified samples are shown in Figures G.2.1 - G.2.7.

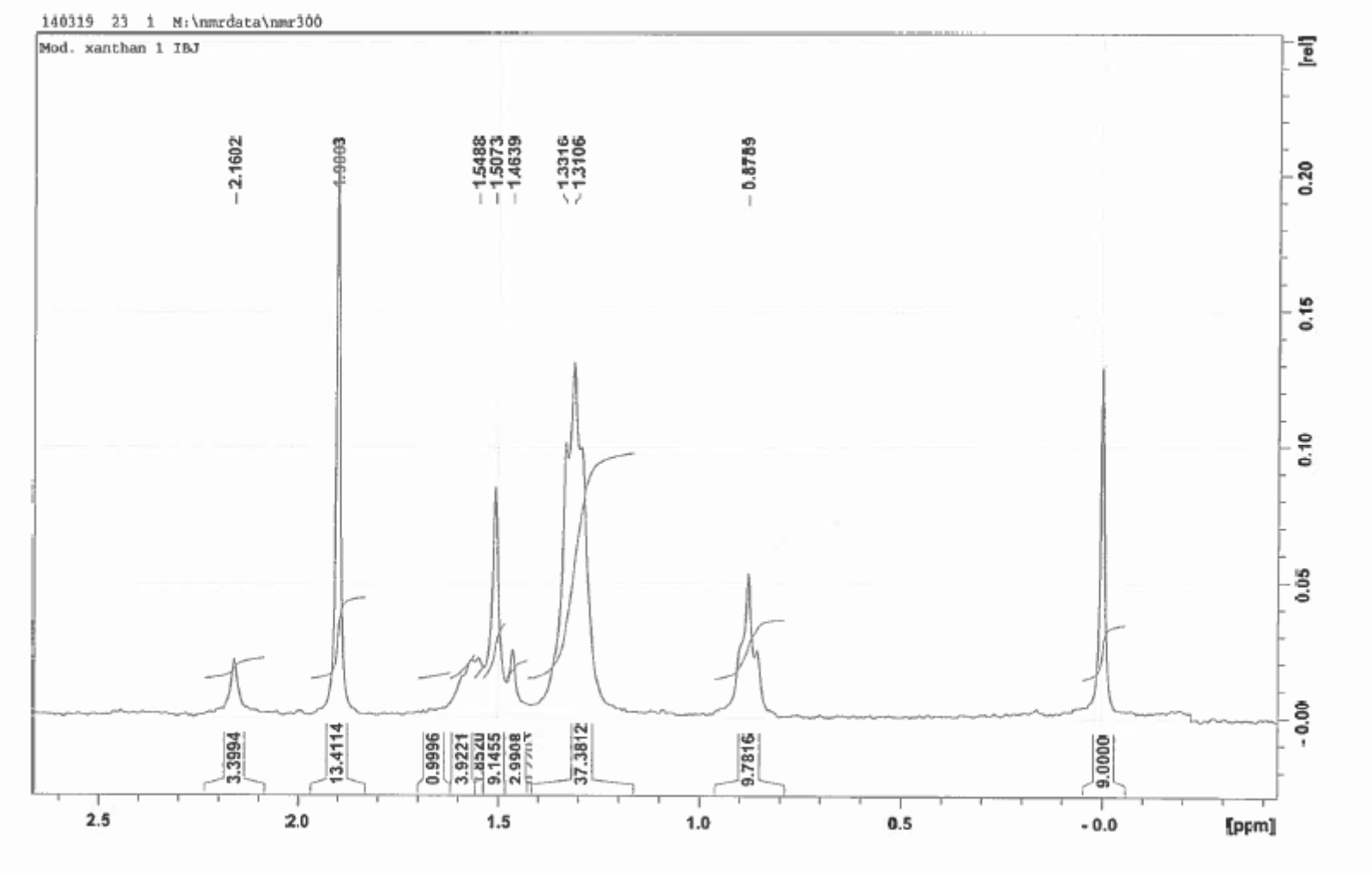

Figure G.2.1: ^{1}H-NMR spectrum of modified sample test1mod1. Analysed with Bruker Avance DPX 300 MHz at 80 °C

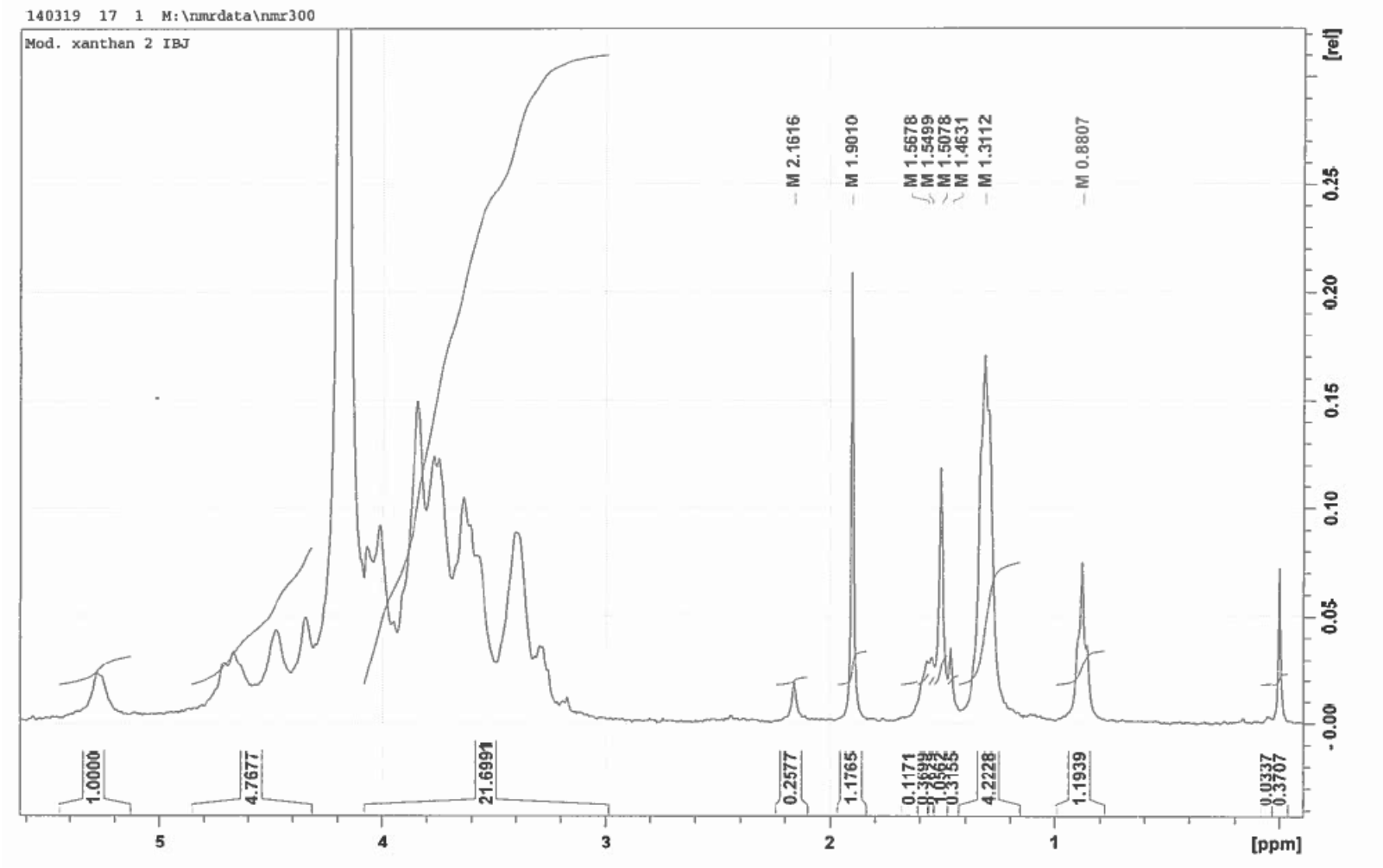

Figure G.2.2: [1]H-NMR spectrum of modified sample test1mod2. Analysed with Bruker Avance DPX 300 MHz at 80 °C

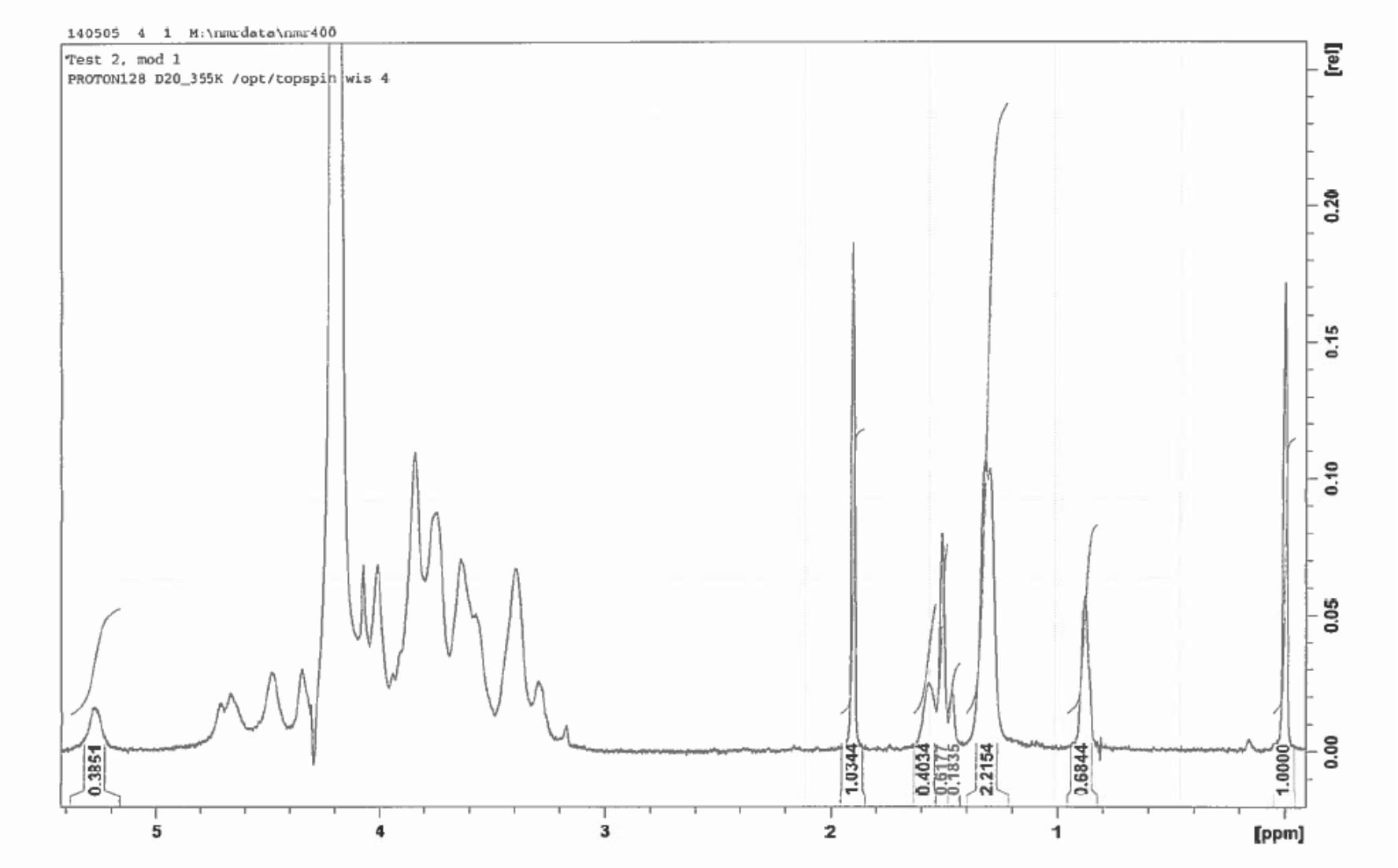

Figure G.2.3: ^{1}H-NMR spectrum of modified sample test2mod1. Analysed with Bruker Avance DPX 300 MHz at 80 °C

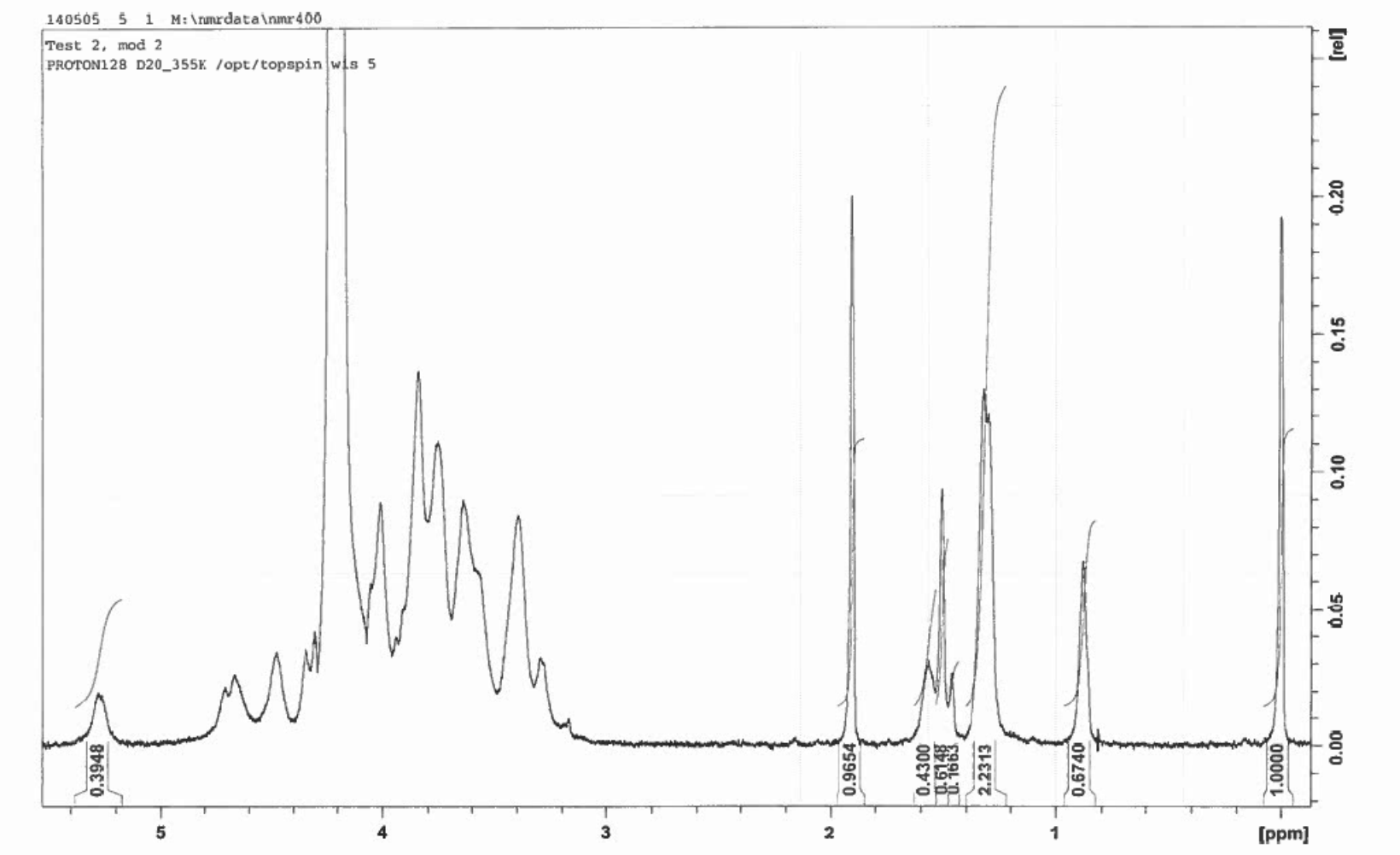

Figure G.2.4: ^{1}H-NMR spectrum of modified sample test2mod2. Analysed with Bruker Avance DPX 300 MHz at 80 °C

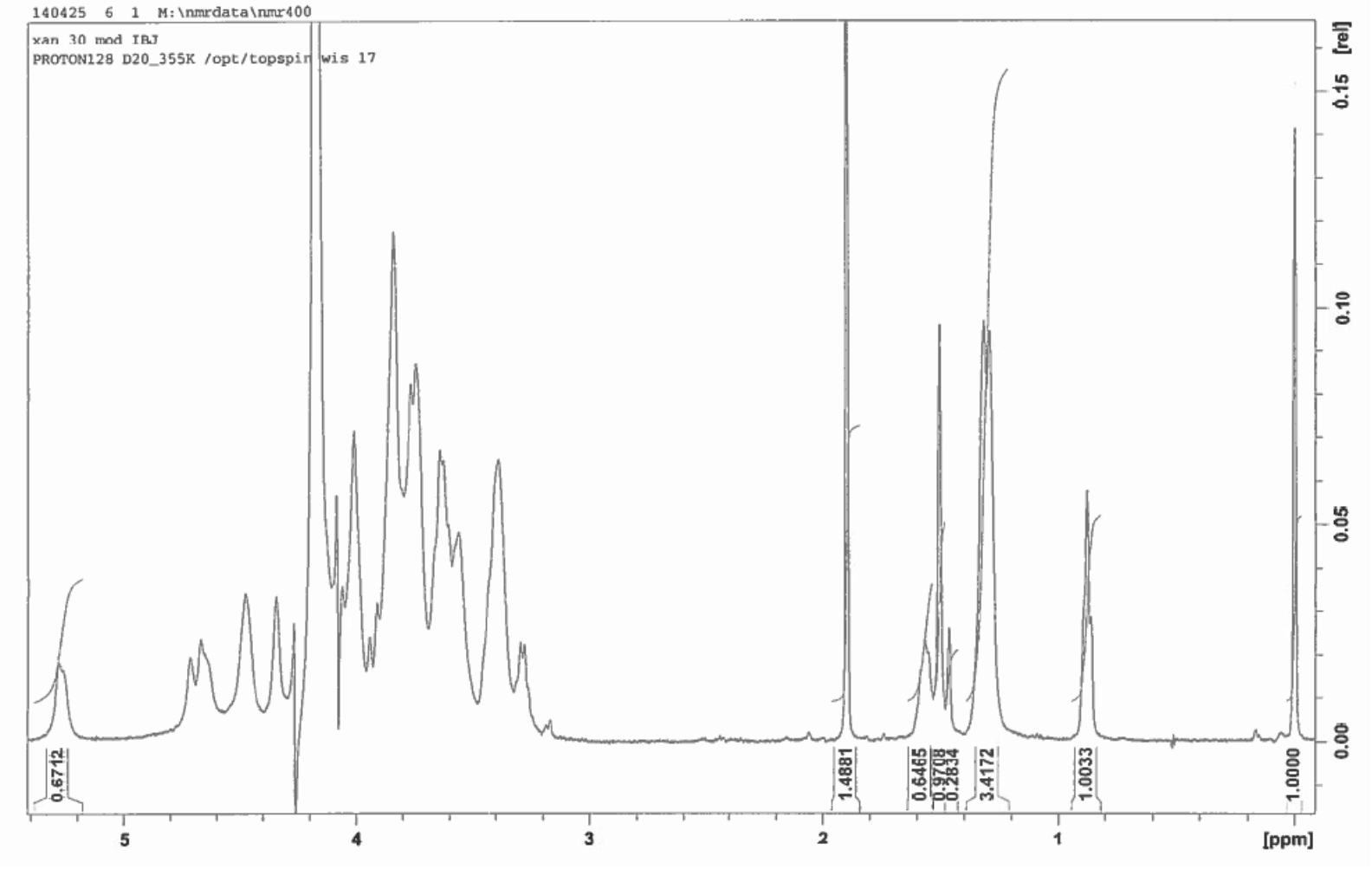

Figure G.2.5: ^{1}H-NMR spectrum of modified sample xan30mod. Analysed with Bruker Avance DPX 400 MHz at 80 °C

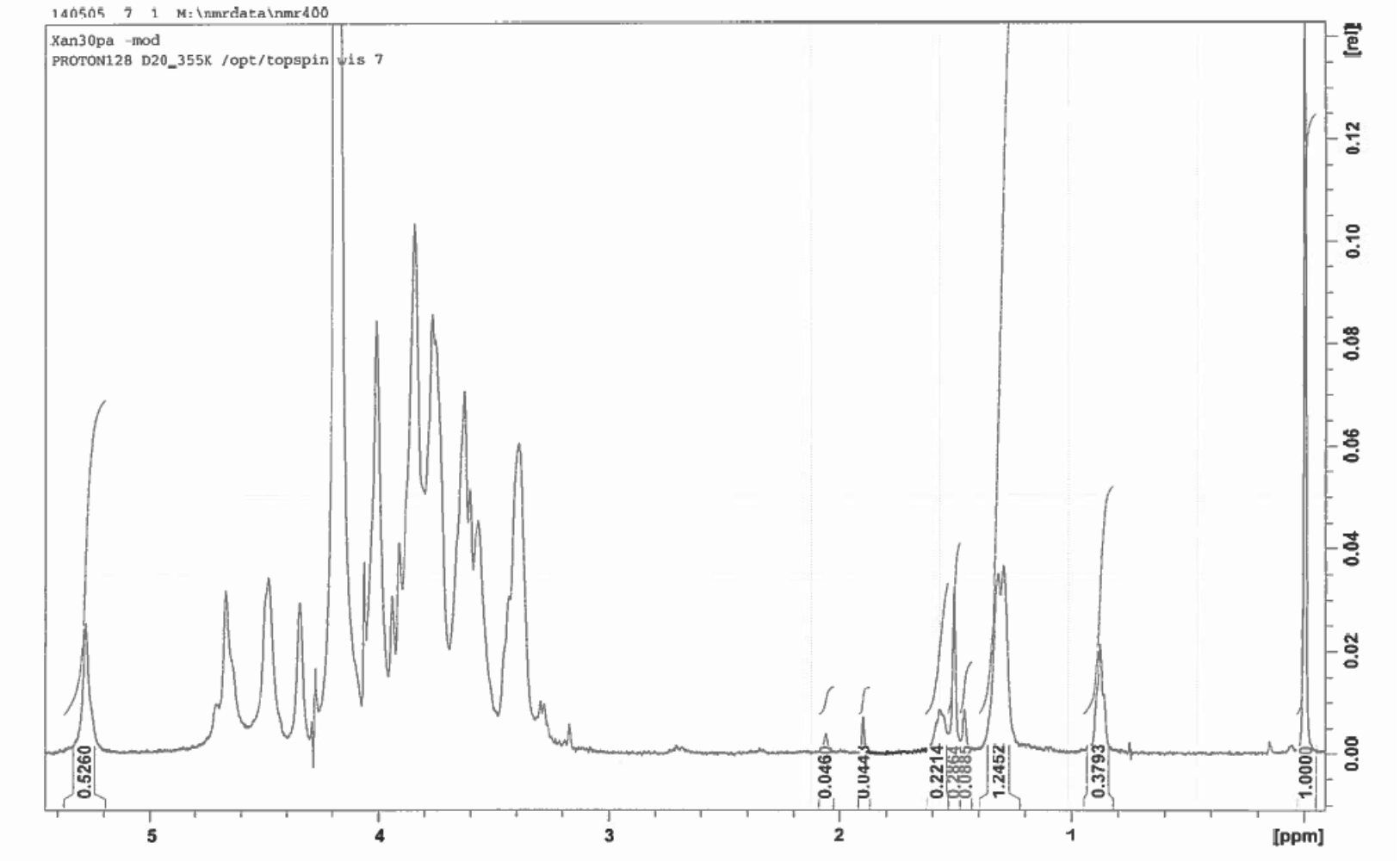

Figure G.2.6: ^{1}H-NMR spectrum of modified sample xan30pamod. Analysed with Bruker Avance DPX 400 MHz at 80 °C

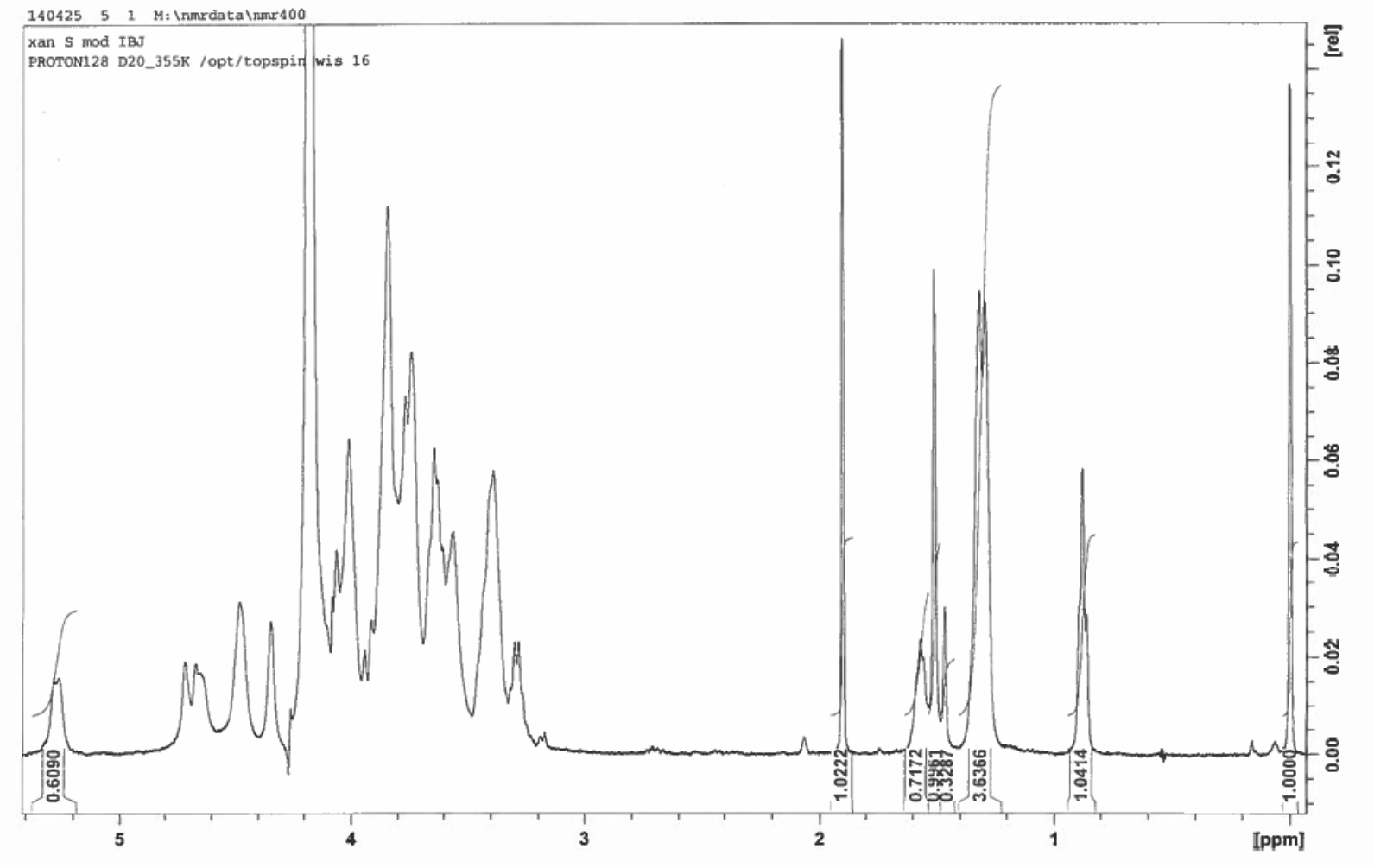

Figure G.2.7: ^{1}H-NMR spectrum of modified sample xanSmod. Analysed with Bruker Avance DPX 400 MHz at 80 °C

G.3 xan-3-94 Samples

The ^{1}H-NMR spectra, with integrals, for the samples xan-3-94-2 and xan-3-94-14 are presented in Figure G.3.1 and G.3.2, respectively.

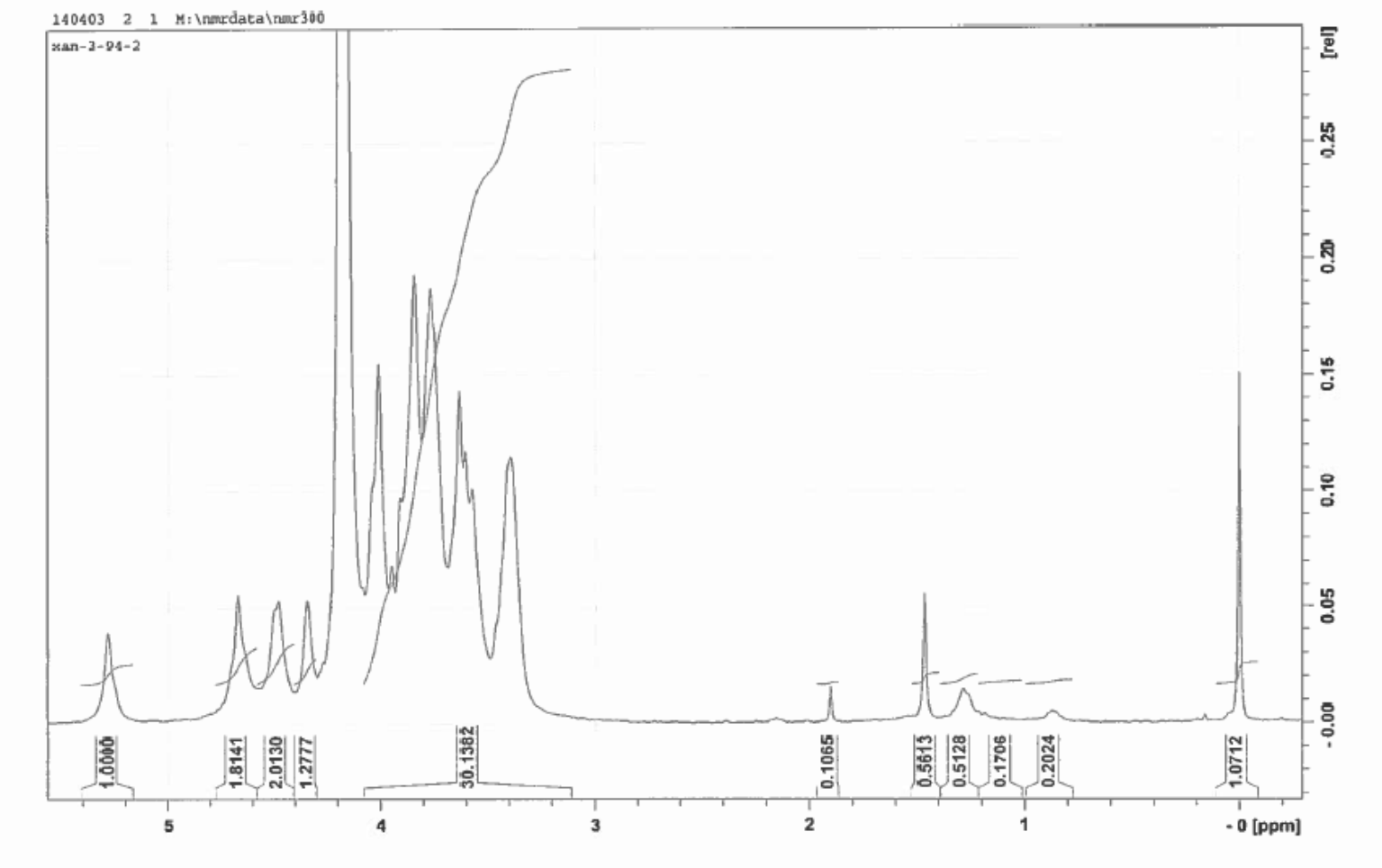

Figure G.3.1: ^{1}H-NMR spectrum of sample xan-3-94-2. Analysed with Bruker Avance DPX 400 MHz at 80 °C

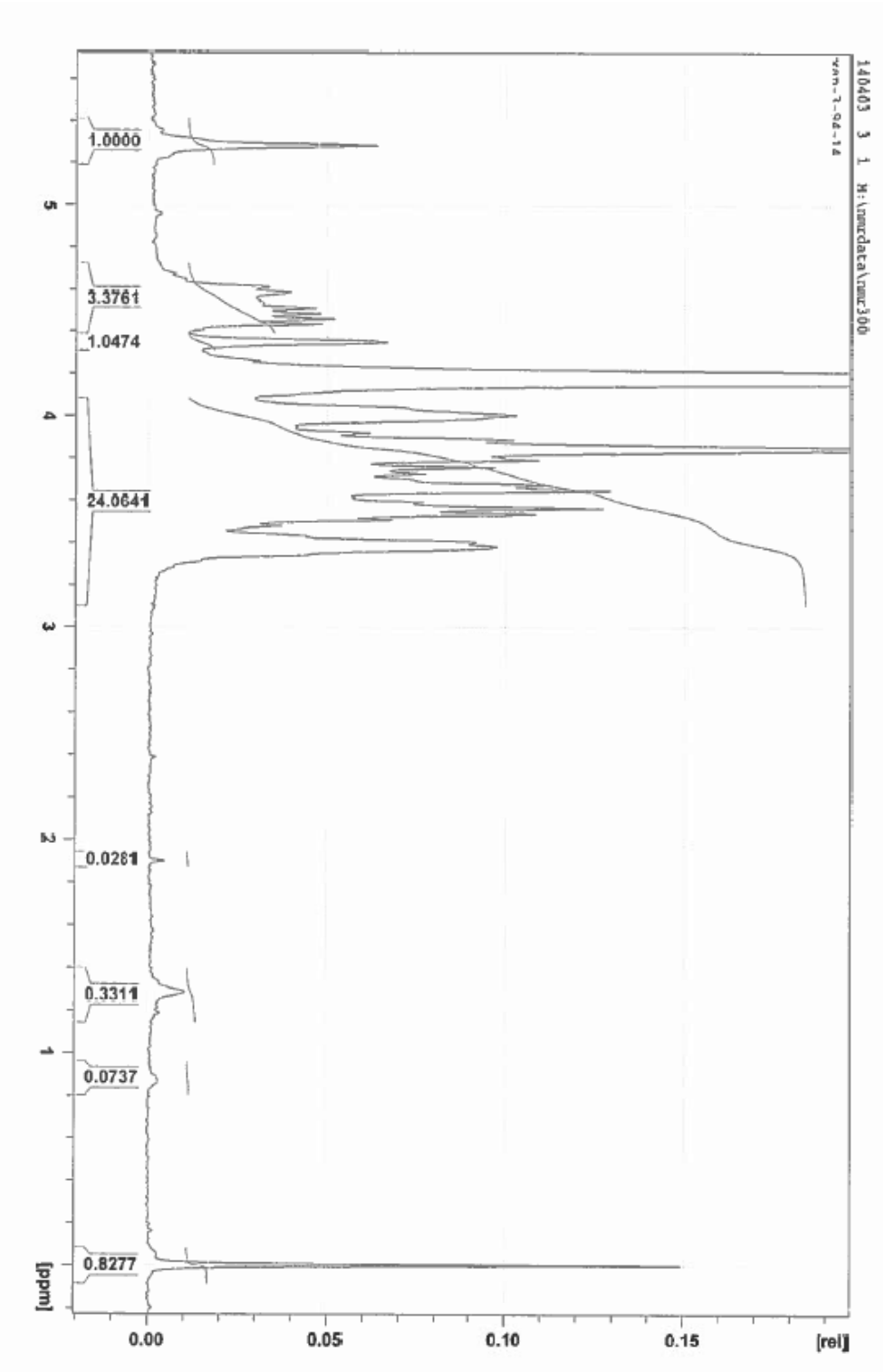

Figure G.3.2: ^{1}H-NMR spectrum of sample xan-3-94-14. Analysed with Bruker Avance DPX 400 MHz at 80 °C

Appendix H

^{1}H-NMR Calculations

H.1 Raw Data and Calculated Degrees of Substitution of Acetyl and Pyruvyl, and Grafting Densities

An overview of the NMR calculations for the test modifications and the modification of the purified sonicated samples is presented in Tables H.1.1 to H.1.3.

H.1.1 Testmodifications

Table H.1.1: Raw data,calculated degrees of substitution of acetyl and pyruvyl, and grafting densities of test modifications.

	test1mod1	**test1mod2**	**test2mod1**	**test2mod2**
V_{TSP} [µL]	5	5	5	5
m_{TSP} [mg]	0.05	0.05	0.05	0.05
n_{TSP} [mol]	2.902E-07	2.902E-07	2.902E-07	2.902E-07
$c_{TSP,0}$ [mol/L]	5.805E-02	5.805E-02	5.805E-02	5.805E-02
$m_{xanthan,0}$ [mg]	6.000	5.700	4.800	4.900
$m_{xanthan,0,corr}$ [mg]	5.520	5.244	4.416	4.508
$V_{H_2O,0}$ [μL]	830	830	830	830
V_{H_2O} µL	600	800	800	800
V_{tot} [μL]	605	805	805	805
$m_{xanthan}$[mg]	3.9904	5.0545	4.2564	4.3451

Continued on next page

Table H.1.1 – *Continued from previous page*

	test1mod1	**test1mod2**	**test2mod1**	**test2mod2**
$c_{xanthan}$ **[g/L]**	6.6506	6.3181	5.3205	5.4313
c_{TSP} **[mol/L]**	4.797E-04	3.605E-04	3.605E-04	3.605E-04
I_{TSP}	9.0000	0.3707	1.0000	1.0000
I_{octyl}	9.7816	1.1939	0.6844	0.6740
I_{Ac}	16.8108	1.4342	1.0344	0.9654
I_{pyr}	9.1455	1.0562	0.6177	0.6148
n_{octyl} **[mol]**	9.463E-07	2.804E-06	5.959E-07	5.869E-07
n_{Ac} **[mol]**	4.042E-04	6.624E-04	2.103E-04	1.923E-04
n_{pyr} **[mol]**	2.199E-04	4.878E-04	1.256E-04	1.224E-04
n'_{RU} **[mol]**	4.334E-06	5.007E-06	4.805E-06	4.917E-06
%octyl	21.8 %	56.0 %	12.4 %	11.9 %
%acetyl	36.2 %	62.7 %	18.3 %	16.7 %
%pyruvyl	19.7 %	46.2 %	11.0 %	10.7 %
M_{RU} **[g/mol]**	896.39	947.28	872.08	870.45
M'_{RU} **[g/mol]**	920.64	1009.57	885.88	883.68
%octyl (n_{octyl}/n'_{RU})	21.8 %	56.0 %	12.4 %	11.9 %

H.1.2 Purified Sonicated Samples xan30, xan30pa, and xanS

Table H.1.2: Raw data andcalculated degrees of substitution of acetyl and pyruvyl for non-modified xan30, xan30pa, and xanS.

	xan30	**xan30pa**	**xanS**
V_{TSP} [µL]	5	5	5
m_{TSP} [mg]	0.05	0.05	0.05
n_{TSP} [mol]	2.902E-07	2.902E-07	2.902E-07
$c_{TSP,0}$ [mol/L]	5.805E-02	5.805E-02	5.805E-02
$m_{xanthan,0}$ [mg]	4.9000	5.1000	4.8000
$m_{xanthan,0,corr}$ [mg]	4.5080	4.6920	4.4160
V_{H2O} [µL]	630	630	630
$V_{xanthansolution}$ [µL]	600	600	600
V_{tot} [muL]	605	605	605
$m_{xanthan}$ [mg]	4.2933	4.4686	4.2057
$c_{xanthan}$ [g/L]	7.1556	7.4476	7.0095
c_{TSP} [mol/L]	0.0005	0.0005	0.0005
I_{TSP}	1	1	1
T_{Ac}	1.3438	0.0398	1.0962
I_{Pyr}	1.0532	0.2955	1.4379
n_{Ac} [mol]	2.703E-04	7.691E-06	2.251E-04
n_{Pyr} [mol]	2.118E-04	5.710E-05	2.952E-04
%acetyl	23.8 %	0.7 %	19.9 %
%pyruvyl	18.6 %	4.9 %	26.1 %
M_{RU} [g/mol]	879.52	850.73	885.52

Table H.1.3: Raw data and grafting densities of modified xan30, xan30pa, and xanS.

	xan30	**xan30pa**	**xanS**
V_{TSP} [µL]	5	5	5
m_{TSP} [mg]	0.05	0.05	0.05
n_{TSP} [mol]	2.902E-07	2.902E-07	2.902E-07
$c_{TSP,0}$ [mol/L]	5.805E-02	5.805E-02	5.805E-02
$m_{xanthan,0}$ [mg]	4.9000	5.1000	4.8000
$m_{xanthan,0,corr}$ [mg]	4.5080	4.6920	4.4160
$V_{H2O,0}$ [µL]	630	630	630

Continued on next page

Table H.1.3 – *Continued from previous page*

	xan30	**xan30pa**	**xanS**
$\boldsymbol{V_{xan}}$ [µL]	600	600	600
$\boldsymbol{m_{xanthan}}$ **[mg]**	4.2933	4.4686	4.2057
$\boldsymbol{V_{tot}}$ [µL]	605	605	605
$\boldsymbol{c_{xanthan}}$ **[g/L]**	7.0964	7.4476	7.0095
$\boldsymbol{c_{TSP}}$ **[mol/L]**	4.797E-04	4.797E-04	4.797E-04
$\boldsymbol{I_{TSP}}$	1.0000	1.0000	1.0000
$\boldsymbol{I_{o}ctyl}$	1.0033	0.3793	1.0414
$\boldsymbol{I_{Ac}}$	1.4881	0.0443	1.0222
$\boldsymbol{I_{Pyr}}$	0.9708	0.2864	0.9961
$\boldsymbol{n_{octyl}}$ **[mol]**	8.736E-07	3.3027E-07	9.06774E-07
$\boldsymbol{n'_{RU}}$ **[mol]**	4.771E-06	5.210E-06	4.635E-06
%octyl	18.3 %	6.3 %	19.6 %
$\boldsymbol{M_{RU}}$	879.52	850.73	885.52
$\boldsymbol{M'_{RU}}$	899.88	857.74	907.32
%octyl	18.3 %	6.3 %	19.6 %

H.2 Calculations

H.2.1 Molecular Weight of Repeating Unit

The number of moles of acetate and pyruvate, n_{Ac} and n_{Pyr}, can be determined by equation H.2.1.

$$n_{Ac} = 3\frac{I_{Ac} \cdot c_{TSP}}{I_{TSP} \cdot c_{xanthan}} \quad \text{and} \quad n_{Pyr} = 3\frac{I_{Pyr} \cdot c_{TSP}}{I_{TSP} \cdot c_{xanthan}} \tag{H.2.1}$$

Here I_{Ac} is the integral of peak corresponding to the methyl group of pyruvate at 1.46 ppm, I_{Pyr} is the peaks corresponding to the methyl groups of the acetyl groups, both bound acetyl and free sodium acetate, at 2.16 ppm and 1.90 ppm, respectively. I_{TSP} is the reference peak at 0.00 ppm, and c_{TSP} and $c_{xanthan}$ is the concentration of the reference

in mol/L and xanthan in g/L, respectively.

The degree of substitution of acetate and pyruvate can be calculated by equation

$$\begin{aligned} DS_{Ac} &= \frac{n_{Ac} \cdot M_{xanthan}}{1 - n_{Ac} \cdot M_{Ac} - n_{Pyr} \cdot M_{Pyr}} \text{ and} \\ DS_{Pyr} &= \frac{n_{Pyr} \cdot M_{xanthan}}{1 - n_{Ac} \cdot M_{Ac} - n_{Pyr} \cdot M_{Pyr}} \end{aligned} \tag{H.2.2}$$

Here $M_{xanthan}$ is the molecular weight of the repeating unit of xanthan without the acetyl and pyruvate groups, M_{Ac} is the molecular weight of acetyl group bound to the mannose, and M_{Pyr} is the molecular weight of pyruvate group bound to the glucose.

The molecular weight of each repeating unit of xanthan can be described by equation H.2.3

$$M_{RU} = M_{xanthan} + DS_{Ac}M_{Ac} + DS_{Pyr}M_{Pyr} \tag{H.2.3}$$

H.2.2 Grafting Density

The grafting density, $\%octyl$, is given by equation (H.2.4).

$$\%octyl = \frac{n_{octyl}}{n'_{RU}} \tag{H.2.4}$$

Here n_{octyl} is the number of moles of octylamine grafted onto the xanthan, which can be calculated from equation H.2.5, and n'_{RU} is the number of moles of modified repeating unit, which can be calculated by H.2.6.

$$n_{octyl} = 3 \cdot \frac{I_{octyl} \cdot n_{TSP}}{I_{TSP}} \tag{H.2.5}$$

$$n_{RU'} = \frac{m_{xanthan}}{M_{RU'}} \tag{H.2.6}$$

During the modification one molecule of water is lost for each molecule of octylamine group grafted onto the xanthan. The molecular weight of modified repeating unit can then be determined by equation H.2.7.

$$M_{RU'} = M_{RU} + \%octyl \cdot M_{octyl} - \%octyl \cdot M_{H_2O} \tag{H.2.7}$$

Here M_{RU} is the molecular weight of a not modified repeating unit, $\%octyl$ is the grafting density, and M_{octyl} and M_{H_2O} is the molecular weight of octylamine and water, respectively.

Iterative calculations is necessary to calculate $\%octyl$ and $M_{RU'}$.

H.3 Calculations of α-Man Content

The number of protons of each repeating unit of xanthan is given by equation (H.3.1)

$$\begin{aligned} \text{Protones of repeating unit} &= 32f_{\beta-Man} + 25f_{ABA} + 14(1 - f_{ABA}) \\ &= 32f_{\beta-Man} + 11f_{ABA} + 14 \end{aligned} \tag{H.3.1}$$

Here $f_{\beta-Man}$ and f_{ABA} is the fraction of β-mannose and α-mannose, respectively. The fraction of α-mannose in the sample, f_{ABA} is given by equation (H.3.2)

$$\begin{aligned} f_{ABA} &= \frac{\dfrac{\text{area of } \alpha\text{-Man H-1 peak}}{\text{protones of } \alpha\text{-Man H-1}}}{\dfrac{\text{area of main peak}}{\text{protones of repeating unit}}} \\ &= \frac{32f_{\beta-Man} + 11f_{ABA} + 14}{R} \end{aligned} \tag{H.3.2}$$

Here R is given by equation (H.3.3).

$$R = \frac{\text{area of } \alpha\text{-Man H1 peak}}{\text{area of main peak}} \tag{H.3.3}$$

By rewriting equation (H.3.2), an equation for calculation of the fraction of α-mannose can be achieved:

$$f_{ABA} = \frac{32f_{\beta-Man} + 14}{R - 11} \tag{H.3.4}$$

The fraction of β-D-mannose, $f_{\beta-Man}$, for xan-3-94-2 and xan-3-94-14, was assumed to be 0 and 0.5, respectively.

Appendix I

Attached CD

The attached CD includes:

- Raw data from intrinsic viscosity measurements with single capillary viscometer
- Raw data from intrinsic viscosity measurements with four-bulb shear dilution viscometer
- ASTRA-files from SEC-MALLS analyses
- Calculations from ^{1}H-NMR